

Chapter 1

Introduction

1.1 Introduction to liquid crystals

The difference between crystals and liquids, the two most common condensed matter phases, is that the molecules in a crystal are ordered whereas in a liquid they are not. The order in a crystal is usually both positional and orientational, in that the molecules are constrained both to occupy specific sites in a lattice and to point their molecular axes in specific directions. The molecules in liquids, on the other hand, diffuse randomly throughout the sample container with the molecular axes tumbling wildly. Interestingly enough, many phases with more order than present in liquids but less order than typical of crystals also exist in nature. These phases are grouped together and called “*liquid crystals*”, since they share properties normally associated with both liquids and crystals.¹

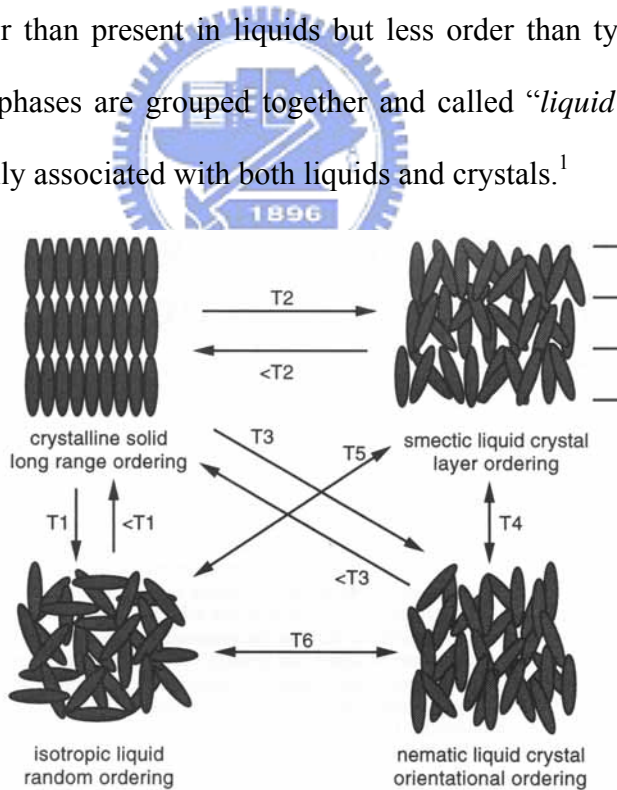
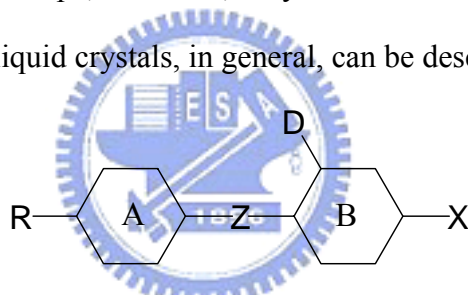


Figure 1.1 Possible melting sequences for a liquid crystalline material.

The liquid crystal can be divided into two categories: 1. lyotropic liquid crystal, the liquid crystalline molecule combines a hydrophobic group at one end with a hydrophilic group at the other end. Such amphiphilic molecules can form ordered structures at certain concentration in both polar and non-polar solvents. 2. Thermotropic liquid crystals, the liquid crystal phase is stable for a certain temperature interval. The most common types of thermotropic liquid crystalline molecule are rod-shaped molecule (calamitic liquid crystal) and disc-like molecules (discotic liquid crystal).

1.1.1 Calamitic liquid crystals

Generally speaking, the geometric structures of nematic and smectic liquid crystalline materials are similar to rod-shape, therefore, they are also called calamitic liquid crystals. The structures of calamitic liquid crystals, in general, can be described as follows:



R is side chain group, X is terminal group, and D is lateral substitution. Two or more saturated and unsaturated rings (A, B) are linked by linking group (Z), which is called core. A and B are usually consisted of cyclic rings. The temperature of mesophase will be promoted while the numbers of cyclic ring are increased. All of the following have been utilized for side chain groups (R):

1. alkyl group, C_nH_{2n+1}
2. alkoxy group, OC_nH_{2n+1}
3. alkenyl group, C_nH_{2n-1}
4. alkeneoxy group, OC_nH_{2n-1}

The length and flexibility of side chain have great effects on the transition temperature and mesophase of liquid crystals. The mesophase tends to form smectic phase from nematic

phase while the length of side chain is increased.

The common linking groups have:

1. dimethylene group and methyleneoxy group
2. ester group
3. containing double bond groups, such as ethylene group, azo group, and imine group
4. acetylene group

Terminal unit is often a small polar substituent (e.g., CN, F, NCS, NO₂), which mainly decide dielectric constant (ϵ) and dielectric anisotropy ($\Delta\epsilon$). A wide range of different lateral substituents (e.g., F, Cl, CN, NO₂, CH₃, CF₃) have been incorporated into many different liquid crystal systems in many different environments. However, the fluoro substituent is the most useful lateral group because of its subtle combination of small size and high electronegativity. It can be thought that lateral substituent sticks out at the side of a molecule that will disrupt molecular packing and reduce liquid crystal phase stability. Figure 2 summaries the possibilities of lateral substitution.

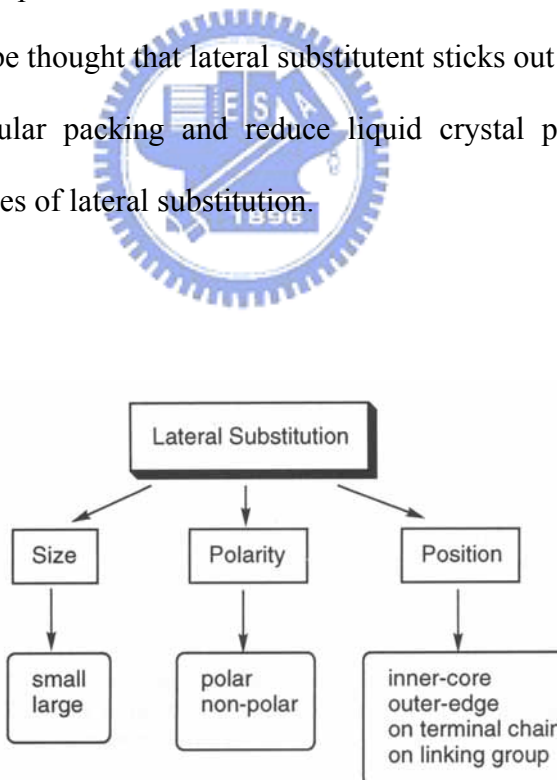


Figure 1.2 The important issues when condidering lateral substitution.

1.2 Introduction to polymer light-emitting materials

In 1990, Burroughes et al. discovered electroluminescent emission from poly(phenylene vinylene)(PPV) which has opened up new research areas for electroactive macromolecules.² Since then, polymer light-emitting diodes (PLEDs) have been studied intensively and various electroluminescent conjugated polymers with good color-tunability have been synthesized through molecular engineering,³ because of their potential applications in a new generation of flat display and lighting technologies.^{4,5} Compared with inorganic electroluminescent (EL) materials, π -conjugated polymers have many virtues such as ease of forming large area, good mechanical flexibility, low fabrication cost, and easy color tuning through molecular design.⁶ Therefore, it is generally expected that PLEDs will be a possible candidate of the next generation display technology. At the same time, polymer light-emitting devices with patterned multi-color emissions have been made by clever device design and construction.

PPV is a bright yellow fluorescent polymer. Its emission maxima at 551 nm (2.25 eV) and 520 nm (2.4 eV) are in the yellow-green region of the visible spectrum. This polymer is insoluble, intractable, and infusible. Any synthesis of PPV directly from a monomer produces an insoluble material, which can not be easily processed. Solution processing by spin-coating is, however, particularly desirable as it yields high-quality transparent thin films for the production of polymer EL devices. This dilemma is conveniently resolved by the use of a solution-processible precursor polymer. The sulfonium precursor route to PPV was introduced by Wessling and Zimmerman,⁷ and was subsequently modified and optimized by other groups.⁸ The principle has been applied, not only to PPV and its derivatives, but also to a whole range of PPV-related copolymers.

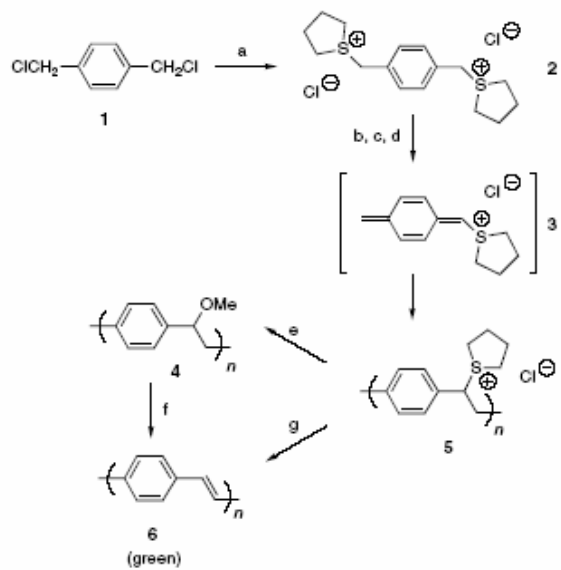


Figure 1.3 Synthesis route of PPV.

Figure 4 shows the synthesis of the most studied dialkoxy-PPV (MEH-PPV). The branched side chain in MEH-PPV has a favorable effect on the solubility of the polymer. Indeed, this polymer dissolves easily in solvents such as tetrahydrofuran, chloroform, or xylene.

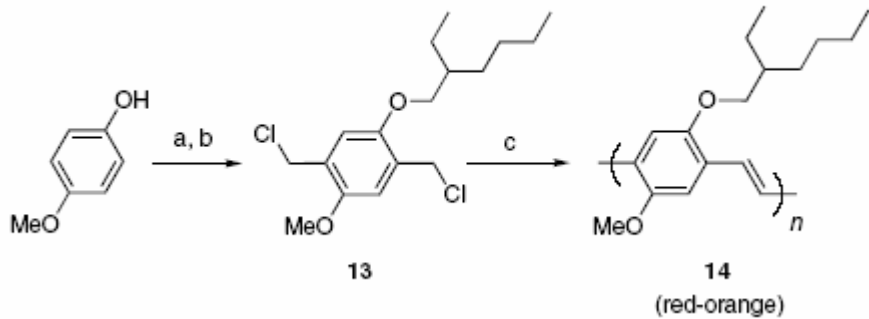


Figure 1.4 Synthesis route of MEH-PPV.

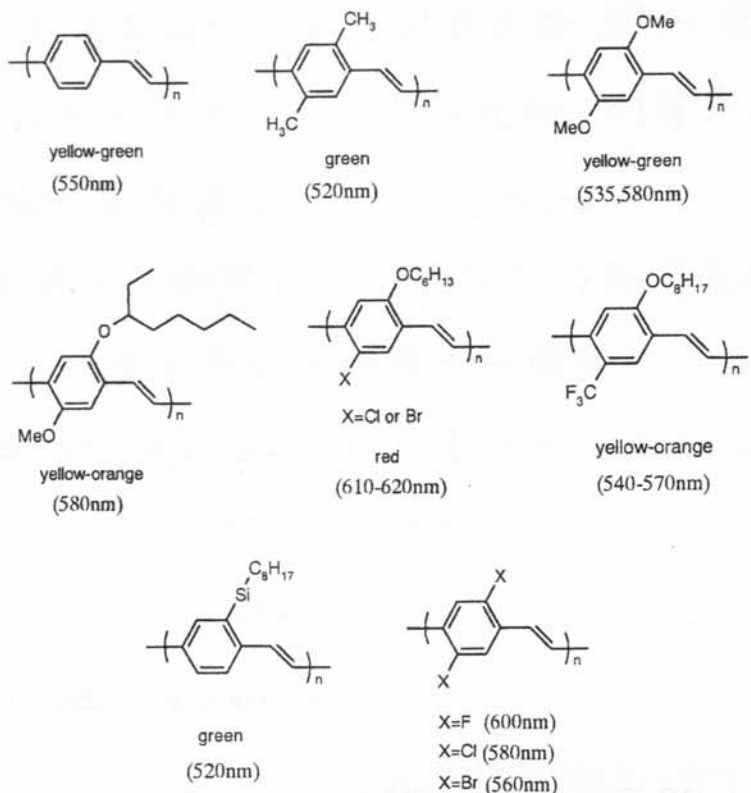


Figure 1.5 PPV derivatives and their emission color range.

Since the successful use of 2-(4-biphenylyl)-5-(4-*tert*-butylphenyl)-1,3,4-oxadiazole (PBD) in sublimed film EL devices. The oxadiazole derivatives become the most extensively investigated classes of electron-conducting/hole-blocking materials. But sublimed PBD layer has tendency to recrystallization and reduce the stability of device. Therefore, how to suppress the recrystallization becomes an important subject. There are a variety of methods that can be used to overcome this issue:

1. electron-transporting materials are doped in inert polymer matrix or fluorescent polymer layer. But molecular oxadiazole derivatives (such as PBD) have some incompatibilities with polymers that lead to phase separation or recrystallization especially at higher temperatures.
2. synthesize large steric hindrance materials such as star-sharp, spiro-linkage or forming

complex with metals.⁹

3. synthesize high Tg materials by molecular design.

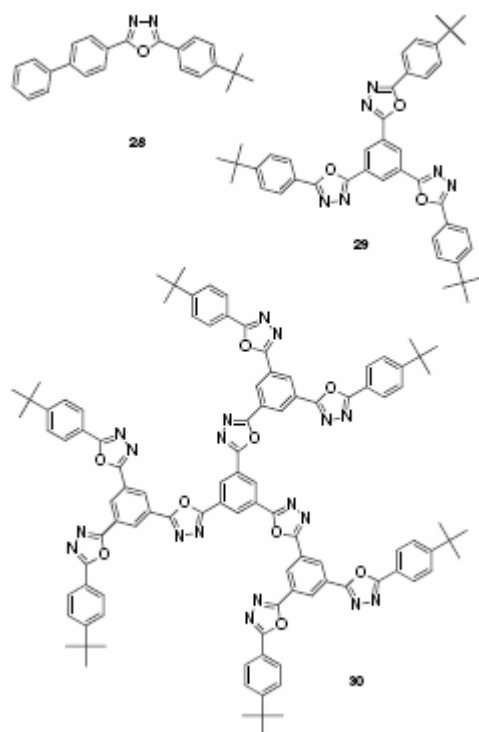


Figure 1.6 Examples of oxadiazole-containing electron-transporting materials.

Most EL polymers inject and transport holes more efficiently than electrons due to the inherent richness of π -electrons in the EL polymers, which results in an unbalance of opposite carrier currents and shift of the recombination zone toward the region near the interface of the polymer and the cathode. In order to obtain highly efficient PLED devices, a balance in the injection and transportation of both holes and electrons into the polymer emissive layer is necessary.¹⁰⁻¹⁴ Therefore, the synthesis of efficient electron transporting polymers is needed to improve EL device performance.

The incorporation of identical redox sites within polymers has been used successfully in

the design of chromophore. Since electron hopping is the main charge-transport mechanism in electron-conducting materials, increasing the number of electron-transporting moiety would therefore seem a promising way to improve the charge-transporting properties. Polymers containing electron-withdrawing units in the main chains or side chains usually have large electron affinities. Polymeric 2,5-diphenyl-1,3,4-oxadiazole-diyl derivatives are the most widely studied classes of electron-injection and/or hole-blocking materials,¹⁵ by virtue of many merits owned by 1,3,4-oxadiazole (OXD) moieties, such as high electron affinity, high photoluminescence (PL) quantum yield, and good thermal stability.¹⁶ In recent years, except oxadiazole derivatives, polyquinolines, polyquinoxalines, polybenzobisazoles, and polypyridines have been demonstrated as electron transporting (ET) polymers due to the good film quality, and the excellent thermal and oxidative stability.¹⁷⁻¹⁹

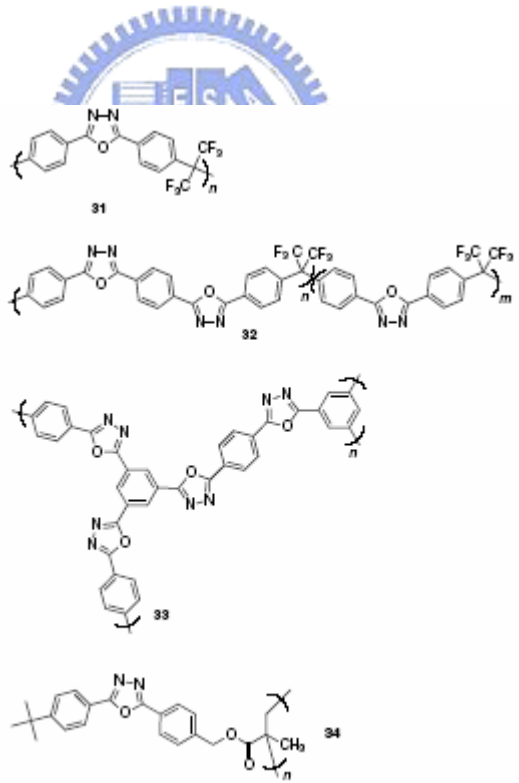


Figure 1.7 Examples of oxadiazole-containing electron-transporting polymers.

On the other hand, in order to achieve highly efficient and luminescent PLED devices, it is also important to suppress the self-quenching process, which is originated from the formation of excimers due to the intermolecular interactions in the solid state. Since large

steric hindrance of lateral substitution will cause the decrease of crystallinity in the resulting polymers, the bulky substitution with symmetrical and asymmetrical structure on the side chains of the polymer can provide the polymer film with an amorphous property.²⁰ In addition, the pseudo-orthogonal arrangement of the rigid pendant groups can reduce the π -stacking and thus to increase the radiative decay quantum efficiency and photostability of the polymers.

A wealth of liquid-crystalline polymers based on non-conjugated polymers has been created.²¹ In contrast, few liquid-crystalline polymers based on conjugated polymers have been generated; nevertheless, those polymers exhibit novel optical and electronic properties and suit to construct electrooptic device. Since 1995, Dyreklev et al. demonstrated an organic polarized EL device based on aligned conjugated polymers that emitted polarized light.²² They realized that such devices would be particularly useful as backlights for conventional LCDs, because they could make the polarizer redundant. High polarization ration (12~200, depending on application) is necessary for backlight application,²³ it is a new challenge to the materials science community to explore highly aligned emitters and practical aligned methods. There are a variety of methods that can be used to achieve orientation, and all of the following have been utilized for organic EL materials:

1. mechanical alignment (stretching or rubbing with a cloth)
2. Langmuir-Blodgett (LB) deposition
3. Liquid-crystalline self-organization
4. alignment on specific substrates

The quality of alignment of a molecular material is often quantified by an orientational “order parameter” S . An upper limit of the polarization ratio R (intensity parallel over intensity perpendicular to molecular alignment) of emitted light is given by the order parameter S of the emitters, with d the dimensionality of the system.

$$S = [R-1] / [R + (d-1)] \quad (1a)$$

Chapter 2

Effects of polar substituents on the properties of 1,3,4-oxadiazole-based liquid crystalline materials containing asymmetric cores

2.1 Abstract

A series of 1,3,4-oxadiazole-based liquid crystals bearing different polar substituents (n-NPO-X, where X = Me, OMe, Cl, F, CN, and NO₂) at phenyl 4-position are synthesized and characterized. These angular oxadiazole-based liquid crystals, which are composed of asymmetric cores containing naphthalene units, exhibit stable mesogenic properties including the nematic and smectic A phases. With the analogous structural design, the transition temperatures, mesomorphic phases, optical properties, and internal quantum efficiencies show strong dependence on the terminal substitution. In general, by increasing the terminal dipoles, the temperature ranges of the mesophases are enhanced, and both of the absorption and photoluminescence spectra are shifted to longer wavelengths.

2.2 Introduction

The design and synthesis of liquid crystals (LC) containing heterocyclic units has been the subject of considerable researches in recent years.²⁴⁻²⁹ Due to more choices in the design of new mesogenic molecules with heterocyclic rings, the polarity and geometry of the molecules are versatile by the introduction of heteroatoms.^{30,31} These factors make dramatic changes in the types of mesophases and the phase transition temperatures in the heterocyclic liquid crystalline materials.

Dipole-dipole interactions and structural shapes are the fundamental elements in the design of liquid crystals.³² However, the role of the polar units in the generation of liquid crystalline phases still needs to be explored in novel heterocyclic systems. It is due to the polar substituents are highly variable, and its attaching sites are also adjustable. Therefore, these benefits allow us to access a wide variety of mesophases simply by changing the polar moieties or their attaching positions.

1,3,4-Oxadiazole-based LC derivatives, which possess asymmetric structures containing the oxadiazole ring in the central position of the mesogenic core, were first proposed by Dimitrowa et al.³³ The introduction of oxadiazole rings can provide not only the lateral dipole from the oxygen and nitrogen atoms, but also the bent shape of the rigid cores. This large lateral dipoles make it possible to exhibit hexagonal columnar phases by using oxadiazole rings as central cores.³⁴ In addition, star-shaped molecules composed of 2,5-diphenyloxadiazole units as rigid arms possess a discotic nematic phase.³⁵ Compounds having both oxadiazole and pyridinium groups may exhibit liquid crystalline properties as well as thermochromic behavior, which shows color change from yellow at room temperature to bright red in the mesophase.³⁶

Choosing terminal moieties is crucial in the generation of specific types of liquid crystalline phases. In this work, a series of 1,3,4-oxadiazole-based liquid crystals with different terminal polar units are synthesized. Their liquid crystalline and photoluminescent

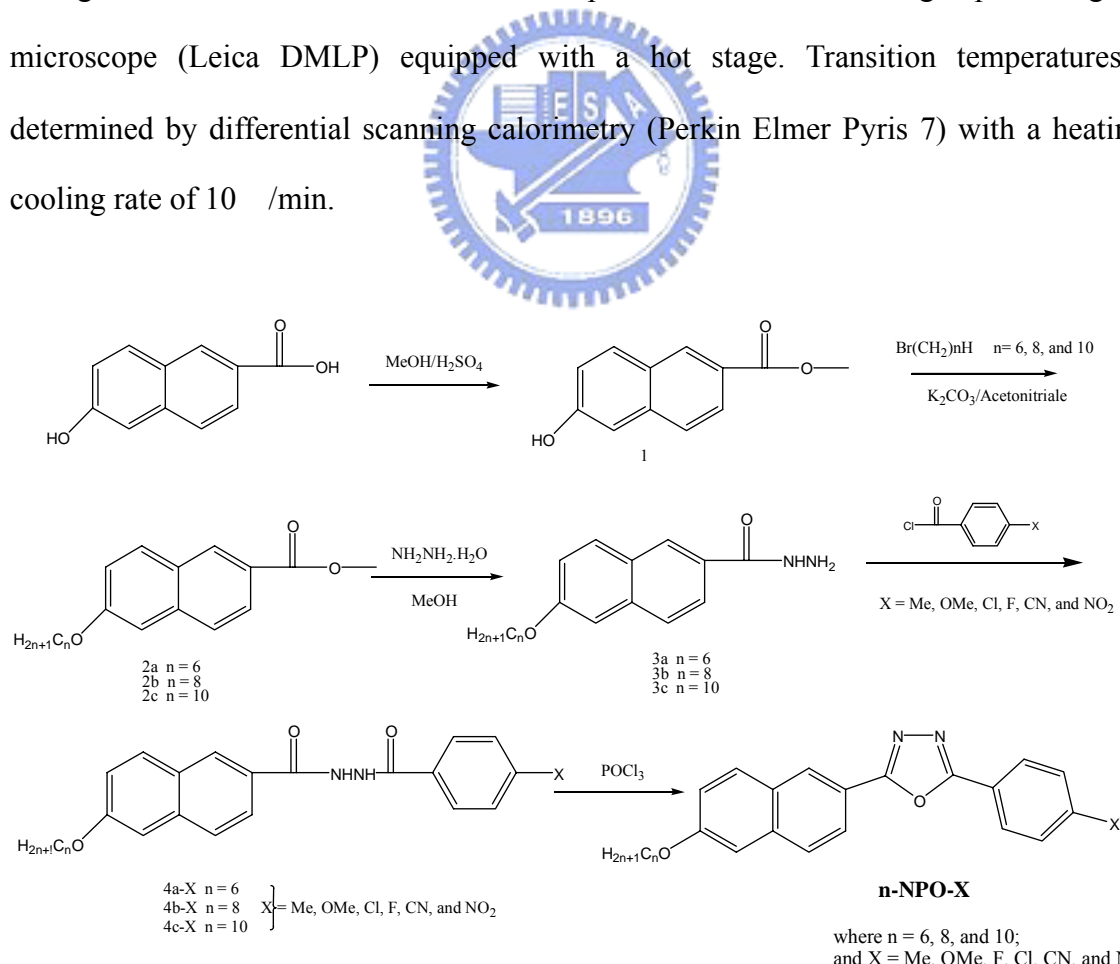
properties with respect to various terminal polarities are also investigated in this study.

2.3 Experimental

2.3.1 Characterization

Chemicals and solvents were reagent grades and purchased from Aldrich, ARCROS, TCI and Lancaster Chemical Co. Pyridine and NMP were distilled to keep anhydrous before use. The other chemicals were used without further purification.

^1H NMR spectra were recorded on a Varian unity 300M Hz spectrometer using CDCl_3 and DMSO-d_6 as solvents. Elemental analyses were performed on a HERAEUS CHN-OS RAPID elemental analyzer. High-resolution electron impact mass data were obtained on a Finnigan-MAT-95XL. The textures of mesophases were studied using a polarizing optical microscope (Leica DMLP) equipped with a hot stage. Transition temperatures were determined by differential scanning calorimetry (Perkin Elmer Pyris 7) with a heating and cooling rate of 10 $^{\circ}\text{C}/\text{min}$.



Scheme 2.1 The synthetic route of 1,3,4-oxadiazole-based materials

2.3.2 Synthesis

The synthetic route of 1,3,4-oxadiazole-based liquid crystalline materials of this study is shown in scheme 2-1. 6-Hydroxy-naphthalene-2-carboxylic acid methyl ester, 1, was prepared using the modification of the procedure described by GÜller *et al.*³⁷ The compounds of 2a-c were obtained by O-alkylation of 6-Hydroxy-naphthalene-2-carboxylic acid methyl ester (1) with appropriate n-alkyl bromides, according to the procedure reported in references.³⁸ The synthetic procedures and chemical analyses of each products are described sequentially as follows:

6-Octyloxy-naphthalene-2-carboxylic acid methyl ester (2b)

Yield: 95%. ¹H NMR (ppm, CDCl₃): 0.89 (t, -CH₃, 3H), 1.30-1.88 (m, -CH₂, 12H), 3.95 (s, -OCH₃, 3H), 4.08 (t, -OCH₂, 2H), 7.13 (s, -C₁₀H₆, 1H), 7.17 (d, *J* = 9 Hz, -C₁₀H₆, 1H), 7.72 (d, *J* = 8.7 Hz, -C₁₀H₆, 1H), 7.81 (d, *J* = 9 Hz, -C₁₀H₆, 1H), 8.00 (d, *J* = 8.4 Hz, -C₁₀H₆, 1H), 8.51 (s, -C₁₀H₆, 1H).

6-Hexyloxy-naphthalene-2-carboxylic acid hydrazide (3a)

A mixture of 2.23 g (7.78 mmol) of 6-hexyloxy-naphthalene-2-carboxylic acid methyl ester and 3.90 g (77.8 mmol) of hydrazine monohydrate were dissolved in methanol. The reaction mixture was refluxed for 24 h. After cooling, the product was poured into water and recrystallized from methanol. Yield: 83%. ¹H NMR (ppm, DMSO-d₆): 0.88 (t, -CH₃, 3H), 1.22-1.79 (m, -CH₂, 8H), 4.09 (t, -OCH₂, 2H), 4.50 (s, -NH₂, 2H), 7.18 (d, *J* = 9 Hz, -C₁₀H₆, 1H), 7.34 (s, -C₁₀H₆, 1H), 7.80-7.90 (m, -C₁₀H₆, 3H), 8.33 (s, -C₁₀H₆, 1H), 9.81 (s, -NH, 1H).

6-Octyloxy-naphthalene-2-carboxylic acid hydrazide (3b)

Yield: 79%. ¹H NMR (ppm, DMSO-d₆): 0.85 (t, -CH₃, 3H), 1.25-1.79 (m, -CH₂, 12H), 4.08 (t, -OCH₂, 2H), 4.52 (s, -NH₂, 2H), 7.17 (d, *J* = 9 Hz, -C₁₀H₆, 1H), 7.33 (s, -C₁₀H₆, 1H), 7.79-7.90 (m, -C₁₀H₆, 3H), 8.33 (s, -C₁₀H₆, 1H), 9.80 (s, -NH, 1H).

6-Decyloxy-naphthalene-2-carboxylic acid hydrazide (3c)

Yield: 82%. ^1H NMR (ppm, DMSO-d₆): 0.84 (t, -CH₃, 3H), 1.24-1.79 (m, -CH₂, 16H), 4.08 (t, -OCH₂, 2H), 4.51 (s, -NH₂, 2H), 7.18 (d, J = 9 Hz, -C₁₀H₆, 1H), 7.34 (s, -C₁₀H₆, 1H), 7.83-7.90 (m, -C₁₀H₆, 3H), 8.33 (s, -C₁₀H₆, 1H), 9.82 (s, -NH, 1H).

4-Methyl-benzoic acid N'-(6-hexyloxy-naphthalene-2-carbonyl)-hydrazide (4a-CH₃)

0.5 g (3.23 mmol) of 4-methyl-benzoyl chloride was added into a solution containing 0.93 g (3.23 mmol) of 6-hexyloxy-naphthalene-2-carboxylic acid hydrazide and 0.26 g (3.23 mmol) of pyridine in 10 ml of NMP. The reaction mixture was stirred for 12 h and then poured into water. The product was filtered and crystallized from methanol. Yield: 70%. ^1H NMR (ppm, DMSO-d₆): 0.83 (t, -CH₃, 3H), 1.21-1.80 (m, -CH₂, 8H), 2.38 (s, -CH₃, 3H), 4.10 (t, -OCH₂, 2H), 7.21 (d, J = 9 Hz, -C₁₀H₆, 1H), 7.31 (d, J = 8.1 Hz, -C₆H₄, 2H), 7.39 (s, -C₁₀H₆, 1H), 7.83-7.95 (m, -C₁₀H₆ and -C₆H₄, 5H), 8.45 (s, -C₁₀H₆, 1H), 10.45 (s, -NH, 1H), 10.52 (s, -NH, 1H).

4-Methyl-benzoic acid N'-(6-octyloxy-naphthalene-2-carbonyl)-hydrazide (4b-CH₃)

Yield: 69%. ^1H NMR (ppm, DMSO-d₆): 0.83 (t, -CH₃, 3H), 1.21-1.80 (m, -CH₂, 12H), 3.38 (s, -CH₃, 3H), 4.11 (t, -OCH₂, 2H), 7.22 (d, J = 9 Hz, -C₁₀H₆, 1H), 7.31 (d, J = 8.4, -C₆H₄, 2H), 7.39 (s, -C₁₀H₆, 1H), 7.83-7.96 (m, -C₁₀H₆ and -C₆H₄, 5H), 8.46 (s, -C₁₀H₆, 1H), 10.46 (s, -NH, 1H), 10.52 (s, -NH, 1H).

4-Methyl-benzoic acid N'-(6-decyloxy-naphthalene-2-carbonyl)-hydrazide (4c-CH₃)

Yield: 79%. ^1H NMR (ppm, DMSO-d₆): 0.84 (t, -CH₃, 3H), 1.24-1.78 (m, -CH₂, 16H), 2.38 (s, -CH₃, 3H), 4.11 (t, -OCH₂, 2H), 7.22 (d, J = 9 Hz, -C₁₀H₆, 1H), 7.31 (d, J = 7.8 Hz, -C₆H₄, 2H), 7.39 (s, -C₁₀H₆, 1H), 7.83-7.97 (m, -C₁₀H₆ and -C₆H₄, 5H), 8.46 (s, -C₁₀H₆, 1H), 10.47 (s, -NH, 1H), 10.52 (s, -NH, 1H).

4-Methoxy-benzoic acid N'-(6-hexyloxy-naphthalene-2-carbonyl)-hydrazide (4a-OMe)

Yield: 90%. ^1H NMR (ppm, DMSO-d₆): 0.88 (t, -CH₃, 3H), 1.21-1.81 (m, -CH₂, 8H), 3.87 (s, -OCH₃, 3H), 4.11 (t, -OCH₂, 2H), 7.17 (d, J = 8.7 Hz, -C₆H₄, 2H), 7.25 (d, J = 8.7 Hz, -C₁₀H₆, 1H), 7.42 (s, -C₁₀H₆, 1H), 7.79-8.11 (m, -C₁₀H₆ and -C₆H₄, 5H), 8.63 (s, -C₁₀H₆, 1H),

10.39 (d, -NH, 2H).

4-Methoxy-benzoic acid N'-(6-octyloxy-naphthalene-2-carbonyl)-hydrazide (4b-OMe)

Yield: 85%. ^1H NMR (ppm, DMSO-d₆): 0.86 (t, -CH₃, 3H), 1.22-1.81 (m, -CH₂, 12H), 3.83 (s, -OCH₃, 3H), 4.11 (t, -OCH₂, 2H), 7.04 (d, J = 8.7 Hz, -C₆H₄, 2H), 7.21 (d, J = 9 Hz, -C₁₀H₆, 1H), 7.39 (s, -C₁₀H₆, 1H), 7.90-7.96 (m, -C₁₀H₆ and -C₆H₄, 5H), 8.46 (s, -C₁₀H₆, 1H), 10.39 (d, -NH, 2H).

4-Methoxy-benzoic acid N'-(6-decyloxy-naphthalene-2-carbonyl)-hydrazide (4c-OMe)

Yield: 82%. ^1H NMR (ppm, DMSO-d₆): 0.86 (t, -CH₃, 3H), 1.24-1.77 (m, -CH₂, 16H), 3.82 (s, -OCH₃, 3H), 4.10 (t, -OCH₂, 2H), 7.04 (d, J = 8.7 Hz, -C₆H₄, 2H), 7.21 (d, J = 9.3 Hz, -C₁₀H₆, 1H), 7.39 (s, -C₁₀H₆, 1H), 7.90-7.93 (m, -C₁₀H₆ and -C₆H₄, 5H), 8.45 (s, -C₁₀H₆, 1H), 10.39 (d, -NH, 2H).

4-Fluoro-benzoic acid N'-(6-hexyloxy-naphthalene-2-carbonyl)-hydrazide (4a-F)

Yield: 77%. ^1H NMR (ppm, DMSO-d₆): 0.88 (t, -CH₃, 3H), 1.23-1.81 (m, -CH₂, 8H), 4.11 (t, -OCH₂, 2H), 7.22 (d, J = 9 Hz, -C₁₀H₆, 1H), 7.34 (s, -C₁₀H₆, 1H), 7.37 (d, J = 8.7 Hz, -C₆H₄, 2H), 7.87-8.03 (m, -C₁₀H₆ and -C₆H₄, 5H), 8.46 (s, -C₁₀H₆, 1H), 10.58 (s, -NH, 2H).

4-Fluoro-benzoic acid N'-(6-octyloxy-naphthalene-2-carbonyl)-hydrazide (4b-F)

Yield: 72%. ^1H NMR (ppm, DMSO-d₆): 0.85 (t, -CH₃, 3H), 1.26-1.80 (m, -CH₂, 12H), 4.11 (t, -OCH₂, 2H), 7.22 (d, J = 9 Hz, -C₁₀H₆, 1H), 7.34 (s, -C₁₀H₆, 1H), 7.37 (d, J = 8.7 Hz, -C₆H₄, 2H), 7.88-8.04 (m, -C₁₀H₆ and -C₆H₄, 5H), 8.46 (s, -C₁₀H₆, 1H), 10.58 (s, -NH, 2H).

4-Fluoro-benzoic acid N'-(6-decyloxy-naphthalene-2-carbonyl)-hydrazide (4c-F)

Yield: 72%. ^1H NMR (ppm, DMSO-d₆): 0.85 (t, -CH₃, 3H), 1.24-1.80 (m, -CH₂, 16H), 4.11 (t, -OCH₂, 2H), 7.22 (d, J = 9 Hz, -C₁₀H₆, 1H), 7.34 (s, -C₁₀H₆, 1H), 7.37 (d, J = 9 Hz, -C₆H₄, 2H), 7.87-8.04 (m, -C₁₀H₆ and -C₆H₄, 5H), 8.46 (s, -C₁₀H₆, 1H), 10.55 (s, -NH, 2H).

4-Chloro-benzoic acid N'-(6-hexyloxy-naphthalene-2-carbonyl)-hydrazide (4a-Cl)

Yield: 80%. ^1H NMR (ppm, DMSO-d₆): 0.88 (t, -CH₃, 3H), 1.23-1.81 (m, -CH₂, 8H), 4.11 (t, -OCH₂, 2H), 7.22 (d, J = 9 Hz, -C₁₀H₆, 1H), 7.39 (s, -C₁₀H₆, 1H), 7.60 (d, J = 8.7 Hz,

-C₆H₄, 2H), 7.88-7.97 (m, -C₁₀H₆ and -C₆H₄, 5H), 8.46 (s, -C₁₀H₆, 1H), 10.60 (s, -NH, 1H), 10.64 (s, -NH, 1H).

4-Chloro-benzoic acid N'-(6-octyloxy-naphthalene-2-carbonyl)-hydrazide (4b-Cl)

Yield: 83%. ¹H NMR (ppm, DMSO-d₆): 0.86 (t, -CH₃, 3H), 1.26-1.81 (m, -CH₂, 12H), 4.11 (t, -OCH₂, 2H), 7.22 (d, *J* = 9 Hz, -C₁₀H₆, 1H), 7.39 (s, -C₁₀H₆, 1H), 7.60 (d, *J* = 8.7 Hz, -C₆H₄, 2H), 7.88-7.97 (m, -C₁₀H₆ and -C₆H₄, 5H), 8.46 (s, -C₁₀H₆, 1H), 10.62 (s, -NH, 1H), 10.64 (s, -NH, 1H).

4-Chloro-benzoic acid N'-(6-decyloxy-naphthalene-2-carbonyl)-hydrazide (4c-Cl)

Yield: 79%. ¹H NMR (ppm, DMSO-d₆): 0.84 (t, -CH₃, 3H), 1.24-1.80 (m, -CH₂, 16H), 4.11 (t, -OCH₂, 2H), 7.21 (d, *J* = 9 Hz, -C₁₀H₆, 1H), 7.38 (s, -C₁₀H₆, 1H), 7.60 (d, *J* = 8.4 Hz, -C₆H₄, 2H), 7.87-7.97 (m, -C₁₀H₆ and -C₆H₄, 5H), 8.46 (s, -C₁₀H₆, 1H), 10.58 (s, -NH, 1H), 10.62 (s, -NH, 1H).

4-Cyano-benzoic acid N'-(6-hexyloxy-naphthalene-2-carbonyl)-hydrazide (4a-CN)

Yield: 77%. ¹H NMR (ppm, DMSO-d₆): 0.86 (t, -CH₃, 3H), 1.26-1.81 (m, -CH₂, 8H), 4.11 (t, -OCH₂, 2H), 7.22 (d, *J* = 9 Hz, -C₁₀H₆, 1H), 7.40 (s, -C₁₀H, 1H), 7.88-7.97 (m, -C₁₀H₆ and -C₆H₄, 3H), 8.02-8.10 (m, -C₁₀H₆ and -C₆H₄, 4H), 8.46 (s, -C₁₀H₆, 1H), 10.67 (s, -NH, 1H), 10.82 (s, -NH, 1H).

4-Cyano-benzoic acid N'-(6-octyloxy-naphthalene-2-carbonyl)-hydrazide (4b-CN)

Yield: 68%. ¹H NMR (ppm, DMSO-d₆): 0.84 (t, -CH₃, 3H), 1.26-1.81 (m, -CH₂, 12H), 4.11 (t, -OCH₂, 2H), 7.22 (d, *J* = 9 Hz, -C₁₀H₆, 1H), 7.39 (s, -C₁₀H, 1H), 7.91-7.97 (m, -C₁₀H₆ and -C₆H₄, 3H), 8.02-8.10 (m, -C₁₀H₆ and -C₆H₄, 4H), 8.46 (s, -C₁₀H₆, 1H), 10.67 (s, -NH, 1H), 10.82 (s, -NH, 1H).

4-Cyano-benzoic acid N'-(6-decyloxy-naphthalene-2-carbonyl)-hydrazide (4c-CN)

Yield: 68%. ¹H NMR (ppm, DMSO-d₆): 0.82 (t, -CH₃, 3H), 1.24-1.80 (m, -CH₂, 16H), 4.11 (t, -OCH₂, 2H), 7.22 (d, *J* = 9 Hz, -C₁₀H₆, 1H), 7.39 (s, -C₁₀H, 1H), 7.88-7.97 (m, -C₁₀H₆ and -C₆H₄, 3H), 8.02-8.10 (m, -C₁₀H₆ and -C₆H₄, 4H), 8.46 (s, -C₁₀H₆, 1H), 10.68 (d,

-NH, 2H).

4-Nitro-benzoic acid N'-(6-hexyloxy-naphthalene-2-carbonyl)-hydrazide (4a-NO₂)

Yield: 77%. ¹H NMR (ppm, DMSO-d₆): 0.88 (t, -CH₃, 3H), 1.22-1.81 (m, -CH₂, 8H), 4.11 (t, -OCH₂, 2H), 7.22 (d, *J* = 9 Hz, -C₁₀H₆, 1H), 7.41 (d, -C₁₀H, 1H), 7.88-7.97 (m, -C₁₀H₆, 3H), 8.15 (d, *J* = 9 Hz, -C₆H₄, 2H), 8.39 (d, *J* = 9 Hz, -C₆H₄, 2H), 8.47 (s, -C₁₀H₆, 1H), 10.70 (s, -NH, 1H), 10.90 (s, -NH, 1H).

4-Nitro-benzoic acid N'-(6-octyloxy-naphthalene-2-carbonyl)-hydrazide (4b-NO₂)

Yield: 83%. ¹H NMR (ppm, DMSO-d₆): 0.85 (t, -CH₃, 3H), 1.22-1.81 (m, -CH₂, 12H), 4.11 (t, -OCH₂, 2H), 7.22 (d, *J* = 8.7 Hz, -C₁₀H₆, 1H), 7.40 (d, -C₁₀H, 1H), 7.88-7.97 (m, -C₁₀H₆, 3H), 8.15 (d, *J* = 9 Hz, -C₆H₄, 2H), 8.37 (d, *J* = 9 Hz, -C₆H₄, 2H), 8.47 (s, -C₁₀H₆, 1H), 10.70 (s, -NH, 1H), 10.91 (s, -NH, 1H).

4-Nitro-benzoic acid N'-(6-decyloxy-naphthalene-2-carbonyl)-hydrazide (4c-NO₂)

Yield: 83%. ¹H NMR (ppm, DMSO-d₆): 0.84 (t, -CH₃, 3H), 1.24-1.81 (m, -CH₂, 16H), 4.11 (t, -OCH₂, 2H), 7.22 (d, *J* = 9 Hz, -C₁₀H₆, 1H), 7.40 (d, -C₁₀H, 1H), 7.88-7.97 (m, -C₁₀H₆, 3H), 8.15 (d, *J* = 8.7 Hz, -C₆H₄, 2H), 8.37 (d, *J* = 9.0 Hz, -C₆H₄, 2H), 8.47 (s, -C₁₀H₆, 1H), 10.69 (s, -NH, 1H), 10.89 (s, -NH, 1H).

2-(6-Hexyloxy-naphthalen-2-yl)-5-p-tolyl-[1,3,4]oxadiazole (6-NPO-CH₃)

0.8 g (2.07 mmol) of 4-methyl-benzoic acid N'-(6-hexyloxy-naphthalene-2-carbonyl)-hydrazide was dissolved in 10 ml of POCl₃. The reaction mixture was heated to 130 overnight, and then cooled to room temperature. Most of POCl₃ in reaction mixture was removed at reduced pressure and poured into water. The product was filtered and crystallized from methanol and chloroform several times to get a white solid; yield 42%. ¹H NMR (ppm, CDCl₃): 0.93 (t, -CH₃, 3H), 1.26-1.90 (m, -CH₂, 8H), 2.46 (s, -CH₃, 3H), 4.11 (t, -OCH₂, 2H), 7.17 (s, -C₁₀H₆, 1H), 7.21 (d, *J* = 8.7 Hz, -C₁₀H₆, 1H), 7.34 (d, *J* = 7.8 Hz, -C₆H₄, 2H), 7.83 (d, *J* = 8.4 Hz, -C₁₀H₆, 2H), 7.85 (d, *J* = 8.4 Hz, -C₁₀H₆, 1H), 8.05 (d, *J* = 8.4 Hz, -C₆H₄, 2H), 8.14 (d, *J* = 8.4 Hz, -C₁₀H₆, 1H), 8.53 (s, -C₁₀H₆, 1H). Anal: calc. for C₂₅H₂₆N₂O₂ C 77.69, H

6.78, N 7.25%; found C 77.98, H 6.80, N 6.85%. HRMS (EI) calc. 386.1994; found 386.1986.

2-(6-Octyloxy-naphthalen-2-yl)-5-p-tolyl-[1,3,4]oxadiazole (8-NPO-CH₃)

White solid; yield 36%. ¹H NMR (ppm, CDCl₃): 0.93 (t, -CH₃, 3H), 1.26-1.90 (m, -CH₂, 12H), 2.46 (s, -CH₃, 3H), 4.11 (t, -OCH₂, 2H), 7.17 (s, -C₁₀H₆, 1H), 7.21 (d, *J* = 8.7 Hz, -C₁₀H₆, 1H), 7.34 (d, *J* = 7.8 Hz, -C₆H₄, 2H), 7.83 (d, *J* = 8.4 Hz, -C₁₀H₆, 1H), 7.85 (d, *J* = 8.4 Hz, -C₁₀H₆, 1H), 8.06 (d, *J* = 8.4 Hz, -C₆H₄, 2H), 8.14 (d, *J* = 8.4 Hz, -C₁₀H₆, 1H), 8.53 (s, -C₁₀H₆, 1H). Anal: calc. for C₂₇H₃₀N₂O₂ C 78.23, H 7.29, N 6.76%; found C 78.46, H 7.41, N 6.65%. HRMS (EI) calc. 414.2307; found 414.2312.

2-(6-Decyloxy-naphthalen-2-yl)-5-p-tolyl-[1,3,4]oxadiazole (10-NPO-CH₃)

White solid; yield 53%. ¹H NMR (ppm, CDCl₃): 0.86 (t, -CH₃, 3H), 1.29-1.90 (m, -CH₂, 16H), 2.46 (s, -CH₃, 3H), 4.11 (t, -OCH₂, 2H), 7.17 (s, -C₁₀H₆, 1H), 7.21 (d, *J* = 9.3 Hz, -C₁₀H₆, 1H), 7.34 (d, *J* = 8.4 Hz, -C₆H₄, 2H), 7.82 (d, *J* = 8.7 Hz, -C₁₀H₆, 1H), 7.85 (d, *J* = 8.4 Hz, -C₁₀H₆, 1H), 8.06 (d, *J* = 8.4 Hz, -C₆H₄, 2H), 8.14 (d, *J* = 9 Hz, -C₁₀H₆, 1H), 8.53 (s, -C₁₀H₆, 1H). Anal: calc. for C₂₉H₃₄N₂O₂ C 78.70, H 7.74, N 6.33%; found C 78.64, H 7.64, N 6.51%. HRMS (EI) calc. 442.2620; found 442.2617.

2-(6-Hexyloxy-naphthalen-2-yl)-5-(4-methoxy-phenyl)-[1,3,4]oxadiazole

(6-NPO-OMe)

White solid; yield 45%. ¹H NMR (ppm, CDCl₃): 0.90 (t, -CH₃, 3H), 1.30-1.90 (m, -CH₂, 8H), 3.91 (s, -OCH₃, 3H), 4.11 (t, -OCH₂, 2H), 7.04 (d, *J* = 9 Hz, -C₆H₄, 2H), 7.17 (s, -C₁₀H₆, 1H), 7.21 (d, *J* = 9 Hz, -C₁₀H₆, 1H), 7.82 (d, *J* = 8.4 Hz, -C₁₀H₆, 1H), 7.85 (d, *J* = 8.4 Hz, -C₁₀H₆, 1H), 8.10-8.17 (m, -C₆H₄ and -C₁₀H₆, 3H), 8.52 (s, -C₁₀H₆, 1H). Anal: calc. for C₂₅H₂₆N₂O₃ C 74.60, H 6.51, N 6.96%; found C 74.27, H 6.55, N 6.80%. HRMS (EI) calc. 402.1943; found 402.1946.

2-(6-Methoxy-phenyl)-5-(6-octyloxy-naphthalen-2-yl)-[1,3,4]oxadiazole (8-NPO-OMe)

White solid; yield 51%. ¹H NMR (ppm, CDCl₃): 0.90 (t, -CH₃, 3H), 1.30-1.90 (m, -CH₂,

12H), 3.91 (s, -OCH₃, 3H), 4.11 (t, -OCH₂, 2H), 7.03 (d, *J* = 9 Hz, -C₆H₄, 2H), 7.16 (s, -C₁₀H₆, 1H), 7.21 (d, *J* = 8.7 Hz, -C₆H₄, 2H), 7.82 (d, *J* = 8.1 Hz, -C₁₀H₆, 1H), 7.85 (d, *J* = 8.1 Hz, -C₁₀H₆, 1H), 8.10-8.17 (m, -C₆H₄ and -C₁₀H₆, 3H), 8.51 (s, -C₁₀H₆, 1H). Anal: calc. for C₂₇H₃₀N₂O₃ C 75.32, H 7.02, N 6.51%; found C 75.15, H 6.45, N 7.16%. HRMS (EI) calc. 430.2256; found 430.2248.

2-(6-Decyloxy-naphthalen-2-yl)-5-(4-methoxy-phenyl)-[1,3,4]oxadiazole (10-NPO-OMe)

White solid; yield 52%. ¹H NMR (ppm, CDCl₃): 0.89 (t, -CH₃, 3H), 1.28-1.90 (m, -CH₂, 16H), 3.91 (s, -OCH₃, 3H), 4.11 (t, -OCH₂, 2H), 7.04 (d, *J* = 9.3 Hz, -C₆H₄, 2H), 7.16 (s, -C₁₀H₆, 1H), 7.21 (d, *J* = 9 Hz, -C₆H₄, 2H), 7.82 (d, *J* = 8.4 Hz, -C₁₀H₆, 1H), 7.85 (d, *J* = 8.4 Hz, -C₁₀H₆, 1H), 8.11-8.17 (m, -C₆H₄ and -C₁₀H₆, 3H), 8.52 (s, -C₁₀H₆, 1H). Anal: calc. for C₂₉H₃₄N₂O₃ C 75.95, H 7.47, N 6.11%; found C 76.10, H 7.22, N 5.89%. HRMS (EI) calc. 458.2569; found 458.2574.

2-(4-Fluoro-phenyl)-5-(6-hexyloxy-naphthalen-2-yl)-[1,3,4]oxadiazole (6-NPO-F)

White solid; yield 87%. ¹H NMR (ppm, CDCl₃): 0.93 (t, -CH₃, 3H), 1.24-1.90 (m, -CH₂, 8H), 4.11 (t, -OCH₂, 2H), 7.18-7.28 (m, -C₁₀H₆ and -C₆H₄, 4H), 7.83 (d, *J* = 8.7 Hz, -C₁₀H₆, 1H), 7.85 (d, *J* = 9 Hz, -C₁₀H₆, 1H), 8.13-8.22 (m, -C₆H₄ and -C₁₀H₆, 3H), 8.53 (s, -C₁₀H₆, 1H). Anal: calc. for C₂₄H₂₃N₂O₂ C 73.83, H 5.94, N 7.17%; found C 73.78, H 6.23, N 7.50%. HRMS (EI) calc. 390.1744; found 390.1740.

2-(4-Fluoro-phenyl)-5-(6-octyloxy-naphthalen-2-yl)-[1,3,4]oxadiazole (8-NPO-F)

White solid; yield 81%. ¹H NMR (ppm, CDCl₃): 0.90 (t, -CH₃, 3H), 1.31-1.90 (m, -CH₂, 12H), 4.11 (t, -OCH₂, 2H), 7.17-7.28 (m, -C₁₀H₆ and -C₆H₄, 4H), 7.83 (d, *J* = 8.7 Hz, -C₁₀H₆, 1H), 7.85 (d, *J* = 8.7 Hz, -C₁₀H₆, 1H), 8.13-8.22 (m, -C₆H₄ and -C₁₀H₆, 3H), 8.52 (s, -C₁₀H₆, 1H). Anal: calc. for C₂₆H₂₇FN₂O₂ C 74.62, H 6.50, N 6.69%; found C 74.22, H 6.57, N 6.55%. HRMS (EI) calc. 418.2057; found 418.2055.

2-(6-Decyloxy-naphthalen-2-yl)-5-(4-fluoro-phenyl)-[1,3,4]oxadiazole (10-NPO-F)

White solid; yield 87%. ^1H NMR (ppm, CDCl_3): 0.88 (t, $-\text{CH}_3$, 3H), 1.26-1.87 (m, $-\text{CH}_2$, 16H), 4.11 (t, $-\text{OCH}_2$, 2H), 7.17-7.28 (m, $-\text{C}_{10}\text{H}_6$ and $-\text{C}_6\text{H}_4$, 4H), 7.84 (d, $J = 8.4$ Hz, $-\text{C}_{10}\text{H}_6$, 1H), 7.85 (d, $J = 9$ Hz, $-\text{C}_{10}\text{H}_6$, 1H), 8.14-8.23 (m, $-\text{C}_6\text{H}_4$ and $-\text{C}_{10}\text{H}_6$, 3H), 8.52 (s, $-\text{C}_{10}\text{H}_6$, 1H). Anal: calc. for $\text{C}_{28}\text{H}_{31}\text{FN}_2\text{O}_2$ C 75.31, H 7.00, N 6.27%; found C 75.58, H 7.18, N 6.09%. HRMS (EI) calc. 446.2370; found 446.2377.

2-(4-Chloro-phenyl)-5-(6-hexyloxy-naphthalen-2-yl)-[1,3,4]oxadiazole (6-NPO-Cl)

White solid; yield 68%. ^1H NMR (ppm, CDCl_3): 0.88 (t, $-\text{CH}_3$, 3H), 1.25-1.90 (m, $-\text{CH}_2$, 8H), 4.07 (t, $-\text{OCH}_2$, 2H), 7.12 (s, $-\text{C}_{10}\text{H}_6$, 1H), 7.18 (d, $J = 9$ Hz, $-\text{C}_{10}\text{H}_6$, 1H), 7.49 (d, $J = 8.4$ Hz, $-\text{C}_6\text{H}_4$, 2H), 7.78 (d, $J = 8.1$ Hz, $-\text{C}_{10}\text{H}_6$, 1H), 7.84 (d, $J = 8.4$ Hz, $-\text{C}_{10}\text{H}_6$, 1H), 8.06-8.11 (m, $-\text{C}_{10}\text{H}_6$ and $-\text{C}_6\text{H}_4$, 3H), 8.46 (s, $-\text{C}_{10}\text{H}_6$, 1H). Anal: calc. for $\text{C}_{24}\text{H}_{23}\text{ClN}_2\text{O}_2$ C 70.84, H 5.70, N 6.88%; found C 70.97, H 5.74, N 6.77%. HRMS (EI) calc. 406.1448; found 406.1441.

2-(4-Chloro-phenyl)-5-(6-octyloxy-naphthalen-2-yl)-[1,3,4]oxadiazole (8-NPO-Cl)

White solid; yield 72%. ^1H NMR (ppm, CDCl_3): 0.90 (t, $-\text{CH}_3$, 3H), 1.33-1.91 (m, $-\text{CH}_2$, 12H), 4.09 (t, $-\text{OCH}_2$, 2H), 7.15 (s, $-\text{C}_{10}\text{H}_6$, 1H), 7.21 (d, $J = 8.7$ Hz, $-\text{C}_{10}\text{H}_6$, 1H), 7.51 (d, $J = 8.1$ Hz, $-\text{C}_6\text{H}_4$, 2H), 7.81 (d, $J = 8.1$ Hz, $-\text{C}_{10}\text{H}_6$, 1H), 7.84 (d, $J = 8.4$ Hz, $-\text{C}_{10}\text{H}_6$, 1H), 8.09-8.14 (m, $-\text{C}_{10}\text{H}_6$ and $-\text{C}_6\text{H}_4$, 3H), 8.50 (s, $-\text{C}_{10}\text{H}_6$, 1H). Anal: calc. for $\text{C}_{26}\text{H}_{27}\text{ClN}_2\text{O}_2$ C 71.80, H 6.26, N 6.44%; found C 71.46, H 6.33, N 6.29%. HRMS (EI) calc. 434.1761; found 434.1767.

2-(4-Chloro-phenyl)-5-(6-decyloxy-naphthalen-2-yl)-[1,3,4]oxadiazole (10-NPO-Cl)

White solid; yield 60%. ^1H NMR (ppm, CDCl_3): 0.89 (t, $-\text{CH}_3$, 3H), 1.25-1.89 (m, $-\text{CH}_2$, 16H), 4.10 (t, $-\text{OCH}_2$, 2H), 7.15 (s, $-\text{C}_{10}\text{H}_6$, 1H), 7.21 (d, $J = 8.7$ Hz, $-\text{C}_{10}\text{H}_6$, 1H), 7.51 (d, $J = 8.7$ Hz, $-\text{C}_6\text{H}_4$, 2H), 7.81 (d, $J = 8.1$ Hz, $-\text{C}_{10}\text{H}_6$, 1H), 7.84 (d, $J = 8.4$ Hz, $-\text{C}_{10}\text{H}_6$, 1H), 8.09-8.15 (m, $-\text{C}_{10}\text{H}_6$ and $-\text{C}_6\text{H}_4$, 3H), 8.51 (s, $-\text{C}_{10}\text{H}_6$, 1H). Anal: calc. for $\text{C}_{28}\text{H}_{31}\text{ClN}_2\text{O}_2$ C 72.63, H 6.75, N 6.05%; found C 72.76, H 6.87, N 5.90%. HRMS (EI) calc. 462.2074; found 462.2073.

4-[5-(6-Hexyloxy-naphthalen-2-yl)-[1,3,4]oxadiazol-2-yl]-benzonitrile (6-NPO-CN)

White solid; yield 52%. ^1H NMR (ppm, CDCl_3): 0.93 (t, $-\text{CH}_3$, 3H), 1.22-1.90 (m, $-\text{CH}_2$, 8H), 4.11 (t, $-\text{OCH}_2$, 2H), 7.18 (s, $-\text{C}_{10}\text{H}_6$, 1H), 7.23 (d, $J = 8.7$ Hz, $-\text{C}_{10}\text{H}_6$, 1H), 7.84-7.88 (m, $-\text{C}_{10}\text{H}_6$ and $-\text{C}_6\text{H}_4$, 4H), 8.13 (d, $J = 8.4$ Hz, $-\text{C}_{10}\text{H}_6$, 1H), 8.29 (d, $J = 9$ Hz, $-\text{C}_6\text{H}_4$, 2H), 8.54 (s, $-\text{C}_{10}\text{H}_6$, 1H). Anal: calc. for $\text{C}_{25}\text{H}_{23}\text{N}_3\text{O}_2$ C 75.54, H 5.83, N 10.57%; found C 75.29, H 6.05, N 10.55%. HRMS (EI) calc. 397.1790; found 397.1792.

4-[5-(6-Octyloxy-naphthalen-2-yl)-[1,3,4]oxadiazol-2-yl]-benzonitrile (8-NPO-CN)

White solid; yield 46%. ^1H NMR (ppm, CDCl_3): 0.90 (t, $-\text{CH}_3$, 3H), 1.25-1.89 (m, $-\text{CH}_2$, 12H), 4.09 (t, $-\text{OCH}_2$, 2H), 7.15 (s, $-\text{C}_{10}\text{H}_6$, 1H), 7.21 (d, $J = 9$ Hz, $-\text{C}_{10}\text{H}_6$, 1H), 7.81-7.86 (m, $-\text{C}_{10}\text{H}_6$ and $-\text{C}_6\text{H}_4$, 4H), 8.12 (d, $J = 8.7$ Hz, $-\text{C}_{10}\text{H}_6$, 1H), 8.25 (d, $J = 8.1$ Hz, $-\text{C}_6\text{H}_4$, 2H), 8.50 (s, $-\text{C}_{10}\text{H}_6$, 1H). Anal: calc. for $\text{C}_{27}\text{H}_{27}\text{N}_3\text{O}_2$ C 76.21, H 6.40, N 9.87%; found C 76.21, H 6.46, N 9.70%. HRMS (EI) calc. 425.2103; found 425.2108.

4-[5-(6-Decyloxy-naphthalen-2-yl)-[1,3,4]oxadiazol-2-yl]-benzonitrile (10-NPO-CN)

Light yellow solid; yield 60%. ^1H NMR (ppm, CDCl_3): 0.89 (t, $-\text{CH}_3$, 3H), 1.28-1.90 (m, $-\text{CH}_2$, 16H), 4.11 (t, $-\text{OCH}_2$, 2H), 7.18 (s, $-\text{C}_{10}\text{H}_6$, 1H), 7.23 (d, $-\text{C}_{10}\text{H}_6$, 1H), 7.84-7.88 (m, $-\text{C}_{10}\text{H}_6$ and $-\text{C}_6\text{H}_4$, 4H), 8.13 (d, $J = 8.7$ Hz, $-\text{C}_{10}\text{H}_6$, 1H), 8.28 (d, $J = 8.7$ Hz, $-\text{C}_6\text{H}_4$, 2H), 8.54 (s, $-\text{C}_{10}\text{H}_6$, 1H). Anal: calc. for $\text{C}_{29}\text{H}_{31}\text{N}_3\text{O}_2$ C 76.79, H 6.89, N 93.26%; found C 76.70, H 7.03, N 9.29%. HRMS (EI) calc. 453.2416; found 453.2409.

2-(6-Hexyloxy-naphthalen-2-yl)-5-(4-nitro-phenyl)-[1,3,4]oxadiazole (6-NPO-NO₂)

Yellow solid; yield 70%. ^1H NMR (ppm, CDCl_3): 0.90 (t, $-\text{CH}_3$, 3H), 1.25-1.90 (m, $-\text{CH}_2$, 8H), 4.11 (t, $-\text{OCH}_2$, 2H), 7.18 (s, $-\text{C}_{10}\text{H}_6$, 1H), 7.23 (d, $J = 9$ Hz, $-\text{C}_{10}\text{H}_6$, 1H), 7.85 (d, $J = 8.7$ Hz, $-\text{C}_{10}\text{H}_6$, 1H), 7.86 (d, $J = 8.9$ Hz, $-\text{C}_{10}\text{H}_6$, 1H), 8.14 (d, $J = 8.7$ Hz, $-\text{C}_{10}\text{H}_6$, 1H), 8.35-8.44 (m, $-\text{C}_6\text{H}_4$, 4H), 8.56 (s, $-\text{C}_{10}\text{H}_6$, 1H). Anal: calc. for $\text{C}_{24}\text{H}_{23}\text{N}_3\text{O}_4$ C 69.05, H 5.55, N 10.07%; found C 68.99, H 5.78, N 10.05. HRMS (EI) calc. 417.1689; found 417.1690.

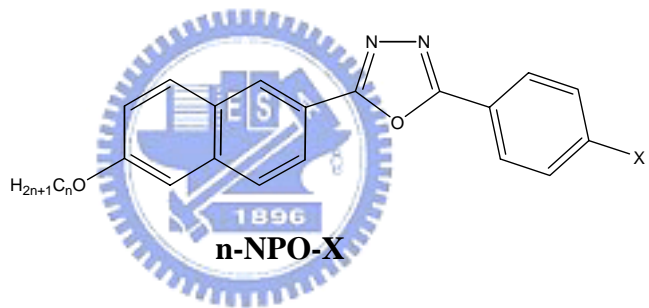
2-(4-Nitro-phenyl)-5-(6-octyloxy-naphthalen-2-yl)-[1,3,4]oxadiazole (8-NPO-NO₂)

Yellow solid; yield 73%. ^1H NMR (ppm, CDCl_3): 0.90 (t, $-\text{CH}_3$, 3H), 1.25-1.92 (m, $-\text{CH}_2$,

12H), 4.12 (t, -OCH₂, 2H), 7.18 (s, -C₁₀H₆, 1H), 7.24 (d, *J* = 8.7 Hz, -C₁₀H₆, 1H), 7.85 (d, *J* = 8.4 Hz, -C₁₀H₆, 1H), 7.87 (d, *J* = 8.7 Hz, -C₁₀H₆, 1H), 8.14 (d, *J* = 8.7 Hz, -C₁₀H₆, 1H), 8.36-8.45 (m, -C₆H₄, 4H), 8.57 (s, -C₁₀H₆, 1H). Anal: calc. for C₂₆H₂₇N₃O₄ C 70.09, H 6.11, N 9.43%; found C 70.38, H 6.20, N 9.05. HRMS (EI) calc. 445.2002; found 445.2004

2-(6-Decyloxy-naphthalen-2-yl)-5-(4-nitro-phenyl)-[1,3,4]oxadiazole (10-NPO-NO₂)

Yellow solid; yield 73%. ¹H NMR (ppm, CDCl₃): 0.88 (t, -CH₃, 3H), 1.28-1.90 (m, -CH₂, 16H), 4.12 (t, -OCH₂, 2H), 7.19 (s, -C₁₀H₆, 1H), 7.24 (d, -C₁₀H₆, 1H), 7.85 (d, *J* = 8.7 Hz, -C₁₀H₆, 1H), 7.87 (d, *J* = 9 Hz, -C₁₀H₆, 1H), 8.15 (d, *J* = 8.7 Hz, -C₁₀H₆, 1H), 8.36-8.45 (m, -C₆H₄, 4H), 8.57 (s, -C₁₀H₆, 1H). Anal: calc. for C₂₈H₃₁N₃O₄ C 71.01, H 6.60, N 8.87%; found C 70.98, H 6.58, N 8.50. HRMS (EI) calc. 473.2315; found 473.2310.



where n = 6, 8, and 10;

and X = Me, OMe, F, Cl, CN, and NO₂

Figure 2.1 Chemical structures of synthesized molecules.

2.4 Results and discussion

2.4.1 Mesophases and thermal properties

Herein a series of 1,3,4-oxadiazole-based liquid crystals containing different polar substituents (figure 2.1) are reported. As previous studies, 2,5-diphenyl-1,3,4-oxadiazole has an exocyclic bond angle ($\sim 134^\circ$) with 3.86 D dipole moment pointed to the oxygen atom of the oxadiazole.³⁹ Therefore, these oxadiazole-based materials also have large exocyclic bond angles and lateral dipole moments.

The phase behavior of these investigated materials is shown in table 2.1. The temperature ranges ($3.1^\circ \text{C} \sim 62.4^\circ \text{C}$) of mesophase are probably influenced by the bending structure of the rigid core, which are originated from the nonlinear 1,3,4-oxadiazole ring, as well as the flexible chain lengths and the polar terminal groups. All compounds with electron-donating terminal groups (-Me and -OMe), i.e. n-NPO-Me and n-NPO-OMe, reveal the nematic (N) phase characterized by the schlieren textures. In contrast, the methoxy-substituted compounds (NPO-OMe) possess a enantiotropic mesophase behavior; however, the methyl-substituted compounds (NPO-Me) display a monotropic nematic phase behavior. Surprisingly, 10-NPO-Me has a focal conic texture indicating a smectic A (SmA) phase, but 10-NPO-OMe has no SmA phase. This might be explained by that the dipole moments of the methoxy group and the oxadiazole unit may be cancelled out due to the opposite directions of their dipoles. This effect is also evidenced by that the isotropization temperatures of n-NPO-Me are higher than those of n-NPO-OMe in their analogues. As it can be seen in figure 2.2, 6-NPO-Me and 6-NPO-OMe both recrystallize before isotropic points. Especially in 6-NPO-OMe, it goes into the N phase at 99.2°C , then part of the domain begins to recrystallize. The N phase becomes isotropic at 112.5°C , and the recrystallized domain melts at 119.5°C . This unusual phenomenon has also been observed in glass-forming liquid crystals.⁴⁰

Table 2.1 Phase behavior of n-NPO-X derivatives^a.

6-NPO-Me	$\begin{array}{c} \text{K} \xrightarrow{112.5 (29.6)} \text{I} \\ \text{K} \xrightarrow{114.8 (-9.5)} \text{K1} \xrightarrow{122.0 (16.7)} \text{I} \\ \text{K} \xleftarrow{86.1 (-24.0)} \text{N} \xleftarrow{106.7 (-0.3)} \text{I} \end{array}$	6-NPO-Cl	$\begin{array}{c} \text{K} \xrightarrow{153.7} \text{SmA} \xrightarrow{156.0} \text{I} \\ \text{K} \xrightarrow{130.3 (-31.5)} \text{SmA} \xrightarrow{153.8 (-4.8)} \text{I} \end{array}$
8-NPO-Me	$\begin{array}{c} \text{K} \xrightarrow{121.7 (29.5)} \text{I} \\ \text{K} \xrightarrow{96.1 (-26.0)} \text{N} \xrightarrow{104.6 (-0.4)} \text{I} \end{array}$	8-NPO-Cl	$\begin{array}{c} \text{K} \xrightarrow{105.1 (4.3)} \text{K1} \xrightarrow{143.1 (35.0)} \text{SmA} \xrightarrow{159.9 (6.1)} \text{I} \\ \text{K} \xrightarrow{100.9 (-4.3)} \text{K1} \xrightarrow{122.4 (-30.0)} \text{SmA} \xrightarrow{157.3 (-6.2)} \text{I} \end{array}$
10-NPO-Me	$\begin{array}{c} \text{K} \xrightarrow{121.0 (32.9)} \text{I} \\ \text{K} \xleftarrow{85.3 (-25.9)} \text{SmA} \xleftarrow{92.9 (-0.6)} \text{N} \xleftarrow{106.7 (-0.6)} \text{I} \end{array}$	10-NPO-Cl	$\begin{array}{c} \text{K} \xrightarrow{88.0 (1.2)} \text{SmE} \xrightarrow{131.6 (26.6)} \text{SmA} \xrightarrow{160.0 (5.5)} \text{I} \\ \text{K} \xrightarrow{85.2 (-1.0)} \text{SmE} \xrightarrow{118.0 (-25.8)} \text{SmA} \xrightarrow{157.5 (-5.6)} \text{I} \end{array}$
6-NPO-OMe	$\begin{array}{c} \text{K} \xrightarrow{91.7 (0.4)} \text{K1} \xrightarrow{99.2 (24.1)} \text{N} \xrightarrow{112.5 (0.1)} \text{I} \\ \text{K} \xrightarrow{107.5 (-14.2)} \text{K2} \xrightarrow{119.5 (18.5)} \text{I} \\ \text{K} \xleftarrow{58.1 (-21.7)} \text{N} \xleftarrow{111.0 (-0.3)} \text{I} \end{array}$	6-NPO-CN	$\begin{array}{c} \text{K} \xrightarrow{130.0 (-1.2)} \text{K1} \xrightarrow{162.7 (30.0)} \text{N} \xrightarrow{167.1 (0.1)} \text{I} \\ \text{K} \xrightarrow{118.4 (-30.4)} \text{N} \xrightarrow{165.5 (-0.3)} \text{I} \end{array}$
8-NPO-OMe	$\begin{array}{c} \text{K} \xrightarrow{109.4 (31.6)} \text{N} \xrightarrow{114.6 (0.2)} \text{I} \\ \text{K} \xleftarrow{79.5 (-26.6)} \text{N} \xleftarrow{113.1 (-0.4)} \text{I} \end{array}$	8-NPO-CN	$\begin{array}{c} \text{K} \xrightarrow{65.5 (9.4)} \text{K1} \xrightarrow{143.3 (26.5)} \text{SmA} \xrightarrow{167.1 (1.8)} \text{I} \\ \text{K} \xrightarrow{42.0 (-8.6)} \text{K1} \xrightarrow{126.4 (-25.8)} \text{SmA} \xrightarrow{165.0 (-1.9)} \text{I} \end{array}$
10-NPO-OMe	$\begin{array}{c} \text{K} \xrightarrow{110.1 (30.9)} \text{N} \xrightarrow{113.2 (0.2)} \text{I} \\ \text{K} \xleftarrow{76.5 (-27.4)} \text{N} \xleftarrow{111.6 (-1.4)} \text{I} \end{array}$	10-NPO-CN	$\begin{array}{c} \text{K} \xrightarrow{89.7 (13.9)} \text{K1} \xrightarrow{132.2 (26.5)} \text{SmA} \xrightarrow{172.5 (3.0)} \text{I} \\ \text{K} \xrightarrow{64.9 (-29.4)} \text{K1} \xrightarrow{118.9 (-26.3)} \text{SmA} \xrightarrow{170.5 (-2.9)} \text{I} \end{array}$
6-NPO-F	$\begin{array}{c} \text{K} \xrightarrow{117.7 (1.9)} \text{K1} \xrightarrow{139.3 (32.1)} \text{I} \\ \text{K} \xrightarrow{99.5 (-1.3)} \text{K1} \xrightarrow{109.7 (-24.5)} \text{SmA} \xrightarrow{128.2 (3.6)} \text{I} \\ \text{K} \xleftarrow{80.5 (3.7)} \text{SmE} \xrightarrow{115.9 (19.5)} \text{SmA} \xrightarrow{134.2 (3.7)} \text{I} \\ \text{K} \xleftarrow{75.6 (-3.4)} \text{SmE} \xrightarrow{96.4 (-19.0)} \text{SmA} \xrightarrow{131.8 (-3.8)} \text{I} \end{array}$	8-NPO-NO ₂	$\begin{array}{c} \text{SmE} \xrightarrow{91.9 (14.1)} \text{SmX} \xrightarrow{143.7 (10.2)} \text{SmA} \xrightarrow{202.6 (4.4)} \text{I} \\ \text{SmE} \xrightarrow{99.9 (-1.5)} \text{SmX} \xrightarrow{139.1 (-10.1)} \text{SmA} \xrightarrow{200.3 (-4.4)} \text{I} \end{array}$
8-NPO-F	$\begin{array}{c} \text{K} \xrightarrow{100.0 (3.6)} \text{SmE} \xrightarrow{127.0 (28.3)} \text{SmA} \xrightarrow{134.9 (4.4)} \text{I} \\ \text{K} \xrightarrow{92.7 (-3.2)} \text{SmE} \xrightarrow{105.9 (-26.7)} \text{SmA} \xrightarrow{132.4 (-4.5)} \text{I} \end{array}$	10-NPO-NO ₂	$\begin{array}{c} \text{K} \xrightarrow{91.0 (19.7)} \text{SmE} \xrightarrow{141.5 (11.2)} \text{SmA} \xrightarrow{203.9 (5.3)} \text{I} \\ \text{K} \xrightarrow{50.0 (-14.9)} \text{SmE} \xrightarrow{137.3 (-11.1)} \text{SmA} \xrightarrow{201.6 (-5.3)} \text{I} \end{array}$
10-NPO-F	$\begin{array}{c} \text{K} \xrightarrow{80.5 (3.7)} \text{SmE} \xrightarrow{115.9 (19.5)} \text{SmA} \xrightarrow{134.2 (3.7)} \text{I} \\ \text{K} \xrightarrow{75.6 (-3.4)} \text{SmE} \xrightarrow{96.4 (-19.0)} \text{SmA} \xrightarrow{131.8 (-3.8)} \text{I} \end{array}$		



^a Transition temperatures () and enthalpies (in parentheses, kJ/mol) were determined by DSC (10 °C/min).

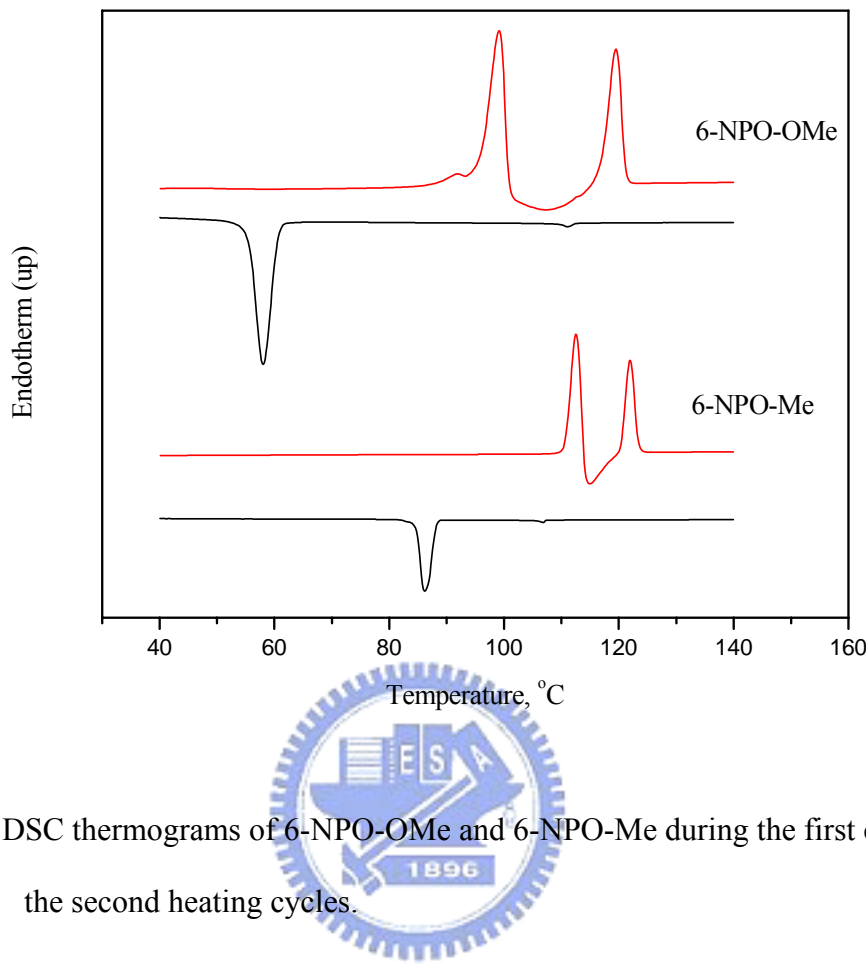


Figure 2.2 DSC thermograms of 6-NPO-OMe and 6-NPO-Me during the first cooling and the second heating cycles.

These LC materials incorporated with strong polar electron-withdrawing terminal groups (F, Cl, CN, and NO_2) exhibit the SmA phase (except 6-NPO-CN). During the cooling process in the polarizing optical microscope (figure 2.3), 10-NPO- NO_2 shows a typical focal-conic texture of the SmA phase at 150 (figure 2.3a), then the mesophase transfers to a paramorphotic arced focal-conic fan texture which is tentatively assigned as the smectic E phase at 130 (figure 2.3b). From literature search it is found that an oxadiazole-based material (2,5-diphenyl-1,3,4-oxadiazole, i.e. structure I in figure 2.4) containing a symmetric core,³³ which is similar to 6-NPO-CN of this report, only possesses a crystalline phase. In comparison with the analogous structure I containing the diphenyl symmetric core, 6-NPO-CN reveals mesomorphic properties owing to the replacement of one phenyl group in

structure I by a naphthalene unit to generate an asymmetric core in 6-NPO-CN. Therefore, the asymmetric cores containing naphthalene units of our molecular design do enhance the formation of liquid crystallinity in this study.

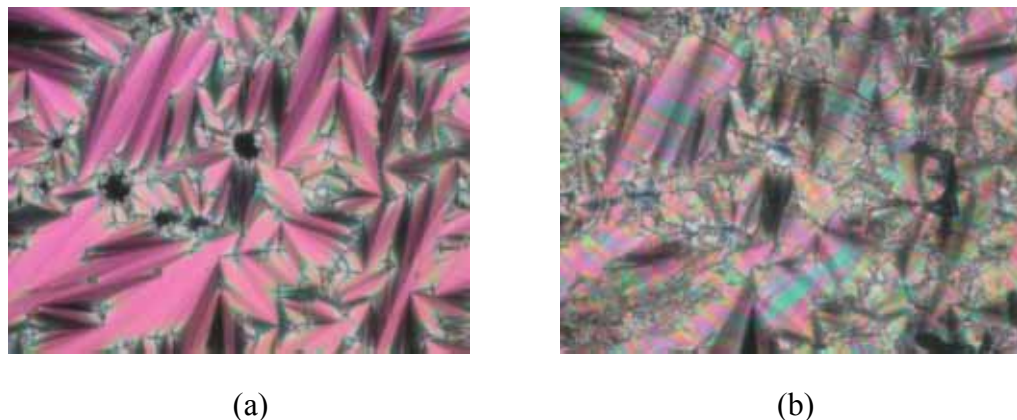


Figure 2.3 Optical textures of compound 10-NPO-NO₂. (a) focal conic texture at 150 (cooling), and (b) the mesophase transfers to paramorphotic arced focal-conic fan texture at 130 (cooling).

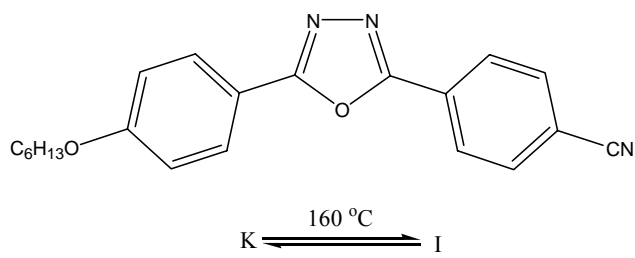
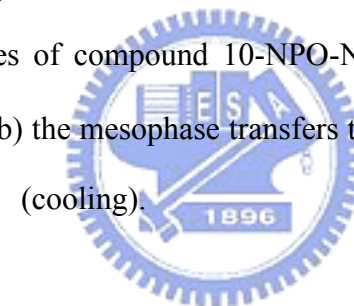


Figure 2.4 Structure I containing a diphenyl symmetric core [10].

Although fluorine has larger electronegativity than chlorine, from the literature,⁴¹ the chloro-substituted system (NPO-Cl) actually generates a larger dipole than the fluoro-substituted system (NPO-F) because of the longer bond from chlorine to carbon. The angular mesogens carrying different terminal groups indeed influence the mesogenic phases and the transition temperatures in 8-NPO-X analogues (see figure 2.5). It shows that both of

the melting temperature and liquid crystallization temperature (on cooling) increase with the terminal dipoles. The clearing temperature and crystallization temperature also have a similar tendency, except the methyl-substituted compound (8-NPO-Me). Another interesting trend is the mesogenic phase range also increases with the terminal dipoles (shown in figure 2.6), especially for the heating procedure, the mesomorphic temperature ranges from 3.1 with methoxy-group (8-NPO-OMe) up to 62.4 with nitro-group (8-NPO-NO₂). From this result, it can be proved that the mesogenic phase ranges of these oxadiazole-based structures can be enlarged by increasing the terminal dipoles, and both of the melting and clearing temperatures can be raised as well.

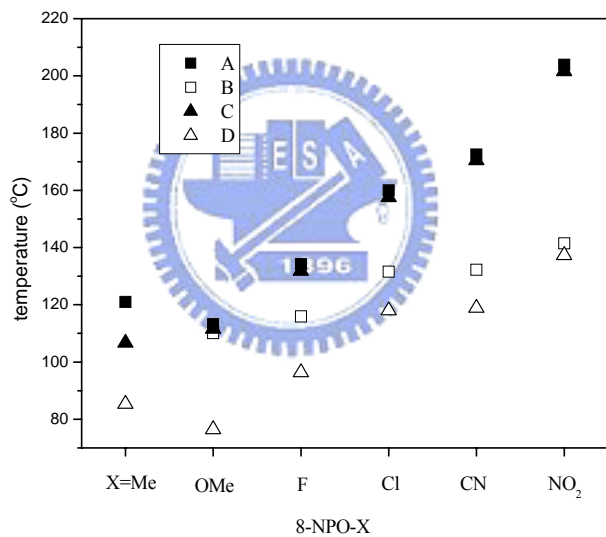


Figure 2.5 The effect of polar substituents on the transition temperatures (dipole increases from left to right). (A) clearing point, (B)melting point, (C) liquid crystallization temperature (on cooling), (D)crystallization temperature.

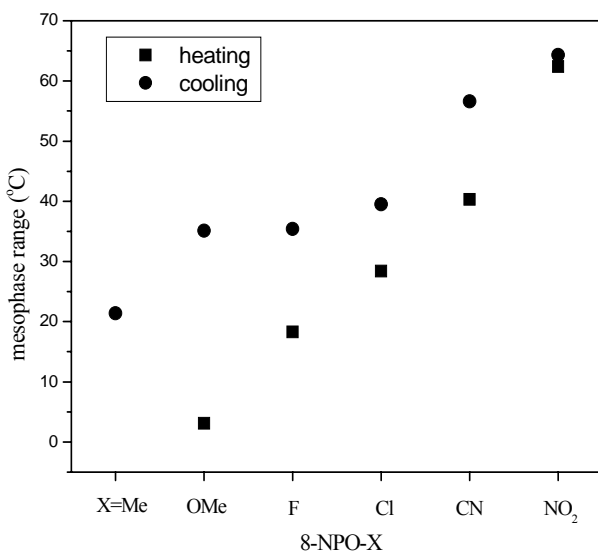


Figure 2.6 The effect of polar substituents on the mesophase range during heating and cooling cycles (dipole increases from left to right).

The optical texture of nematic liquid crystals is an important diagnostic for the presence of a biaxial phase. It has been proposed that the elastic constants of a biaxial nematic should produce only two-brush ($|s|=\frac{1}{2}$) patterns.⁴² In our system, when the nematic samples (n-NPO-Me and n-NPO-OMe) are placed between two untreated glass plates, a schlieren texture consisting of only 2-brush disclinations and absence of 4-brush disclinations ($|s|=1$) is observed in the nematic phase (shown in figure 2.7). As reported, bent-shaped or boomerang-shaped materials may be candidates for a biaxial nematic phase (N_b).^{43,44} Hence, the mesogenic unit containing 1,3,4-oxadiazole provides a large exocyclic bond angle, which makes it possible to be an N_b material.

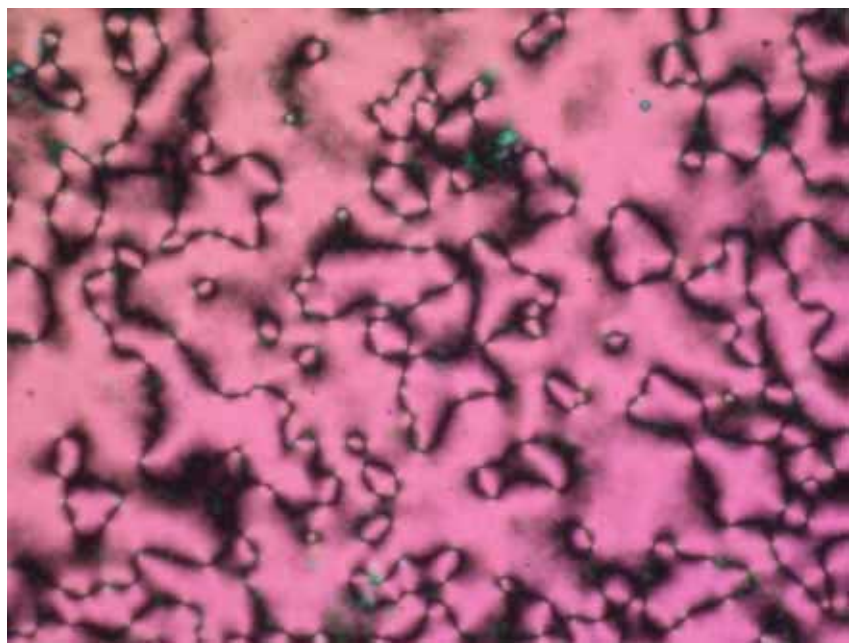


Figure 2.7 Schlieren texture exhibited by the nematic phase of compound 6-NPO-OMe (sandwiched between two untreated glass plates). Note that only 2-brush disclinations, $|s| = \frac{1}{2}$, are observed.

2.4.2 Photoluminescent properties

The absorption spectra of synthesized materials (n-NPO-X) in solution (chloroform) are depicted in figure 2.8. It is noted that similar absorption patterns between 300 and 400 nm are observed in various substituted derivatives of 8-NPO-X (X = Me, OMe, F, and Cl). Nevertheless, both of the cyano- and nitro-substituted compounds have longer wavelengths of absorption. Except the fluoro-substituted compounds (n-NPO-F), a general polar substituent effect is observed, i.e. stronger dipole substituted groups result in larger red shifts ($\text{NO}_2 > \text{CN} > \text{Cl} > \text{OMe} > \text{Me}$) of absorption. Moreover, the strongest polar substituent effect, which results in the largest red shift (>30 nm), can be observed in the nitro-substituted compound (8-NPO-NO₂). The largest red shift in 8-NPO-NO₂ may be due to the electronic effect,⁴⁵ which lowers the LUMO level (as p-doped semiconductors) and reduces the energy

gap.

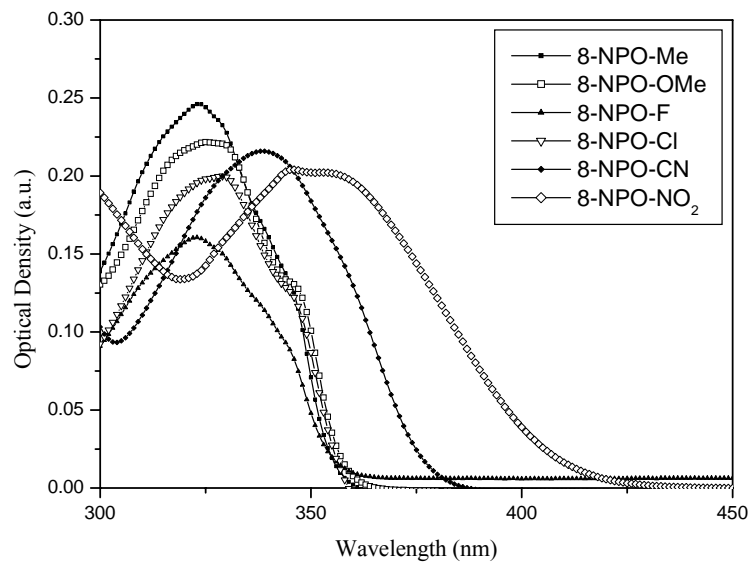


Figure 2.8 Normalize absorption spectra of 8-NPO-X derivatives in solution (chloroform).

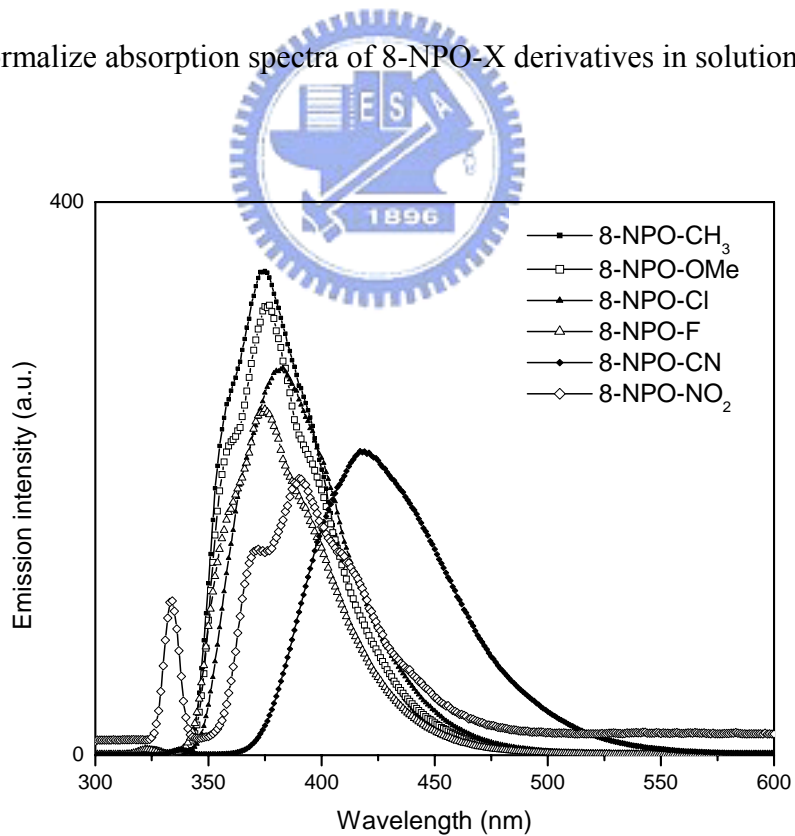


Figure 2.9 Normalized PL spectra of 8-NPO-X derivatives in solution (chloroform).

The normalized photoluminescence (PL) spectra are shown in figure 2.9, and the peak positions are summarized in table 2.2. The emission colors of these 8-NPO-X derivatives are all in the purple region. The methyl-substituted compound (8-NPO-Me) has the shortest wavelength in PL, whereas the stronger dipole substituted compounds have longer wavelengths of PL emission. The cyano-substituted compound (8-NPO-CN) has the longest emission wavelength, which may be due to the elongated conjugation length of the cyano group in conjunction with the mesogenic core. The relative PL quantum yields of these materials are measured in contrast to 8-NPO-Me. The chloro-substituted compound (8-NPO-Cl) has the highest quantum yield and the nitro-substituted compound (8-NPO-NO₂) has the lowest quantum yield. The quenching effect induced by the nitro-substitution has also been observed by Wong et al.,⁴⁶ which is due to the photocurrent generated by the nitro-substituent.

Table 2.2 Absorption and photoluminescence spectra of 8-NPO derivatives.



	8-NPO- Me	8-NPO- OMe	8-NPO- F	8-NPO- Cl	8-NPO- CN	8-NPO- NO ₂
Absorption peaks, nm	323	325	323	329	338	346
Emission peak (PL), nm	374	377	375	383	417	390
Rel. quantum yield	1	1.05	0.95	1.3	1.05	0.05

PL dichroic (D_{PL}) behavior of these materials are also examined. The emission intensity is highest when the polarizer is parallel to the rubbing direction of the aligned cell, and lowest

in the direction perpendicular to it. This property yields a PL dichroic ratio $D_{PL} = I_{\parallel} / I_{\perp}$, where I_{\parallel} and I_{\perp} are values of the PL intensities parallel and perpendicular to the rubbing direction, respectively.⁴⁷ The values of D_{PL} are estimated from 1.4 to 3.4 at the corresponding temperatures (table 2.3) where it shows the highest values of D_{PL} . These results indicate that the conjugated cores are aligned predominantly along the rubbing direction. 10-NPO-Me possesses the largest $D_{PL} = 3.4$ at 100 °C, which means this material has the highest order parameter among these oxadiazole derivatives.

Table 2.3 PL dichroic ratio (D_{PL}) and order parameter of n-NPO-X in various conditions.

	10-NPO -Me	6-NPO- OMe	10-NPO ES-F	10-NPO -Cl	10-NPO -CN	10-NPO -NO ₂
Maximum PL dichroic ratio ^a , ($D_{PL} = I_{\parallel} / I_{\perp}$)	3.4 (100 °C)	1.8 (85 °C)	1.9 (110 °C)	1.4 (150 °C)	1.7 (130 °C)	1.6 (150 °C)
Order parameter ^b	0.44	0.21	0.23	0.11	0.19	0.17

^a The PL dichroic ratio ($D_{PL} = I_{\parallel} / I_{\perp}$) is obtained from the photoluminescence spectra (by the highest intensities of I_{\parallel} and I_{\perp}) at the temperatures where it shows the highest value of D_{PL} , respectively.

^b Order parameter = $(I_{\parallel} - I_{\perp}) / (I_{\parallel} + 2I_{\perp})$

2.5 Conclusion

A new class of mesomorphic molecules consisting of 1,3,4-oxadiazole-based mesogenic cores is prepared. These bent-shaped molecules exhibit the nematic and smectic A phases. In general, the mesogenic phases and optical properties of these oxadiazole-based LC materials have strong connections with their terminal functional groups. By increasing the terminal dipoles, the mesophase ranges are enhanced, and both of the absorption and photoluminescence spectra are shifted toward longer wavelengths.



Chapter 3

Novel Alternating Fluorene-Based Conjugated Polymers

Containing Oxadiazole Pendants with Various Terminal Groups

3.1 ABSTRACT:

A series of soluble alternating fluorene-based copolymers containing symmetrical and asymmetrical 1,3,4-oxadiazole (OXD) pendants with various terminal groups are synthesized by palladium-catalyzed Suzuki coupling reaction. These polymers possess higher glass transition temperatures than that of the analogous dialkoxy-substituted polymer (PFPOC₆) consisting of the same backbone without OXD pendants. The photophysical and electrochemical properties of these polymers are affected by the polar effect (electron-withdrawing group, -CN, and electron-donating group, -R or -OR) and the size effect (the size of the grafted side chain) of the OXD pendants. Owing to the large steric hindrance of OXD pendants, the aggregation of these polymers in solids is reduced, which results in almost identical PL emissions in both solution and solid states. The bulky OXD pendants on the polymer side chains can provide the polymer films with lower HOMO and LUMO energy levels, and better electron injection property. Since only one emission peak is observed in both PL and EL spectra of these polymers, it is evidenced that effective energy transfer from the OXD pendants to the conjugated polymer backbones has occurred and thus to eliminate the light emission from the OXD pendants. These asymmetrical OXD substituted polymers have higher quantum yields and less aggregation in the solid state than the symmetrical OXD substituted polymers. The symmetrical OXD substituted polymer (P1) has a longer PL emission wavelength than the asymmetrical OXD substituted polymers (P2-P8), which may be due to the improvement of the coplanarity between the polymer backbone and the symmetrical OXD pendants, and/or the introduction of two

electron-withdrawing OXD pendants.



3.2 Introduction

Polymer light-emitting diodes (PLEDs) have been studied intensively during the past decade because of their potential applications in a new generation of flat display and lighting technologies.^{48,49} Compared with inorganic electroluminescent (EL) materials, -conjugated polymers have many virtues such as ease of forming large area, mechanical flexibility, low fabrication cost, and easy color tuning through molecular engineering.⁵⁰ Therefore, it is generally expected that PLEDs will be a possible candidate of the next generation display technology.

In order to obtain highly efficient PLED devices, a balance in the injection and transportation of both holes and electrons into the polymer emissive layer is necessary.⁵¹⁻⁵⁵ However, most EL polymers inject and transport holes more efficiently than electrons due to the inherent richness of π -electrons in the EL polymers, which results in an unbalance of opposite carrier currents and a shift of the recombination zone toward the region near the interface of the polymer and the cathode. Thus, the synthesis of efficient electron transporting polymers is needed to improve EL device performance. Polymers containing electron-withdrawing units in the main chains or side chains usually have large electron affinities. In recent years, polyquinolines, polyquinoxalines, polybenzobisazoles, and polypyridines have been demonstrated as electron transporting (ET) polymers due to the good film quality, and the excellent thermal and oxidative stability.⁵⁶⁻⁵⁸ Molecular and polymeric 2,5-diphenyl-1,3,4-oxadiazole-diyl derivatives are the most widely studied classes of electron-injection and/or hole-blocking materials,⁵⁹ by virtue of many merits owned by 1,3,4-oxadiazole (OXD) moieties, such as prominent electron affinity, high photoluminescence (PL) quantum yield, and good thermal stability.⁶⁰ On the other hand, in order to achieve highly efficient and luminescent PLED devices, it is important to suppress the self-quenching process, which is originated from the formation of excimers due to the intermolecular interactions in the solid state. Since large steric hindrance of lateral

substitution will cause the decrease of crystallinity in the resulting polymers, the bulky substitution with symmetrical and asymmetrical structure on the side chains of the polymer can provide the polymer film with an amorphous property.⁶¹ In addition, the pseudo-orthogonal arrangement of the rigid pendant groups can reduce the π -stacking and thus to increase the radiative decay quantum efficiency and photostability of the polymers.^{62, 59c} In this paper, we report a series of alternating fluorene-based copolymers containing symmetrical and asymmetrical substituted OXD pendants with different terminal groups (on the side chains of the polymers). The electrochemical, spectroscopic, and thermal properties of these polymers with respect to various terminal OXD groups are also investigated in this study.

3.3 Experimental Section

3.3.1 Measurements.

¹H NMR spectra were recorded on a Varian unity 300M Hz spectrometer using CDCl₃ solvent. Elemental analyses were performed on a HERAEUS CHN-OS RAPID elemental analyzer. Transition temperatures were determined by differential scanning calorimetry (Perkin Elmer Pyris 7) with a heating and cooling rate of 10 °C/min. Thermogravimetric analysis (TGA) was conducted on a Du Pont Thermal Analyst 2100 system with a TGA 2950 thermogravimetric analyzer under a heating rate of 20 °C/min. Gel permeation chromatography (GPC) analysis was conducted on a Water 1515 separation module using polystyrene as a standard and THF as an eluant. UV-visible absorption spectra were recorded in dilute chloroform solutions (10⁻⁵ M) on a HP G1103A spectrophotometer, and fluorescence spectra were obtained on a Hitachi F-4500 spectrophotometer. Fluorescence quantum yields were determined by comparing the integrated PL density of a reference 9,10-diphenylanthracene in toluene with a known quantum yield (ca. 5 * 10⁻⁶ M, quantum yield = 1.0). Cyclic voltammetry (CV) was performed at a scanning rate of 100 mV/s on a



BAS 100 B/W electrochemical analyzer, which was equipped with a three-electrode cell. Pt wire was used as a counter electrode, and an Ag/AgCl was used as a reference electrode in the CV measurement. The polymer thin film was cast onto a Pt disc as a working electrode with ferrocene as a standard in acetonitrile, and 0.1 M tetrabutylammonium hexafluorophosphate (TBAPF₆) was used as a supporting electrolyte. Polymer thin films were spin-coated on a quartz substrate from chloroform solution with a concentration of 10 mg/ml (this condition consists with the electroluminescent device).

3.3.2 Materials.

Chemicals and solvents were reagent grades and purchased from Aldrich, ARCROS, TCI, and Lancaster Chemical Co. Dichloromethane and THF were distilled to keep anhydrous before use. The other chemicals were used without further purification.

The synthetic routes of monomers (M1-M8) are shown in Scheme 3.1. Firstly, 2,5-dibromo-*p*-xylene was oxidized with potassium permanganate in pyridine to afford 2,5-dibromoterephthalic acid and 2,5-dibromo-4-methyl-benzoic acid. After then, the acid group was further esterified to give 2,5-dibromo-terephthalic acid dimethyl ester (1) and 2,5-dibromo-4-methyl-benzoic acid methyl ester (2), which were synthesized by the modified procedure of ref 63. After the ester groups had been converted to benzoyl hydrazides (3 and 4), they were reacted with various aryl chloride to form compounds 5 and 6. Finally, monomers (M1-M8) were produced by the dehydrative cyclization of hydrazides in POCl₃.

2,5-Dicromo-terephthaloyldihydrazides (3). A mixture of 3.19 g (9.07 mmol) of methyl-2,5-dibromoterephthalate and 4.53 g (90.70 mmol) of hydrazine monohydrate was dissolved in 35 ml methanol, and then refluxed for 24 h. After cooling, the product was poured into water and recrystallized from methanol. Yield: 83%. ¹H NMR (ppm, DMSO-d₆): 4.51 (s, 4H), 7.58 (s, 2H), 9.69 (s, 2H).

2,5-Dicromo-4-methyl-benzoic acid hydrazide (4). Yield: 78%. ^1H NMR (ppm, DMSO-d₆): 2.33 (s, 3H), 7.52 (s, 1H), 7.68 (s, 1H), 9.57 (s, 1H).

Compound 5. 0.81 g (3.02 mmol) of 4-octyloxy-benzoylchloride was added into a solution containing 0.53 g (1.51 mmol) of (1) and 0.25 ml (3.02 mmol) of pyridine in 10 ml of NMP. The reaction mixture was stirred for 12 h and then poured into water. The product was filtered and crystallized from methanol. Yield: 73%. ^1H NMR (ppm, DMSO-d₆): 0.83 (t, 6H), 1.21-1.80 (m, 24H), 4.04 (t, 4H), 7.02 (d, J = 9 Hz, 4H), 7.78 (s, 2H), 7.89 (d, J = 8.7 Hz, 4H), 10.55 (s, 2H), 10.58 (s, 2H).

Benzoic acid *N*-(2,5-dibromo-4-methyl-benzoyl)-hydrazide (6-2). Yield: 81%. ^1H NMR (ppm, DMSO-d₆): 2.38(s, 3H), 7.49-7.62 (m, 3H), 7.68 (s, 1H), 7.77 (s, 1H), 7.91 (d, J = 8.4 Hz, 2H), 10.38 (s, 1H), 10.44 (s, 1H).

4-Methyl-benzoic acid *N'*-(2,5-dibromo-4-methyl-benzoyl)-hydrazide (6-3). Yield: 66%. ^1H NMR (ppm, DMSO-d₆): 2.37 (s, 3H), 2.38(s, 3H), 7.30 (d, J = 8.1 Hz, 2H), 7.68 (s, 1H), 7.76 (s, 1H), 7.84 (d, J = 7.5 Hz, 2H), 10.40 (s, 1H), 10.58 (s, 1H).

4-Methoxy-benzoic acid *N'*-(2,5-dibromo-4-methyl-benzoyl)-hydrazide (6-4). Yield: 88%. ^1H NMR (ppm, DMSO-d₆): 2.38(s, 3H), 3.82 (s, 3H), 7.03 (d, J = 8.7Hz, 2H), 7.68 (s, 1H), 7.76 (s, 1H), 7.90 (d, J = 8.7 Hz, 2H), 10.36 (s, 1H), 10.51 (s, 1H).

4-Octyloxy-benzoic acid *N'*-(2,5-dibromo-4-methyl-benzoyl)-hydrazide (6-5). Yield: 79%. ^1H NMR (ppm, DMSO-d₆): 0.83 (t, 3H), 1.25-1.79 (m, 12H), 2.38 (s, 3H), 4.03 (t, 2H), 7.00 (d, J = 8.7 Hz, 2H), 7.68 (s, 1H), 7.76 (s, 1H), 7.87 (d, J = 9 Hz, 2H), 10.37 (s, 1H), 10.50 (s, 1H).

4-Cyano-benzoic acid *N'*-(2,5-dibromo-4-methyl-benzoyl)-hydrazide (6-6). Yield: 82%. ^1H NMR (ppm, DMSO-d₆): 2.38 (s, 3H), 7.67 (s, 1H), 7.77 (s, 1H), 8.00 (d, J = 8.4 Hz, 2H), 8.05 (d, J = 8.1 Hz, 2H), 10.59 (s, 1H), 10.97 (s, 1H).

Thiophene-2-carboxylic acid *N'*-(2,5-dibromo-4-methyl-benzoyl)-hydrazide (6-7). Yield: 63%. ^1H NMR (ppm, DMSO-d₆): 2.38 (s, 3H), 7.20 (t, J = 5.1 Hz, 1H), 7.65 (s, 1H), 7.77 (s,

1H), 7.86 (d, J = 9.3 Hz, 1H), 7.88 (d, J = 8.4 Hz, 1H), 10.47 (s, 1H), 10.71 (s, 1H).

Naphthalene-1-carboxylic acid N'-(2,5-dibromo-4-methyl-benzoyl)-hydrazide (6-8).

Yield: 71%. 1 H NMR (ppm, DMSO-d₆): 2.39 (s, 3H), 7.56-7.78 (m, 6H), 8.00 (d, J = 7.2 Hz, 1H), 8.06 (d, J = 7.2 Hz, 1H), 8.36 (d, J = 8.7 Hz, 1H), 10.58 (s, 1H), 10.64 (s, 1H).

Monomer 1 (M1). 0.8 g (1.02 mmol) of (4a) was dissolved in 100 ml of POCl₃. The reaction mixture was heated to 130°C overnight, and then cooled to room temperature. Most POCl₃ in reaction mixture was removed at reduced pressure and poured into water. The product was filtered and crystallized from methanol and chloroform several times to get a yellow solid.

Yield: 74%. 1 H NMR (ppm, CDCl₃): 0.88 (t, 6H), 1.30-1.86 (m, 24H), 4.05 (t, 4H), 7.03 (d, J = 9 Hz, 4H), 8.08 (d, J = 8.7 Hz, 4H), 8.51 (s, 2H). Anal. Calcd for C₃₈H₄₄Br₂N₂₄O₄: C, 58.47; H, 5.68; N, 7.18. Found: C, 58.20; H, 5.79; N, 7.07.

2-(2,5-Dibromo-4-methyl-phenyl)-5-phenyl-[1,3,4]oxadiazole (M2). Yield: 56%. 1 H NMR (ppm, CDCl₃): 2.46(s, 3H), 7.52-7.65 (m, 3H), 8.14-8.17 (m, 2H), 8.24(s, 1H). Anal. Calcd for C₁₅H₁₀Br₂N₂O: C, 45.72; H, 2.56; N, 7.11. Found: C, 46.06; H, 2.87; N, 6.87.

2-(2,5-Dibromo-4-methyl-phenyl)-5-p-tolyl-[1,3,4]oxadiazole (M3). Yield: 68%. 1 H NMR (ppm, CDCl₃): 2.45 (s, 3H), 2.46 (s, 3H), 7.33 (d, J = 7.8 Hz, 2H), 7.64 (s, 1H), 8.02 (d, J = 8.4 Hz, 2H), 8.22 (s, 1H). Anal. Calcd for C₁₆H₁₂Br₂N₂O: C, 47.09; H, 2.96; N, 6.86. Found: C, 47.07; H, 3.23; N, 6.80.

2-(2,5-Dibromo-4-methyl-phenyl)-5-(4-methoxy-phenyl)-[1,3,4]oxadiazole (M4). Yield: 44%. 1 H NMR (ppm, CDCl₃): 2.46 (s, 3H), 3.90 (s, 3H), 7.02 (d, J = 9 Hz, 2H), 7.64 (s, 1H), 8.07 (d, J = 8.7 Hz, 2H), 8.22 (s, 1H). Anal. Calcd for C₁₆H₁₂Br₂N₂O₂: C, 45.31; H, 2.85; N, 6.61. Found: C, 45.09; H, 3.09; N, 6.51.

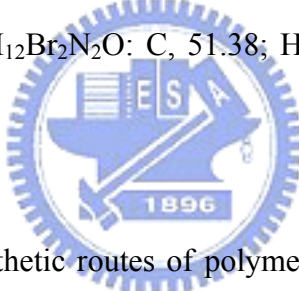
2-(2,5-Dibromo-4-methyl-phenyl)-5-(4-octyloxy-phenyl)-[1,3,4]oxadiazole (M5). Yield: 81%. 1 H NMR (ppm, CDCl₃): 0.90 (t, 3H), 1.20-1.51 (m, 10H), 1.77 (m, 2H), 2.46 (s, 3H), 4.04 (t, 2H), 7.00 (d, J = 8.7 Hz, 2H), 7.64 (s, 1H), 8.05 (d, J = 8.7 Hz, 2H), 8.22 (s, 1H). Anal. Calcd for C₂₃H₂₆Br₂N₂O₂: C, 52.89; H, 5.02; N, 5.36. Found: C, 53.13; H, 5.34; N,

5.30.

4-[5-(2,5-Dibromo-4-methyl-phenyl)-[1,3,4]oxadiazol-2-yl]-benzonitrile (M6). Yield: 88%. ^1H NMR (ppm, CDCl_3): 2.48 (s, 3H), 7.67 (s, 1H), 7.84 (d, $J = 8.4\text{Hz}$, 2H), 8.25 (s, 1H), 8.26 (d, $J = 8.1\text{ Hz}$, 2H). Anal. Calcd for $\text{C}_{16}\text{H}_9\text{Br}_2\text{N}_3\text{O}$: C, 45.86; H, 2.16; N, 10.03. Found: C, 45.82; H, 2.49; N, 10.07.

2-(2,5-Dibromo-4-methyl-phenyl)-5-thiophen-2-yl-[1,3,4]oxadiazole (M7). Yield: 88%. ^1H NMR (ppm, CDCl_3): 2.45 (s, 3H), 7.20 (t, $J = 5.1\text{ Hz}$, 1H), 7.59 (d, $J = 5.1\text{ Hz}$, 1H), 7.63 (s, 1H), 7.85 (d, $J = 5.1\text{ Hz}$, 1H), 8.19 (s, 1H). Anal. Calcd for $\text{C}_{13}\text{H}_8\text{Br}_2\text{N}_2\text{OS}$: C, 39.03; H, 2.02; N, 7.00. Found: C, 39.37; H, 2.34; N, 6.92.

2-(2,5-Dibromo-4-methyl-phenyl)-5-naphthalen-1-yl-[1,3,4]oxadiazole (M8). Yield: 68%. ^1H NMR (ppm, CDCl_3): 2.41 (s, 3H), 7.56-7.68 (m, 4H), 7.88-8.23 (m, 4H), 9.30 (d, $J = 8.1\text{ Hz}$, 1H). Anal. Calcd for $\text{C}_{19}\text{H}_{12}\text{Br}_2\text{N}_2\text{O}$: C, 51.38; H, 2.72; N, 6.31. Found: C, 51.32; H, 3.01; N, 6.28.



Polymerization. The synthetic routes of polymers (P1-P8) are shown in Scheme 3.2. General procedure of polymerization is proceeded through the Suzuki coupling reaction. A mixture of 2,7-bis(4,4,5,5-tetramethyl-1,3,2-dioxaborolan-2-yl)-9,9-dioctylfluorene (1 equiv), dibromo compounds M1-M8 (1 equiv), and tetrakis(triphenylphosphine) palladium (1.0 mol %) was added in a degassed mixture of toluene ([monomer] = 0.2 M) and aqueous 2 M potassium carbonate (3:2 in volume). The mixture was vigorously stirred and reacted at 87 °C for 72 h. After the mixture was cooled to room temperature, it was poured into 200 ml of methanol. A fibrous solid was obtained by filtration, and the solid was sequentially washed with methanol, water, and methanol.

P1. Yield: 51%. ^1H NMR (ppm, CDCl_3): 0.61-1.41 (m, 46H), 1.69-2.00 (m, 10H), 3.88 (br, 4H), 6.73 (d, $J = 8.4\text{ Hz}$, 4H), 7.37-7.55 (m, 8H), 7.81 (d, $J = 7.2\text{ Hz}$, 2H), 8.37 (s, 2H). Anal. Calcd for $\text{C}_{63}\text{H}_{76}\text{N}_4\text{O}_4$: C, 79.37; H, 8.04; N, 5.88. Found: C, 78.10; H, 7.97; N, 5.60.

P2. Yield: 23%. ^1H NMR (ppm, CDCl_3): 0.66-1.20 (m, 22H), 1.91 (br, 4H), 2.46 (s, 3H), 7.22-7.59 (m, 10H), 7.76-7.81 (m, 2H), 8.14 (s, 1H). Anal. Calcd for $\text{C}_{40}\text{H}_{42}\text{N}_2\text{O}$: C, 84.77; H, 7.47; N, 4.94. Found: C, 83.26; H, 7.45; N, 4.83.

P3. Yield: 40%. ^1H NMR (ppm, CDCl_3): 0.66-1.23 (m, 22H), 1.92 (br, 4H), 2.28 (s, 3H), 2.46 (s, 3H), 7.03 (d, $J = 7.8$ Hz, 2H), 7.36-7.50 (m, 7H), 7.74-7.82 (m, 2H), 8.12 (s, 1H). Anal. Calcd for $\text{C}_{41}\text{H}_{44}\text{N}_2\text{O}$: C, 84.79; H, 7.64; N, 4.82. Found: C, 83.44; H, 7.55; N, 4.62.

P4. Yield: 35%. ^1H NMR (ppm, CDCl_3): 0.74-1.26 (m, 22H), 2.1 (br, 4H), 2.48 (s, 3H), 3.77 (s, 3H), 6.75 (br, 2H), 7.41-7.84 (m, 9H), 8.14 (s, 1H). Anal. Calcd for $\text{C}_{41}\text{H}_{44}\text{N}_2\text{O}_2$: C, 82.51; H, 7.43; N, 4.69. Found: C, 81.42; H, 7.50; N, 4.48.

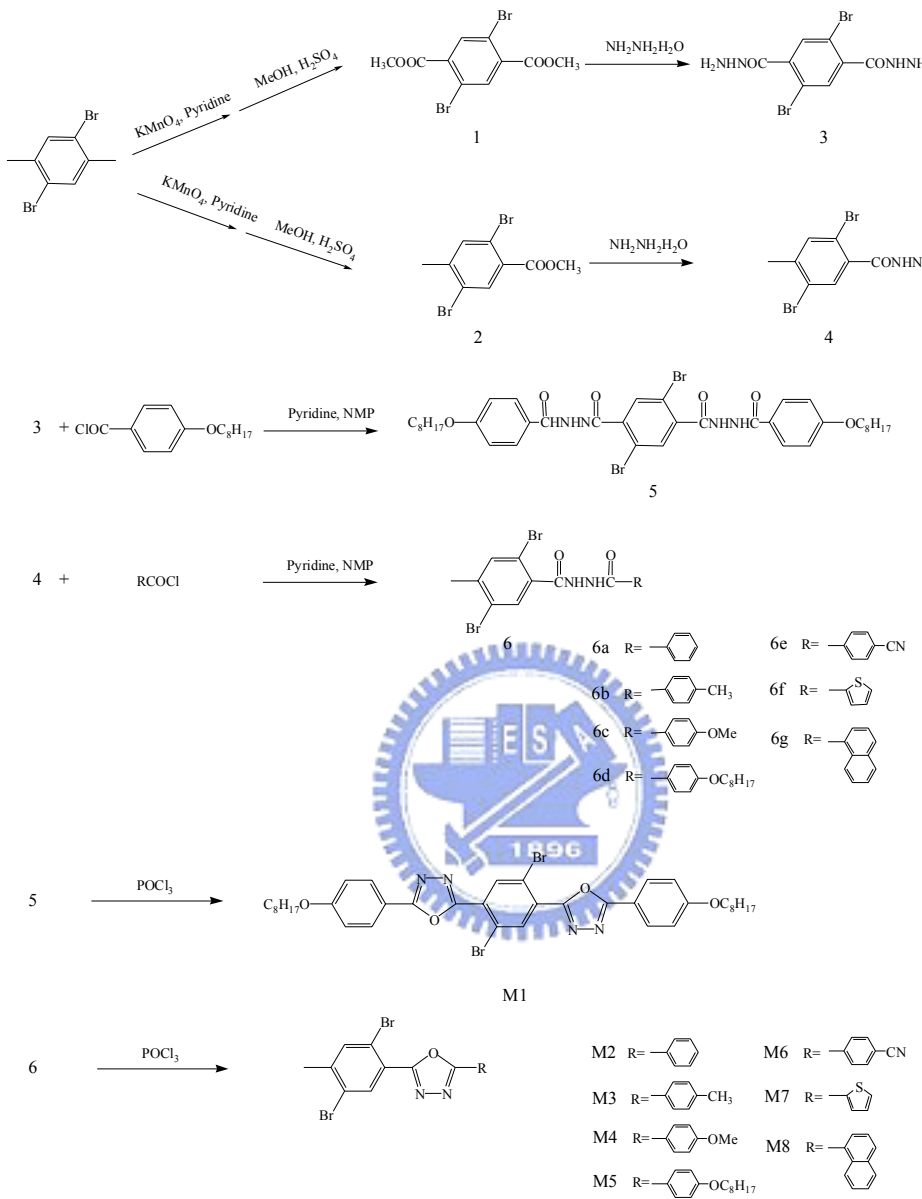
P5. Yield: 78%. ^1H NMR (ppm, CDCl_3): 0.68-1.41 (m, 35H), 1.74-2.07 (m, 6H), 2.47 (s, 3H), 3.90 (br, 2H), 6.77 (d, $J = 8.4$ Hz, 2H), 7.41-7.83 (m, 9H), 8.15 (s, 1H). Anal. Calcd for $\text{C}_{48}\text{H}_{58}\text{N}_2\text{O}_2$: C, 82.95; H, 8.41; N, 4.03. Found: C, 82.03; H, 8.27; N, 3.71.

P6. Yield: 54%. ^1H NMR (ppm, CDCl_3): 0.68-1.26 (m, 22H), 1.95 (br, 4H), 2.50 (s, 3H), 7.35-7.86 (m, 11H), 8.21 (s, 1H). Anal. Calcd for $\text{C}_{41}\text{H}_{41}\text{N}_3\text{O}$: C, 83.21; H, 6.98; N, 7.10. Found: C, 82.26; H, 6.91; N, 6.73.

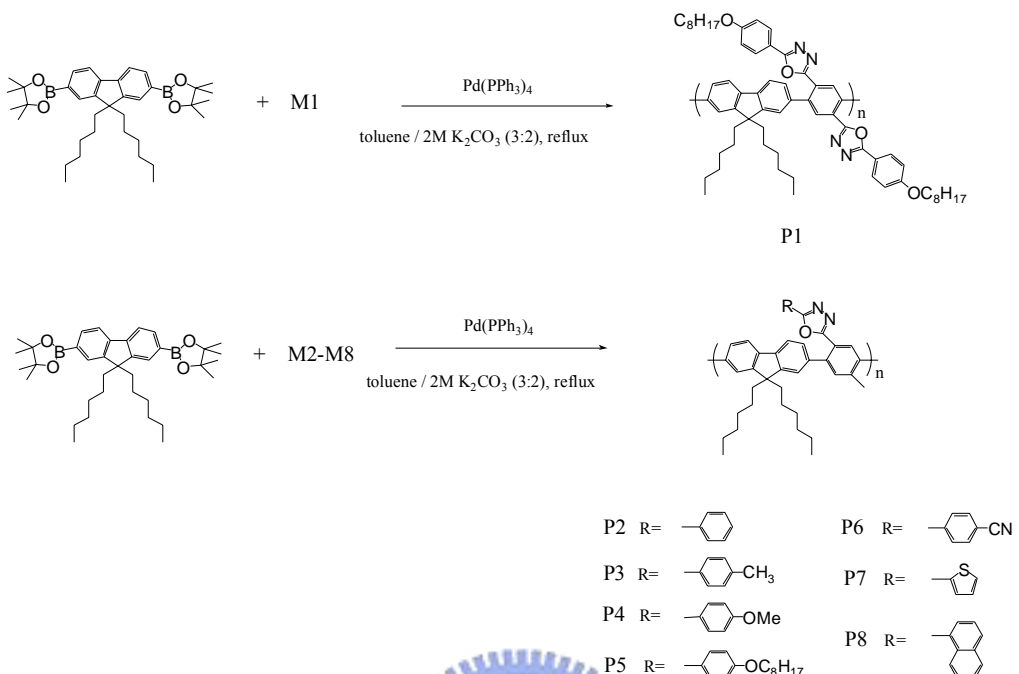
P7. Yield: 88%. ^1H NMR (ppm, CDCl_3): 0.75-1.20 (m, 22H), 2.04 (br, 4H), 2.48 (s, 3H), 6.95 (br, 1H), 7.37-7.49 (m, 7H), 7.76-7.85 (m, 2H), 8.11 (s, 1H). Anal. Calcd for $\text{C}_{38}\text{H}_{40}\text{N}_2\text{OS}$: C, 79.68; H, 7.04; N, 4.89. Found: C, 78.47; H, 7.14; N, 4.69.

P8. Yield: 63%. ^1H NMR (ppm, CDCl_3): 0.48-1.20 (m, 22H), 1.92 (br, 4H), 2.48 (s, 3H), 7.12 (br, 1H), 7.39-7.55 (m, 8H), 7.80-7.87 (m, 4H), 8.20 (s, 1H), 9.04 (br, 1H). Anal. Calcd for $\text{C}_{44}\text{H}_{44}\text{N}_2\text{O}$: C, 85.67; H, 7.19; N, 4.54. Found: C, 84.20; H, 7.31; N, 4.08.

Scheme 3.1 Synthetic Routes of Monomers



Scheme 3.2 Synthetic Route of Polymers



3.4 Results and Discussion

3.4.1 Synthesis and Characterization

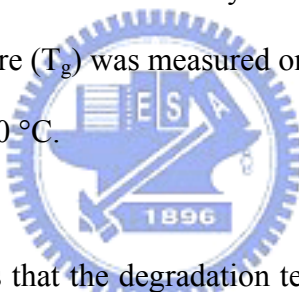
The synthetic routes of monomers (M1-M8) and polymers (P1-P8) are shown in Schemes 3.1 and 3.2. All these polymers were easily dissolved in common organic solvents, such as chloroform, THF, dichloromethane, and toluene to form good transparent films on glass substrates. The average molecular weights were measured by gel permeation chromatography (GPC) with polystyrene as a standard and THF as an eluting solvent. The related data obtained from GPC are given in Table 3.1. The number-average molecular weights (M_n) of polymers are between 4900 and 25200 g/mol, and the polydispersity indexes (PDI) are found between 1.2 and 2.8. The thermal stability of the polymers in nitrogen was evaluated by thermogravimetric analysis (TGA), and their corresponding data are also summarized in Table 3.1.

Table 3.1 Molecular Weights and Thermal Properties of Polymers

Polymer	Yield (%)	M _n	PDI	T _d ^a (°C)	T _g ^b (°C)
P1	51	4900	1.2	398	119
P2	23	6700	1.7	418	109
P3	40	14800	1.5	421	125
P4	35	26600	2.8	414	128
P5	78	24500	2.7	410	85
P6	54	25200	2.6	422	148
P7	88	12200	1.9	407	120
P8	63	6500	1.7	446	132

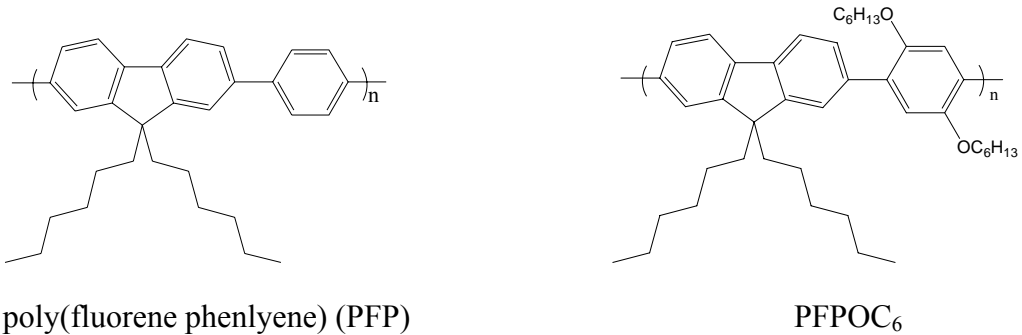
^a Temperature of 5 % weight loss was measured by TGA in nitrogen.

^b The glass transition temperature (T_g) was measured on the first cooling cycle after the sample had been heated to 280 °C.



The TGA analysis indicates that the degradation temperatures (T_d) of 5% weight loss in nitrogen are between 398 and 446 °C. The results of TGA reveal that the polymers are quite stable in nitrogen and, compared with the other polymers (P2-P8) containing asymmetrical OXD pendants, P1 containing symmetrical OXD pendants has the lowest T_d. The glass transition temperatures (T_g) and melting temperatures of these polymers were determined by differential scanning calorimetry (DSC) in nitrogen atmosphere at a scanning rate of 10 °C/min. Their glass transition temperatures are shown between 85 and 148 °C, whereas their melting temperatures are not observed even up to 280 °C. The long flexible alkoxy substituted OXD polymer, P5, has the lowest T_g and the polar cyano substituted OXD polymer, P6, demonstrates the highest T_g. In contrast to P1 containing symmetrical OXD pendants, analogous P5 containing asymmetrical OXD pendants possesses lower T_g (34 °C lower). Comparing P8 with P2, when the phenyl group is replaced with bulky a naphthyl

group in the terminal group of OXD pendants, an increase of 23 °C in T_g is observed in P8. In comparison with the analogous structure without oxadiazole pendants, i.e. poly (fluorene phenlyene) (PFP),⁶⁴ the degradation temperatures of these novel polymers are higher than that of PFP (T_d is 398 °C), and the glass transition temperatures of these polymers are also higher than that of PFPOC₆ (T_g is 72 °C).



3.4.2 Optical Properties

The photophysical characteristics of the monomers and polymers were studied by PL and UV-visible absorption in both dilute chloroform solutions and thin films. The optical properties of the monomers and polymers are summarized in Tables 3.2-3.3 and Figures 3.1-3.5 serially. It is noted that similar absorption patterns between 250 and 400 nm are observed in various substituted monomers, except M1. As expected, both of the absorption and PL spectra are affected by the substituted terminal groups. Compared with those of M2, the maximum absorption and PL wavelengths of M3-M8 increase as the polar substituents and π -excessive thiophene (naphthalene) substituents are attached to the OXD rings. Interestingly, compared with that of M4 ($\lambda_{PL,sol} = 370$ nm) containing OMe pendant terminal group, the emission wavelength of M6 ($\lambda_{PL,sol} = 361$ nm), in which the polar cyano group is attached to the OXD segment, is not efficiently enlarged. This phenomenon is contrary to our previous study, where the cyano group attached to the chromophoric core will elongate the conjugation and result in a longer emission wavelength.⁶⁵ Whereas, the PL emission spectra of the polymers have shown that the cyano-substituted polymer P6 has a longer emission

wavelength ($\lambda_{PL,sol} = 430$ nm) than that of the alkoxy-substituted polymer P4 ($\lambda_{PL,sol} = 405$ nm).

Table 3.2 Absorption and PL Emission Spectral Data of Monomers in Chloroform

Monomer	λ_{abs}^a (nm)	$\lambda_{PL,sol}^b$ (nm)
M1	337	418
M2	283	347
M3	286	352
M4	297	370
M5	299	372
M6	290	361
M7	302	367
M8	320	379

^a Wavelength of the maximum absorbance.

^b Wavelength of the maximum PL emission.

The absorption spectra of synthesized polymers in dilute solutions (chloroform) are depicted in Figure 3.1. It is noticed that the polymers with asymmetric OXD pendants exhibit two absorption peaks; except P8. The absorption spectrum of P8 shows only one peak, which may be due to the overlap of absorption peaks in both OXD pendants and polymer main chains. The shorter absorption ranging at 290-305 nm is originated from the absorption of the conjugated OXD segments, which is confirmed by the same maximum absorption of polymer P5 and monomer M5 (Figure 3.2a). The identical absorption maximum of the OXD segment in dilute solutions before and after the polymerization suggests that the electronic interactions between the conjugated oxadiazole segments and the polymer backbones are quite limited.⁶⁶ The result also implies that part of the conjugated

OXD units (the phenyl-oxadiazole-phenyl conjugated unit) in the asymmetrical side-chain structures twist away from the plane of the conjugated polymer backbone. The longer wavelength peak in the region of 310-370 nm is attributed to the electron transition of -

* along the conjugated backbone of the polymer. Comparing Figures 3.1-3.3, the polymer main-chain absorption peaks of the solution and film samples (Figure 3.2a) are almost identical. This result indicates that the conformation of the polymer chains is very similar in both solution and solid states; in addition, the polymer assembly is in a rather disordered state and refrains from aggregation by this molecular design even in the solid state.

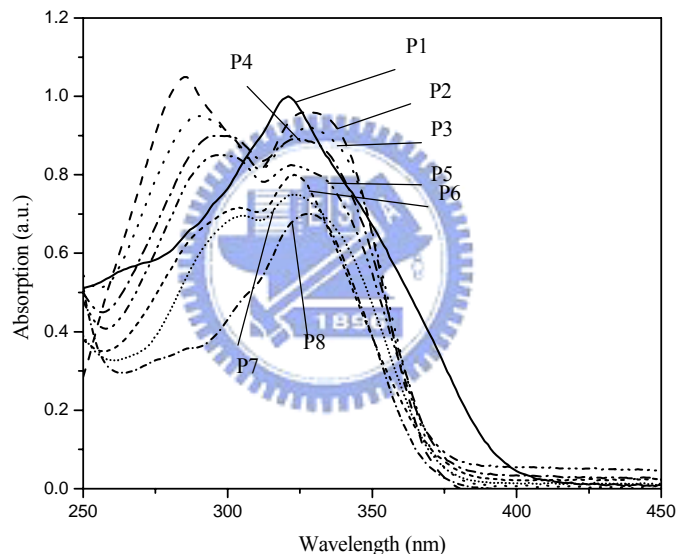


Figure 3.1 UV-visible spectra of polymer solutions in dilute chloroform.

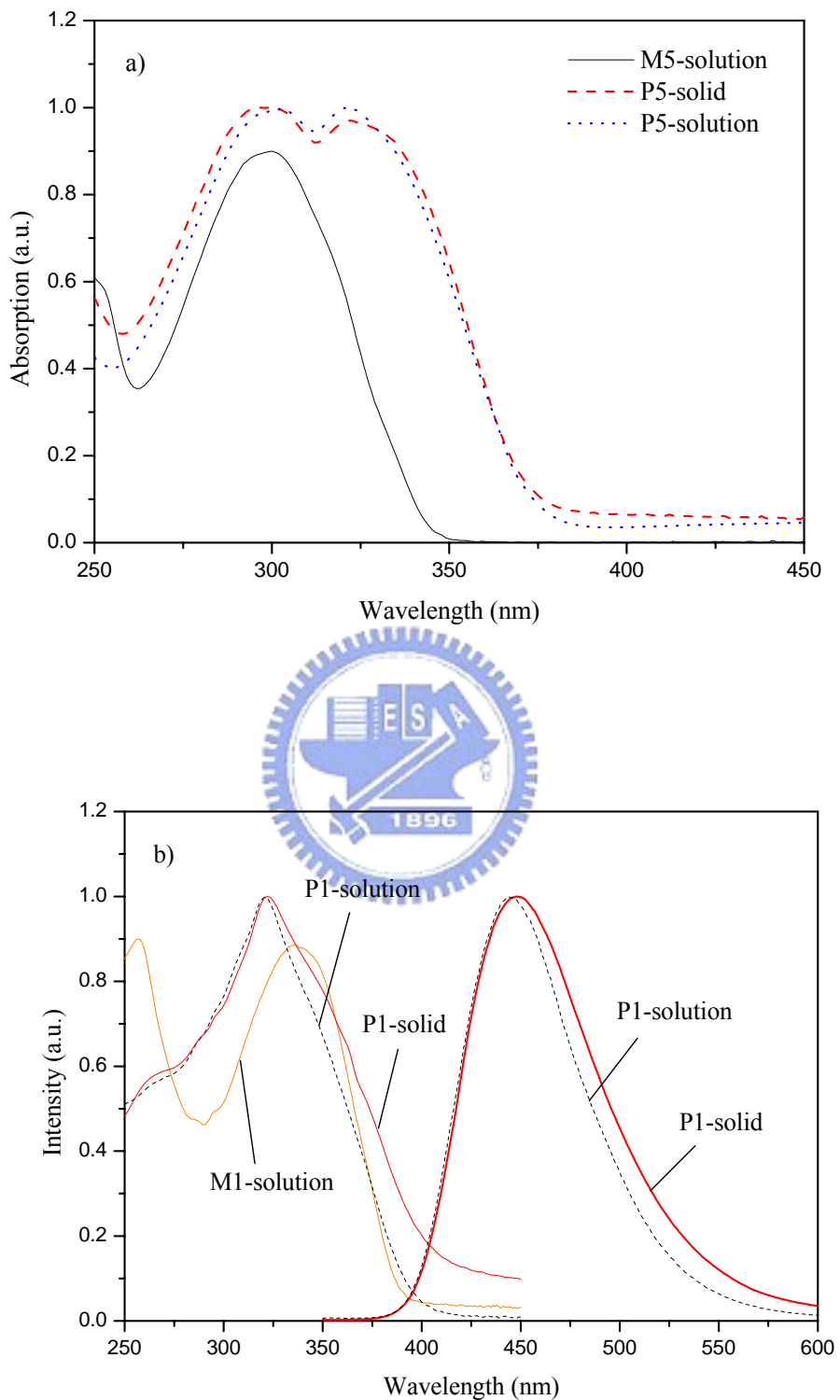


Figure 3.2 (a) UV-visible spectra of M5 and P5. (b) UV-visible and PL emission spectra of M1 and P1.

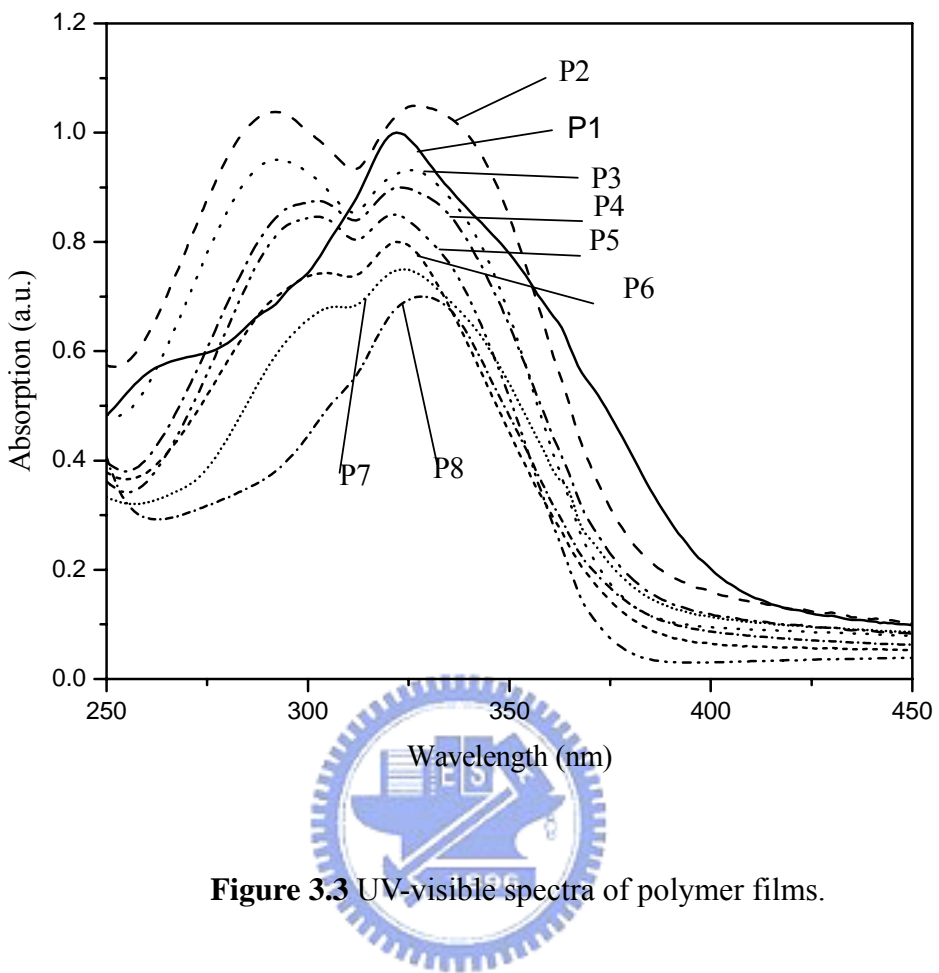


Figure 3.3 UV-visible spectra of polymer films.

The maximum absorption value of P1 (321 nm) comes from the fluorene backbone, which can be proved by similar maximum absorption values of all polymers P1-P8 (321-329 nm), regardless of various oxadiazole pendant groups in P1-P8. The absorption strength of OXD segments in P1 (containing symmetrical OXD pendants) does not appear as a peak but only shows a shoulder around 337 nm (see Figure 3.2b), which corresponds to the absorption peak of M1. This phenomenon illustrates that the fluorene and both symmetrical OXD segments of P1 do not twist away from the conjugated plane of the polymer backbone and induce an elongated conjugation. In addition, the absorption strength of P1 does not show any absorption peak in the region of 270-320 nm (which corresponds to M5 absorption). It implies the conjugated OXD units of P1 keep better coplanarity and do not twist away from

the conjugated plane. We also observe the solid state absorption spectrum of P1 (as shown in Figure 3.2b) has a tail in the low energy region around 370-600 nm, it also proves that P1 has a better coplanarity between the symmetrical OXD pendants and the polymer backbone.

Compared with analogous PFP ($\lambda_{\text{abs}} = 370$ nm), our polymers exhibit blue-shifted absorption maxima (41-49 nm). The blue shifts of the absorption maxima may be ascribed to two reasons. One is that the coplanarity of the polymer backbone is lost due to the asymmetrical bulky substituents, which cause the steric hindrance and induce the distortion of the backbone. Therefore, the conjugation of polymer backbone is interrupted and induces a blue shift of the absorption maximum. The other is that as mentioned previously the OXD pendants act as electron-withdrawing substituents on the side of the polymer backbone. The electron-withdrawing substituted groups decrease the electron density of the polymer backbone and reduce the absorption maximum.⁶⁴

Table 3.3 Absorption and PL Emission Spectral Data of Polymers in Chloroform and in Thin

Polymer	$\lambda_{\text{abs,sol}}^{\text{a}}$	$\lambda_{\text{abs,film}}^{\text{a}}$	Band	$\lambda_{\text{PL,sol}}^{\text{a}}$	$\lambda_{\text{PL,film}}$	$\Phi_{\text{PL,sol}}^{\text{c}}$	fwhm_{sol}
	(nm)	(nm)	gap ^b	(nm)	(nm)		(nm)
Solid Films							
P1	321	322	3.14	445	447	0.15	70
P2	327	327	3.33	405	411	0.30	60
P3	329	326	3.32	402	407	0.39	58
P4	325	323	3.32	405	412	0.36	58
P5	322	321	3.33	404	409	0.31	58
P6	323	322	3.32	430	430	0.17	68
P7	323	324	3.33	409	415	0.26	61
P8	328	328	3.34	410	410	0.38	62

^a Wavelength of the maximum absorbance or PL emission.

^b Band gaps were calculated from the onsets of UV-visible absorption spectra of polymer solutions.

^c PL quantum yield in CHCl₃.

The optical band gap energies obtained from UV-visible absorption in solutions are also given in Table 3.3. The band gap energies of polymers were determined by the intersection of tangents through the turning point of the lower energy side of the spectrum and the lengthened baseline for each polymer. The optical band gaps of asymmetrical OXD substituted polymers from the edge absorption of solution samples are almost identical (3.32-3.34 eV), regardless of terminal functional groups (P2-P8) of OXD pendants. Nevertheless, the symmetrical OXD substituted polymer (P1) has a red-shifted absorption curve and a smaller band gap (3.14 eV). The smaller band gap may be due to the introduction of two electron-withdrawing OXD moieties, and/or a better coplanarity between the polymer backbone and the symmetrical substituents in P1. In comparison with PFP, all band gap energies of these polymers are larger than that of PFP (2.92 eV).

The fluorescence quantum yield (Φ_{PL}), the PL emission maxima (λ_{PL}), and the full width at half-maximum (fwhm) values are also presented in Table 3.3-3.3. All emission data given here were obtained by the excitation at the maximum absorption peaks. In dilute solutions, all these polymers only show one emission peak ranging from 402 to 445 nm (Figure 3.4). Emissions from the OXD pendants are not observed, even when polymers are excited at the absorption peak of the OXD pendants. This indicates the existence of efficient energy transfer from the OXD pendants to the polymer backbone. Except P6, all asymmetrical OXD substituted polymer solutions and films have PL emission in the purple region (Figures 3.4 and 3.5). Among these purple-emitting polymers, the electron-donating substituted groups (CH₃, OCH₃, and OC₈H₁₇) in P3-P5 do not seem to affect the emission spectra significantly as compared with that of P2. However, in contrast to P3-P5, when the electron-withdrawing

cyano group is introduced into the terminal group of OXD pendants in P6, an obvious red shift (about 25 nm) can be observed in the PL spectrum. The symmetrical OXD substituted polymer (P1), apparently, has a longer PL emission wavelength than the other asymmetrical OXD substituted polymers (P2-P8). This result may be due to the improvement of the coplanarity between the polymer backbone and the symmetrical OXD pendants, and/or the introduction of two electron-withdrawing OXD pendants.

The PL spectra of polymer thin films are shown in Figure 3.5. These asymmetrical and symmetrical OXD substituted polymers emit purple and blue color light, respectively. Compared with the spectra of asymmetrical OXD substituted polymers (P2-P8) in solutions, the PL emission peaks of solid films only show a small red shift (the maximum red-shifted value is 7 nm). In contrast to the asymmetrical OXD substituted polymers, the thin film PL peak of P1 is just red-shifted for 2 nm but the emission spectrum shows slight tails in the low energy ends, which may be due to the aggregation of polymer chains in the solid state. The PL quantum yield will be decreased when pendant groups (side chains) are conjugated with the polymer main chains.^{59c, 66, 67} It may be due to the multifarious conjugated forms which can not confine the excitons efficiently, hence the PL quantum yield decreases in the OXD substituted polymer. It is interesting to note that the PL quantum yield of the symmetrical OXD substituted polymer (P1) is lower than those of asymmetrical OXD substituted polymers (P2-P8), which may be due to the different degree of conjugation between the OXD pendants and the backbone in the symmetrical and asymmetrical structures, respectively.

Compared with PFP, side-chain conjugated PPV (OPO-PPV), and cross-conjugated PPE (PPE-PPV),^{61c, 67b} these OXD substituted polymers (P1-P8) exhibit almost identical spectra in the solution and thin film samples. This result is distinct from PFP, OPO-PPV, and PPE-PPV, which have significant red-shifted spectra in the thin film samples as compared with the solution samples. The results demonstrate that the configuration of the OXD

substituted polymers in our study is not affected by the variation of the state in these polymers. It can be understood by the enhanced steric effect between the OXD pendant groups and the polymer backbone, which consequently increases interchain distances and suppresses the formation of aggregation efficiently. In comparison with PFP, the PL spectra of all our polymers (no matter in solution or solid states) exhibit structureless emission spectra, it is different from PFP which possesses a well-resolved vibronic band in the emission spectrum. This phenomenon suggests that the OXD pendants can efficiently enhance the amorphism of the polymers and reduce the vibronic structures in the solid state.

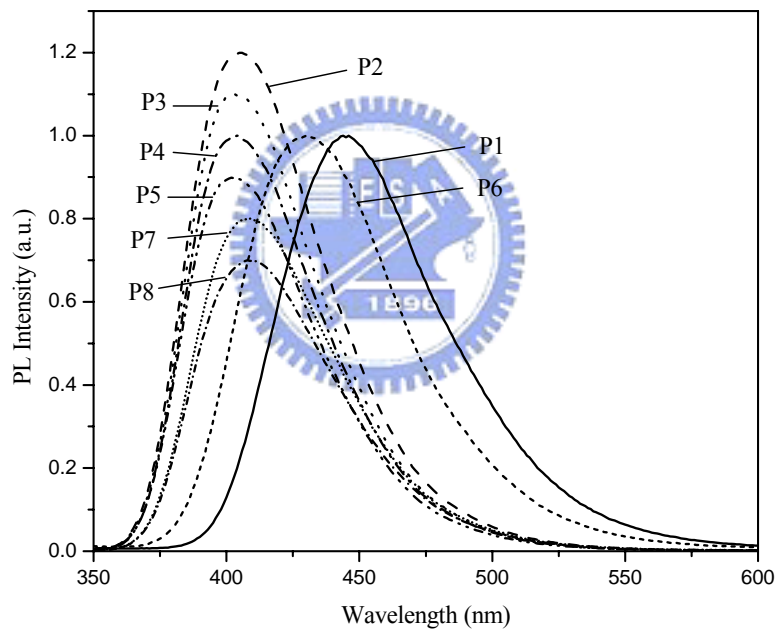


Figure 3.4 PL spectra of polymer solutions in dilute chloroform.

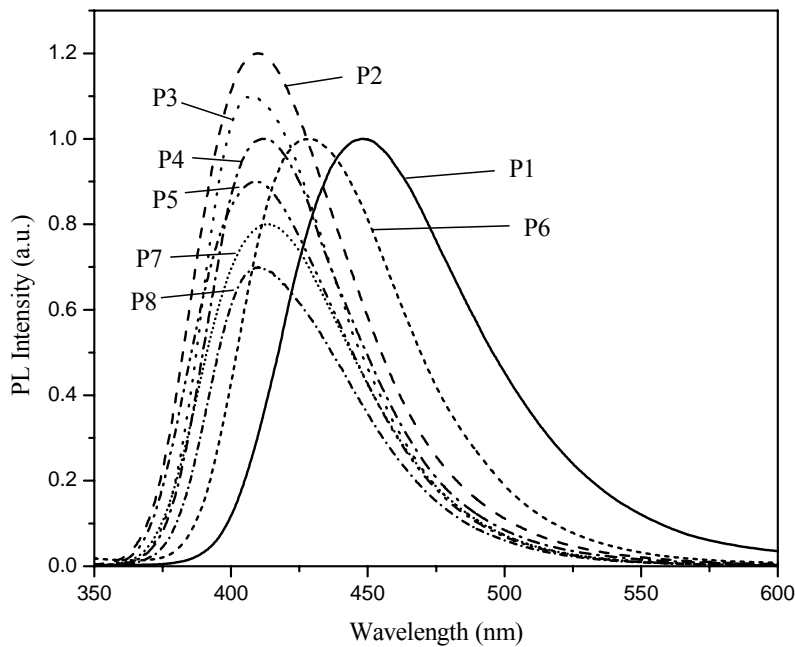


Figure 3.5 PL spectra of polymer films.

Klemm and co-workers reported that the full width at half-maximum (fwhm) values of alkoxy-substituted PPV-PPE hybrid polymers strongly depend on the length of the attached side chains.⁶⁸ The fwhm value increases from 36 nm in PPV-PPE hybrid polymers containing longer side chains (-OC₁₈) to 67 nm in PPV-PPE hybrid polymers containing shorter side chains (-OC₈). They explain that the smaller fwhm value of the long side-chain polymers is due to the emission coming from isolated main-chain fluorophores, however, the larger fwhm value of the short side-chain polymers is a contribution of isolated main-chain fluorophores and a certain degree of aggregation. In our synthetic polymers, the fwhm values of the emission curves of the polymers in the solution and solid states are almost independent of the terminal groups (P2-P5 and P7-P8) of the OXD pendants. Only about 10 nm of increase in the fwhm value was observed in symmetrical P1 and asymmetrical P6 (with a strong electron-withdrawing cyano substituent attached to the end of the OXD

pendant). The strong polar groups of the cyano terminals in the pendants of P6 may induce more or less intramolecular and/or intermolecular interactions and consequently broaden the fwhm value. Otherwise, comparing P5 with P2-P4 of our polymers containing OXD pendants, the fwhm value of the long terminal side-chain polymer (P5) is almost identical with those of short terminal side-chain polymers (P2-P4). From this result, we can generally conclude that the asymmetrical OXD pendants can provide good steric hindrance and reduce aggregation, except OXD pendants containing strong polar cyano groups (such as P6). In general, the lowest quantum yields of P1 (due to the symmetrical pendant structure) and P6 (due to the strong polar cyano-substituent) are also correlated to their largest fwhm values.

In summary of the absorption and PL results, we can conclude the photophysical properties are strongly affected by the OXD pendants. In asymmetrical substituted polymers, the absorption maximum peaks and optical band gaps are almost independent of the electronic effect (electron-withdrawing group, -CN, electron-donating group, -R or -OR) and size effect (the size of the terminal functional group) of the substituted OXD pendants. However, the PL emission peaks and the quantum yields are affected by the electronic effect. When the strong electron-withdrawing cyano group is attached to the terminal phenyl group of the OXD pendant, the PL emission peak is red shifted and the quantum yield is reduced. Except P6, these polymers have similar PL emission peaks as that of PFP ($\lambda_{\text{abs,sol}} = 408 \text{ nm}$, $\lambda_{\text{abs,film}} = 422 \text{ nm}$), but they show larger stoke shifts than that of PFP. As a symmetrical OXD substituted polymer, P1 has an almost identical absorption maximum value as those of asymmetrical substituted polymers, but relatively it possesses a longer PL emission peak and a lower quantum yield.

3.4.3 Electrochemical Properties

To fit the energy band structural scheme of PLED device, it is necessary to determine the energy levels of the highest occupied molecular orbital (HOMO) and the lowest unoccupied molecular orbital (LUMO) of each component, which was carried out by CV to investigate the redox behavior of the polymer thin films. The potential estimated here was based on the reference energy level of ferrocene (4.8 eV below the vacuum level) according to the following equation:²¹ $E^{\text{HOMO}}/E^{\text{LUMO}} = [-(E^{\text{onset}} - 0.45) - 4.8] \text{ eV}$. The onset potentials were determined from the intersection of two tangents drawn at the rising and background currents of the cyclic voltammogram. A crude estimation of the LUMO levels of reduction polymers were deduced from the HOMO values and the optical band gaps.

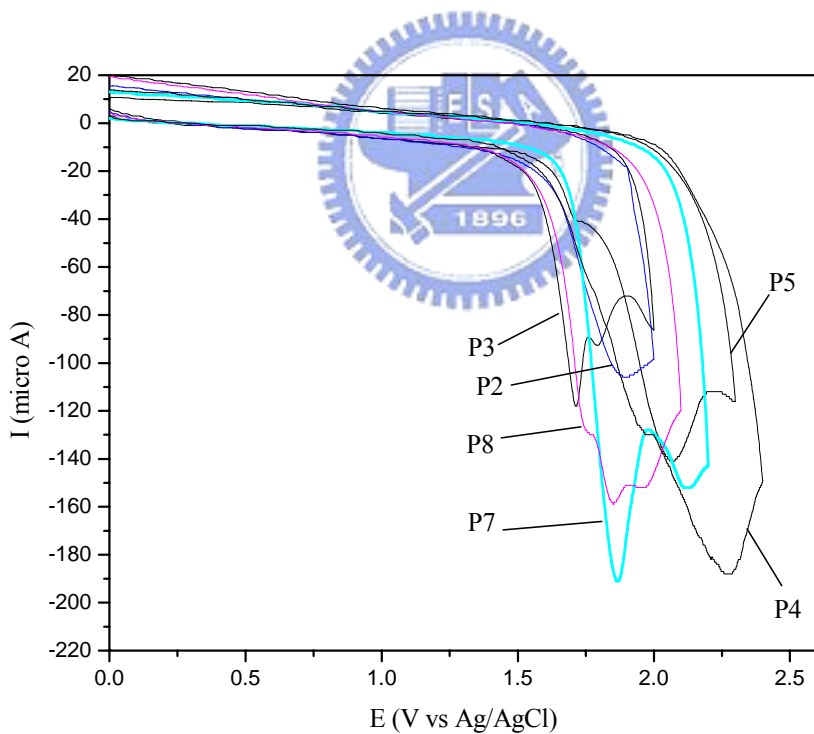


Figure 3.6 Cyclic voltammograms of polymers during the oxidation process.

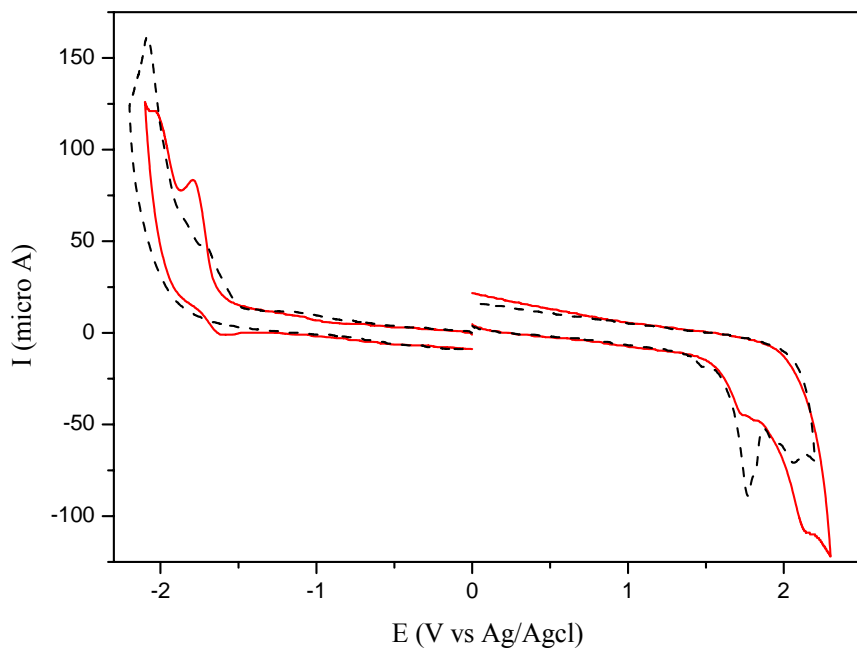


Figure 3.7 Cyclic voltammograms of P1 and P6.

These polymers have the same backbone structure of poly(fluorene-co-alt-phenylene) with different substituents on the OXD pendants which are attached to the phenylene groups. It is interesting to evaluate that how do these OXD pendants modulate the electrochemical behavior of these polymers. As shown in Figures 3.6 and 3.7, most of the polymers possess two anodic peaks, which can be attributed to two different blocks in the OXD pendants and polymer backbones of the copolymers, respectively. Since the reduction potentials are difficult to be measured, only P1 and P6 can be determined, which may be due to their strong electron-withdrawing property. The asymmetrical substituted polymers (P2-P5) show oxidized peaks irreversibly at potentials ranging from 1.72 to 1.98 V (Table 3.4) and the onset potentials of oxidation between 1.57 and 1.62 V in the anodic scan. Comparing P3-P5 with P2, it seems that the electron-donating groups slightly reduce the overall electron-withdrawing effect of the OXD pendants. Compared with P2, the oxidized onset

potentials of P7 and P8 are not remarkably changed by the replacement of the phenyl group with the π -excessive thiophene and naphthalene groups.

As for P6 with cyano-substituted OXD pendants, the oxidation onset potential is 1.39 V and reduction onset potential is -1.51 V. It is obvious that P6 is much easier to be reduced than the other polymers, this is probably due to the strong electron-withdrawing cyano group which increases the overall electron-withdrawing effect of OXD pendants. Compared with P2, the HOMO energy level of P6 can be easily adjusted for 0.4 eV by changing the terminal functional groups of OXD pendants with CN terminals. As for the symmetrical OXD substituted polymer (i.e. P1), the oxidation onset potential is 1.74 V and reduction onset potential is -1.65 V. The band gap obtained from the difference of onset potentials between the reduction and oxidation processes is estimated to be 3.20 V, which is close to that obtained from the absorption edge in the UV-visible spectrum (3.14 V).

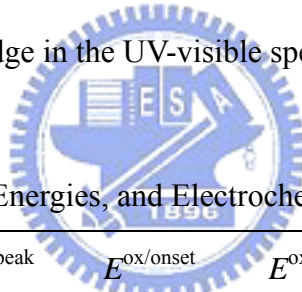


Table 3.4 HOMO and LUMO Energies, and Electrochemical Properties of Polymers

polymer	$E^{\text{red/onset}}$ (V)	$E^{\text{red/peak}}$ (V)	$E^{\text{ox/onset}}$ (V)	$E^{\text{ox/peak}}$ (V)	E^{HOMO} (eV)	E^{LUMO} (eV)
P1	-1.65	-1.79	1.55	1.74	-5.90	-2.70 ^a
P2			1.62	1.90	-5.97	-2.64 ^b
P3			1.57	1.72	-5.92	-2.60 ^b
P4			1.58	1.98	-5.93	-2.61 ^b
P5			1.61	1.73	-5.96	-2.63 ^b
P6	-1.51	-1.72	1.39	1.50	-5.74	-2.84 ^a
P7			1.69	1.87	-6.04	-2.71 ^b
P8			1.60	1.77	-5.95	-2.61 ^b

^a LUMO Energies were obtained from the cyclic voltammetry.

^b LUMO Energies were deduced from HOMO values and optical band gaps.

The OXD pendants act as electron-withdrawing substituents on the backbones of poly(fluorine-co-alt-phenylene)s and thus decrease the LUMO levels (-2.60 to -2.84) of all polymers as compared to that of PFP (HOMO = -5.36, LUMO= -2.47). The lower LUMO potentials of these polymers indicates that the incorporation of electron-withdrawing OXD pendants increases the electron affinities and reduces the LUMO levels of wide band gap polymers (such as PFP) to match the work function of the cathode. From these results, we can conclude that both HOMO and LUMO energy levels can be adjusted not only by the OXD pendants of the polymer backbone but also by the attached functional groups of the OXD pendants.

3.4.4 Electroluminescent (EL) Properties of PLED Devices

The CV and UV-visible results show that both HOMO and LUMO energy levels of our new polymers do not match the work functions of indium-tin oxide (ITO) anode and Al cathode. Therefore, we choose PEDOT and Ca as the anode and cathode, respectively, to overcome these large energy barriers. A series of double-layer EL devices with the configuration of ITO/PEDOT:PSS/Polymer/Ca/Al were made by spin-coating the polymer solutions (with a concentration of 10 mg/ml) onto PEDOT coated glass substrates, and their EL data are demonstrated in Table 3.5.

The current-voltage and luminescence-voltage, i.e. EL response, curves of one typical PLED device (ITO/PEDOT:PSS/P3/Ca/Al) are displayed in Figure 8. All these devices show turn-on voltages for current from 6.5 to 8.5 V and turn-on voltages for light from 7 to 9 V (shown in Table 3.5). Compared with P2 without flexible ends on OXD pendants, P5 with OC₈ terminals on OXD pendants has a higher turn-on voltage. This result may be due to the intrinsic insulation property of the long alkoxy side chains in P5 which consequently increases the turn-on voltage. The attainable maximum luminance is 462 cd/m² at 15 V for P8 as an emitter. These similar turn-on voltages for current and light illustrate that a matched

balance of injection and transportation in charge is achieved. The balanced injection and transportation of both charge carriers may be due to the limited electronic interactions between the cross-conjugated OXD pendants and the conjugated polymer backbone.^{15c}

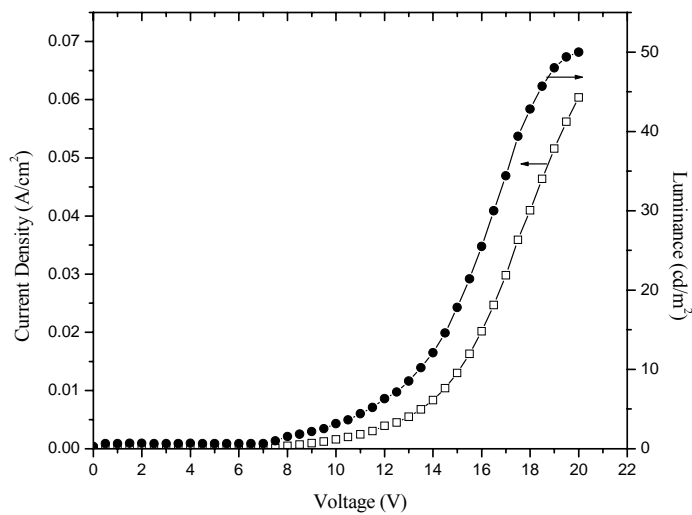


Figure 3.8 Current-voltage and luminescence-voltage characteristics of ITO/PEDOT:PSS/P3/Ca/Al device.



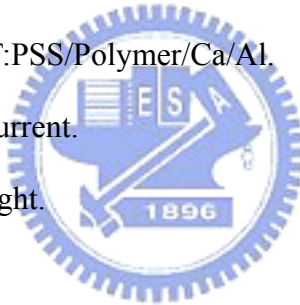
Table 3.5 EL Data of PLED Devices^a

Polymer	$\lambda_{\text{max, EL}}$ (nm)	V_{on}^{b} (V)	V_{on}^{c} (V)	Max. Brightness (cd/m ²)
P1	452	7.5	7.5	126
P2	408	7.5	7.5	29
P3	409	7.5	7.5	51
P4	423	8.5	8.5	104
P5	406	8.5	9.0	376
P6	431	6.5	7.0	306
P7	416	7.0	7.0	82
P8	417	6.5	7.0	462

^a Device structure: ITO/PEDOT:PSS/Polymer/Ca/Al.

^b V_{on} is the turn-on voltage of current.

^c V_{on} is the turn-on voltage of light.



As shown in Figure 3.9, these devices of asymmetrical OXD substituted polymers give purple to blue emission colors and the EL emission peaks are between 406 and 452 nm (Table 3.5). The EL emission peaks, general speaking, are well matched with the corresponding PL emission peaks of the thin films (Table 3.4). This indicates that the similar radiative excited states are involved in both EL and PL processes. In contrast to all asymmetrical OXD substituted polymers, the emission spectra (Figure 10) of P1 at different voltages are slightly voltage-dependent. Since the absorption and fluorescence data reveal that P1 forms excimers due to the aggregation in the solid film, the EL spectra of P1 are red shifted and become broader by increasing voltage.

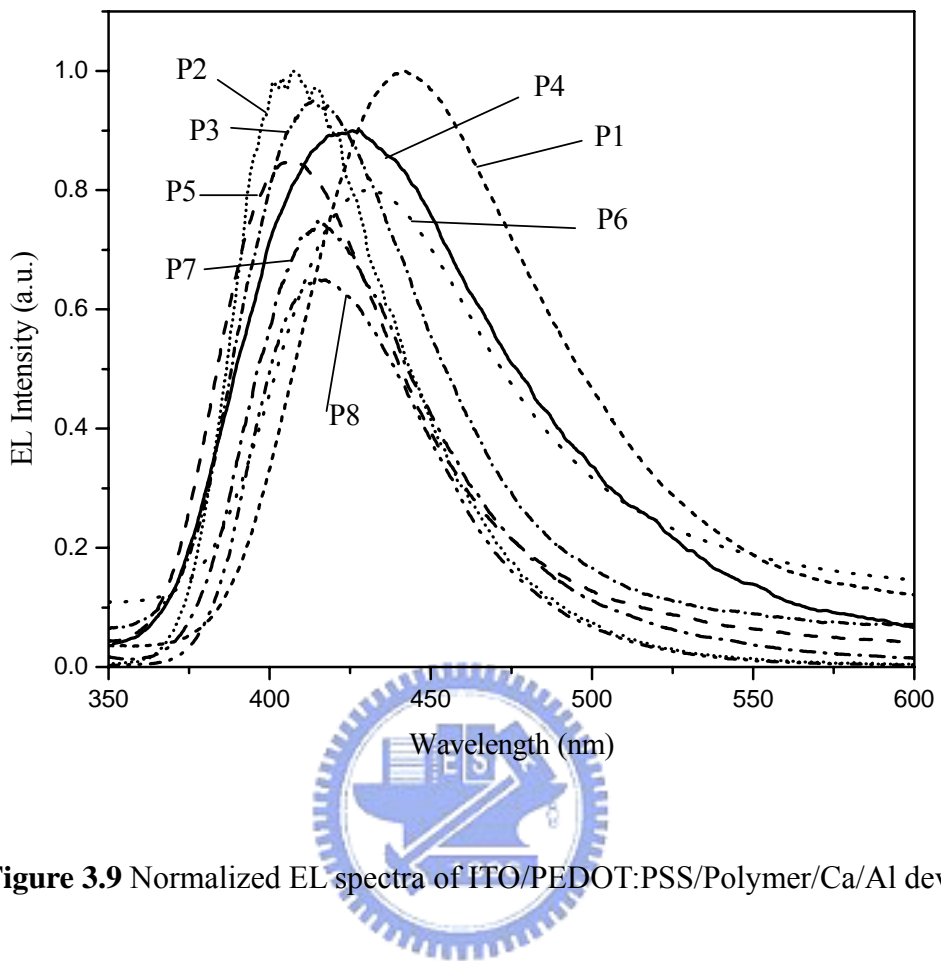


Figure 3.9 Normalized EL spectra of ITO/PEDOT:PSS/Polymer/Ca/Al devices.

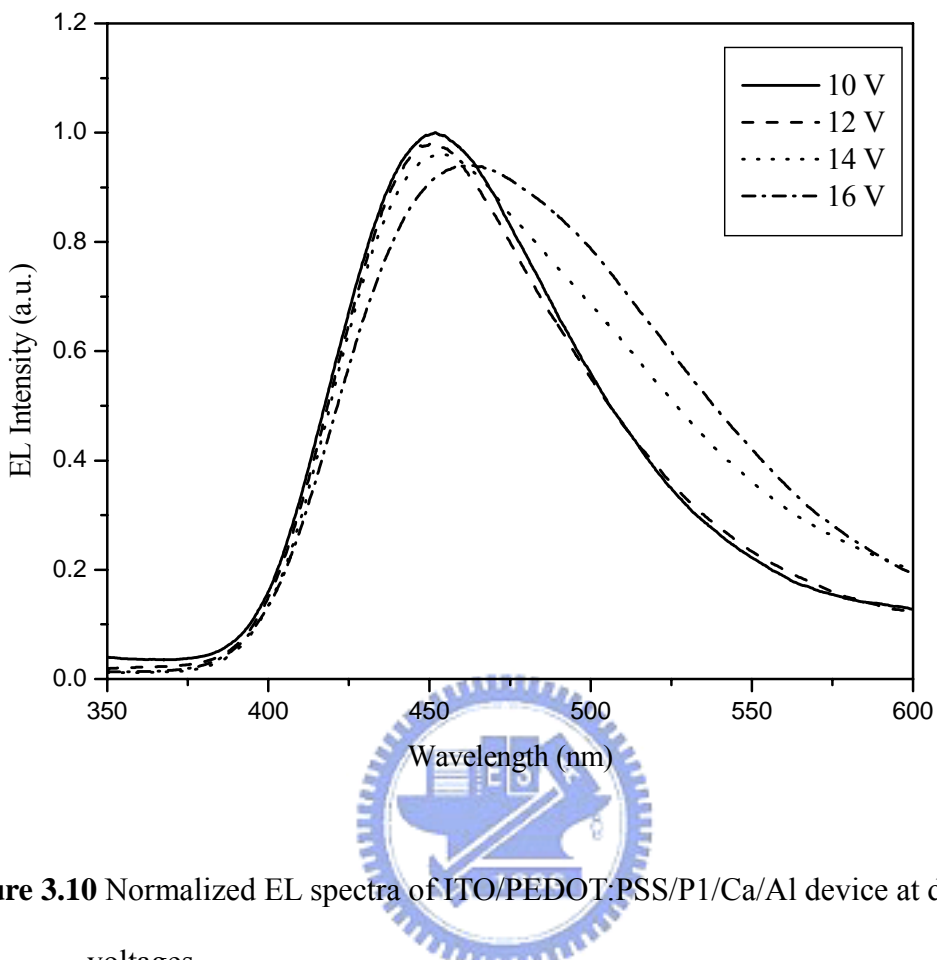


Figure 3.10 Normalized EL spectra of ITO/PEDOT:PSS/P1/Ca/Al device at different voltages.

3.5 Conclusion

A series of soluble alternating fluorene-based copolymers with OXD pendants were synthesized by palladium-catalyzed Suzuki coupling reaction. These polymers exhibit good thermal stability up to 400 °C and possess higher glass transition temperatures than that of the analogous dialkoxy-substituted polymer (PFPOC₆) consisting of the same backbone without OXD pendants. Their photophysical and electrochemical properties are not only affected by the OXD pendants, but also affected by the terminal functional groups. Owing to the large steric hindrance of OXD pendants, the aggregation of these polymers in solid state is reduced, which results in almost identical PL emissions in both solution and solid states.

The incorporation of OXD pendants into polymer backbone leads to mitigating the interchain interaction and improving the electron affinity and charge-injection properties effectively. Since only one emission peak is observed in both PL and EL spectra of these polymers, it is evidenced that effective energy transfer from the OXD pendants to the conjugated polymer backbones has occurred and thus to eliminate the light emission from the OXD pendants. By comparing P1 with P5, we recognize that asymmetrical OXD substituted polymers possess better properties (higher quantum yield and lower aggregation in the solid state) than the symmetrical OXD substituted polymer. The symmetrical OXD substituted polymer (P1) has a longer PL emission wavelength than the asymmetrical OXD substituted polymers (P2-P8), which may be due to the improvement of the coplanarity between the polymer backbone and the symmetrical OXD pendants, and/or the introduction of two electron-withdrawing OXD pendants.



Acknowledgement. We thank the financial support from the National Science Council of Taiwan (ROC) through NSC 92-2113-M-009-016.

Chapter 4

Synthesis and Characterization of Poly(fluorene)-Based Copolymers Containing Various 1,3,4-Oxadiazole Pendants

4.1 Abstract

A series of soluble alternating poly(fluorene)-based copolymers containing electron-transporting 1,3,4-oxadiazole (OXD) and hole-transporting carbazole pendants attached to the C-9 position of fluorene units by long alkyl spacers were synthesized. These copolymers possess mesogenic and non-mesogenic pendants attached to a rigid mesogenic poly(fluorene) (PF) backbone. All these polymers exhibit glass-forming liquid crystalline properties, including the nematic and smectic A (SmA) phases, and reveal much wider mesophasic temperature ranges than that of PF. The thermal properties and mesomorphism of these conjugated polymers are mainly affected by the nature of these pendants, and thus the mesophasic temperature ranges and glass-forming properties are greatly enhanced by introducing the OXD pendants. In addition, the tendencies of crystallization and aggregation of PF are also suppressed by introducing the OXD pendants. A single layer device with P4 as an emitter shows a turn-on voltage of 5 V and a bright luminescence of 2694 cd/m^2 at 11 V with a power efficiency of 1.28 cd/A at 100 mA/cm^2 .

4.2 Introduction

Poly(fluorene) (PF) is a well-known high mobility hole transporting blue-emitting polymer for practical applications in polymer light-emitting diodes (PLEDs).^{69,70} This material displays extremely high photoluminescence (PL) efficiencies in both solution and solid states.^{71,72} However, PF has two major deficiencies as potential candidates for blue PLEDs. Firstly, PF tends to aggregate and form excimers on heating during device formation or operation under forward biases, therefore, which leads to blue-green emission and fluorescence quenching.^{73,74} Secondly, there is an unbalance in charge injection and transportation due to large injection barriers and different charge carrier mobilities.⁷⁵ In order to overcome these drawbacks, the physicochemical properties of PF are improved via side-chain substitution at the C-9 position of the fluorene units. When bulky groups are incorporated into the C-9 position of the fluorene units, it can not only provide large steric hindrance and reduce interchain interaction but also enhance good thermal and morphological stability without substantially changing the electronic properties of the polymer backbone.^{76,77} In addition, the introduction of electron-deficient OXD groups into the C-9 position of the fluorene units will increase electron affinity of resulting polymers, and lead to a more balanced charge injection and transportation as well as recombination.^{78,79}

Linearly polarized blue organic light-emitting diodes have been demonstrated by taking advantage of the thermotropic mesomorphism to be aligned on a rubbing polyimide (PI) substrate.⁸⁰⁻⁸² These liquid crystalline materials possess a potential for spontaneous uniaxial alignment of nematic mesomorphism by spin-coating on a rubbing substrate and therefore they are enabled to generate polarized light emission. PF and monodisperse oligofluorenes are among the most promising candidates for efficient polarized blue luminescence.⁸³⁻⁸⁹ One of the best devices with monodisperse oligofluorenes as an emitter displays polarized electroluminescence (EL) and the dichroic ratio is as high as 31.⁹⁰ It also was found that the side-chain length, pendant structure, and molecular aspect ratio affect the solid morphology,

thermotropic properties, and phase transition temperatures of the resulting polymers. Moreover, the absorption and photoluminescence dichroic ratios are influenced as well.^{91, 92}

Herein, we synthesize the first series of PF with electron-transporting mesogenic pendants in the C-9 position of the fluorene units by long alkyl spacers. This design is based on the consideration that the mesogenic groups with electron-transporting capacity are introduced as pendants to the hole-transporting PF backbones. We hope these functionalized polymers can take advantage of introducing bulky mesogenic pendants to avoid the tendency of spontaneous aggregation and crystallization normally encountered with PF, and to enhance the charge carrier balance as well as the mesophasic temperature range. On the other hand, we also introduce non-mesogenic groups to the PF backbones as pendants for comparative purposes. These intrinsic features help us to investigate the effect of mesogenic pendants on electronic, photonic, and thermotropic properties of the resulting polymers.



4.3 Experimental

4.3.1 Measurements

¹H NMR spectra were recorded on a Varian unity 300M Hz spectrometer using CDCl₃ solvent. Elemental analyses were performed on a HERAEUS CHN-OS RAPID elemental analyzer. Transition temperatures were determined by differential scanning calorimetry (Perkin Elmer Diamond) with a heating and cooling rate of 10 °C/min. The mesophases were studied using a polarizing optical microscope (Leica DMLP) equipped with a hot stage. Thermogravimetric analysis (TGA) was conducted on a Du Pont Thermal Analyst 2100 system with a TGA 2950 thermogravimetric analyzer under a heating rate of 20 °C/min. Gel permeation chromatography (GPC) analysis was conducted on a Water 1515 separation module using polystyrene as a standard and THF as an eluant. UV-visible absorption spectra were recorded in dilute chloroform solutions (10⁻⁵ M) on a HP G1103A spectrophotometer, and fluorescence spectra were obtained on a Hitachi F-4500 spectrophotometer. Polymer thin

films were spin-coated on a quartz substrate from chloroform solutions with a concentration of 10 mg/ml (this condition consists with that of the electroluminescent device). Fluorescence quantum yields were determined by comparing the integrated PL density of a reference 9,10-diphenylanthracene in toluene with a known quantum yield (ca. $5 * 10^{-6}$ M, quantum yield = 1.0). Cyclic voltammetry (CV) was performed at a scanning rate of 100 mV/s on a BAS 100 B/W electrochemical analyzer, which was equipped with a three-electrode cell. Pt wire was used as a counter electrode, and an Ag/AgCl was used as a reference electrode in the CV measurement. The polymer thin film was cast onto a Pt disc as a working electrode with ferrocene as a standard in acetonitrile, and 0.1 M tetrabutylammonium hexafluorophosphate (TBAPF₆) was used as a supporting electrolyte. A series of double-layer EL devices with the configuration of ITO/PEDOT:PSS/Polymer/Ca/Al were made by spin-coating the polymer solutions (with a concentration of 10 mg/ml) onto PEDOT coated glass substrates. The thicknesses of these films were measured on a Sloan DektakIIA surface profilometer. The thickness of PEDOT was about 40 nm, and the thicknesses of these polymers for P1 and P2-P4 were about 60 nm and 80 nm, respectively. The thickness of these films was measured on a Sloan DektakIIA surface profilometer. The thickness of PEDOT was about 40nm, and the thickness of these polymers for P1 was about 60 nm, for P2-P4 was about 80 nm. The luminance-current-voltage characteristics were recorded on a power source (Keithley 2400) and photometer (MINOLTA CS-100A). To align the LC state into a monodomain, polymers were spin-coated from a 1 wt% solution in chloroform at 2500 rpm onto a glass substrate coated with a polyimide alignment layer. After vacuum-drying, pristine films were thermally annealed at corresponding mesomorphic temperature ranges for 30-60 min then cooled to room temperature.

4.3.2 Materials

Chemicals and solvents were reagent grades and purchased from Aldrich, ARCROS, TCI

and Lancaster Chemical Co. Dichloromethane and THF were distilled to keep anhydrous before use. The other chemicals were used without further purification. Compounds 2-7 and fluorine derivative monomer were synthesized by modified procedures (shown in Scheme 1) which have been described in ref 93-98.

M1. 2.25 g (4.77 mmol) of 7a was added to a solution of 2,7-dibromofluorene (0.72 g, 2.22 mmol) in THF at 0 °C. The solution was heated to 60 °C and stirred for 3 h then cooled to room temperature. After evaporation of the solvent, the residue was purified by chromatograph. Yield: 76%. ^1H NMR (ppm, CDCl_3): 0.58 (br, 4H), 1.07-1.45 (m, 24H), 1.73-1.80 (m, 4H), 1.83-1.94 (m, 4H), 2.44 (s, 6H), 4.00 (t, 4H), 6.98 (d, J = 9 Hz, 4H), 7.31 (d, J = 8.7 Hz, 4H), 7.44-7.46 (m, 4H), 7.50-7.54 (m, 2H), 8.00 (d, J = 8.1 Hz, 4H), 8.03 (d, J = 9 Hz, 4H). Anal. Calcd for $\text{C}_{63}\text{H}_{68}\text{Br}_2\text{N}_4\text{O}_4$: C, 68.47; H, 6.20; N, 5.07. Found: C, 68.38; H, 6.28; N, 4.80.

M2. Yield: 82%. ^1H NMR (ppm, CDCl_3): 0.58 (br, 4H), 1.06-1.48 (m, 24H), 1.80-1.90 (m, 4H), 1.91-1.94 (m, 4H), 2.45 (s, 6H), 4.07 (t, 4H), 7.15 (s, 2H), 7.19 (d, J = 8.7 Hz, 2H), 7.33 (d, J = 8.4 Hz, 4H), 7.43-7.46 (m, 4H), 7.50-7.53 (m, 2H), 7.81 (d, J = 8.4 Hz, 2H), 7.83 (d, J = 8.7 Hz, 2H), 8.05 (d, J = 8.4 Hz, 4H), 8.12 (d, J = 8.7 Hz, 4H), 8.51 (s, 1H). Anal. Calcd for $\text{C}_{71}\text{H}_{72}\text{Br}_2\text{N}_4\text{O}_4$: C, 70.76; H, 6.02; N, 4.65. Found: C, 70.70; H, 6.18; N, 4.60.

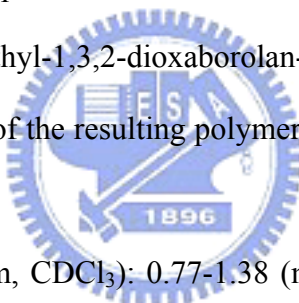
M3. Yield: 73%. ^1H NMR (ppm, CDCl_3): 0.58 (br, 4H), 1.06-1.58 (m, 24H), 1.75-1.80 (m, 4H), 1.89-1.94 (m, 4H), 2.45 (s, 6H), 3.99 (t, 4H), 6.97 (d, J = 8.4 Hz, 4H), 7.33 (d, J = 8.4 Hz, 4H), 7.44-7.47 (m, 4H), 7.51-7.54 (m, 2H), 7.57 (d, J = 8.4 Hz, 4H), 7.70 (d, J = 8.4 Hz, 4H), 8.03 (d, J = 8.1 Hz, 4H), 8.16 (d, J = 8.1 Hz, 4H). Anal. Calcd for $\text{C}_{75}\text{H}_{76}\text{Br}_2\text{N}_4\text{O}_4$: C, 71.65; H, 6.09; N, 4.46. Found: C, 71.31; H, 6.27; N, 4.49.

M4. Yield: 89%. ^1H NMR (ppm, CDCl_3): 0.51 (br, 4H), 1.07-1.26 (m, 8H), 1.68-1.70 (m, 4H), 1.77-1.82 (m, 4H), 4.17 (t, 4H), 7.19 (t, 4H), 7.28-7.35 (m, 6H), 7.40-7.48 (m, 8H), 8.05 (d, J = 7.8 Hz, 4H). Anal. Calcd for $\text{C}_{49}\text{H}_{46}\text{Br}_2\text{N}_2$: C, 71.53; H, 5.64; N, 3.41. Found: C,

71.77; H, 5.98; N, 3.43.

Polymerization

The synthetic route of polymers is shown in Scheme 2. A general procedure of polymerization is proceeded through the Suzuki coupling reaction. For polymers P1-P3, a mixture of 2,7-bis(4,4,5,5-tetramethyl-1,3,2-dioxaborolan-2-yl)-9,9-dihexyllfluorene (1 equiv), dibromo compound (1 equiv), and tetrakis(triphenylphosphine) palladium (1.0 mol%) were added in a degassed mixture of toluene ([monomer] = 0.2 M) and aqueous 2 M potassium carbonate (3:2 in volume). The mixture was vigorously stirred at 87 °C for 72 h. After the mixture was cooled to room temperature, it was poured into 200 ml of methanol. A fibrous solid was obtained by filtration. The solid was washed sequentially with methanol, water, and methanol. A similar procedure is carried out for the synthesis of P4, and the feed ratio of 2,7-bis(4,4,5,5-tetramethyl-1,3,2-dioxaborolan-2-yl)-9,9-dihexyllfluorene / M1 / M4 is 2/1/1. The actual m/n ration of the resulting polymer (P4) is about 1:1, which is calculated from proton NMR.



P1. Yield: 53%. ^1H NMR (ppm, CDCl_3): 0.77-1.38 (m, 50H), 1.70-1.76 (m, 4H), 2.11 (br, 8H), 2.42 (s, 6H), 3.96 (t, 4H), 6.95 (d, J = 8.7 Hz, 4H), 7.29 (d, J = 8.1 Hz, 4H), 7.68-7.85 (m, 12H), 7.98-8.04 (m, 8H). Anal. Calcd for $\text{C}_{88}\text{H}_{100}\text{N}_4\text{O}_4$: C, 82.72; H, 7.89; N, 4.38. Found: C, 82.72; H, 7.89; N, 4.05.

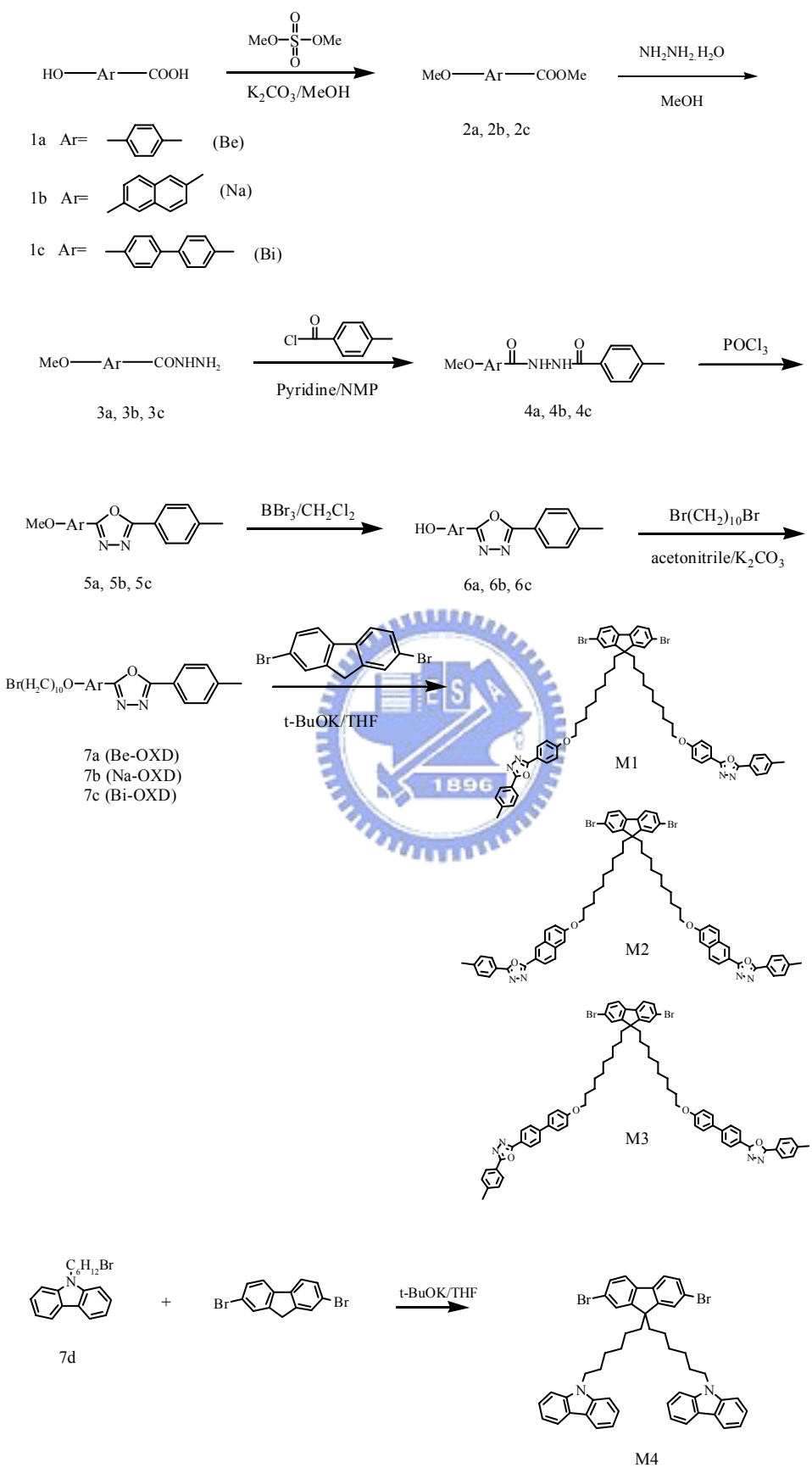
P2. Yield: 61%. ^1H NMR (ppm, CDCl_3): 0.77-1.41 (m, 50H), 1.75-1.80 (m, 4H), 2.12 (br, 8H), 2.42 (s, 6H), 4.00 (t, 4H), 7.09-7.21 (m, 4H), 7.30-7.35 (m, 4H), 7.68-7.85 (m, 16H), 8.02-8.15 (m, 6H), 8.48 (s, 2H). Anal. Calcd for $\text{C}_{96}\text{H}_{104}\text{N}_4\text{O}_4$: C, 83.68; H, 7.61; N, 4.07. Found: C, 82.93; H, 7.60; N, 3.82.

P3. Yield: 79%. ^1H NMR (ppm, CDCl_3): 0.77-1.38 (m, 50H), 1.67-1.73 (m, 4H), 2.13 (br, 8H), 2.42 (s, 6H), 3.93 (t, 4H), 6.93 (d, J = 8.4 Hz, 4H), 7.30 (d, J = 7.8 Hz, 4H), 7.53-7.82 (m, 20H), 8.00 (d, J = 7.8 Hz, 4H), 8.12 (d, J = 8.4 Hz, 4H). Anal. Calcd for $\text{C}_{100}\text{H}_{108}\text{N}_4\text{O}_4$: C, 83.99; H, 7.61; N, 3.92. Found: C, 83.61; H, 7.61; N, 3.67.

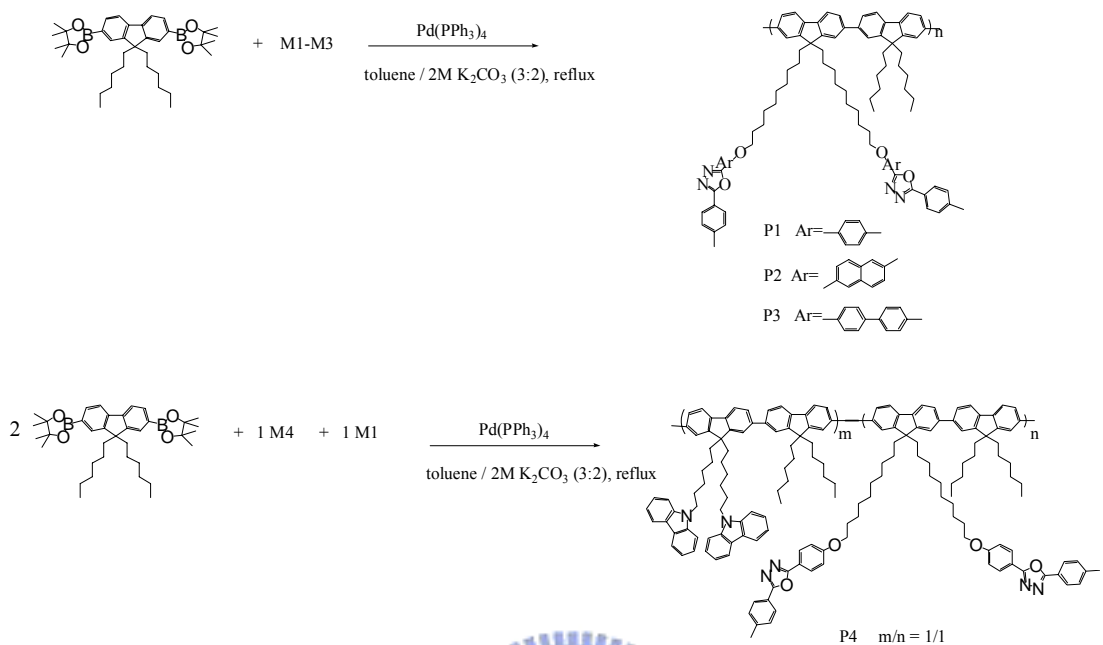
P4. Yield: 82%. ^1H NMR (ppm, CDCl_3): 0.65-1.40 (m, 84H), 1.78 (br, 8H), 2.11 (br, 16H), 3.98 (t, 4H), 4.18 (br, 4H), 6.94 (d, $J = 9$ Hz, 4H), 7.15 (t, 4H), 7.25-7.36 (m, 12H), 7.60-7.88 (m, 24H), 7.96-8.05 (m, 12H).



Scheme 4.1 Synthetic Routes of Monomers



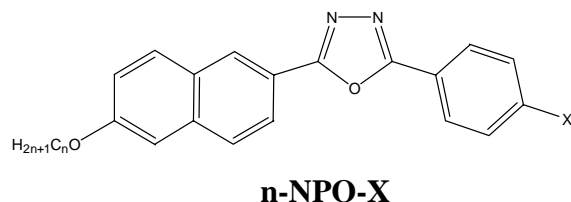
Scheme 4.2 Synthetic Route of Polymers



4.4. Results and Discussion

4.4.1 Synthesis and Characterization

Our previous study reveals that 2-(6-alkoxy-naphthalen-2-yl)-5-phenyl-[1,3,4]oxadiazoles containing various substituents at phenyl 4-position (n-NPO-X) exhibit stable mesogenic properties



where $n = 6, 8$, and 10

and $X = \text{Me, OMe, F, Cl, CN, and NO}_2^{93}$

including the nematic and SmA phases.⁹³ These LC materials incorporated with strong polar electron-withdrawing terminal groups (F, Cl, CN, and NO₂) exhibit the SmA phase and tend to form highly ordered smectic E (SmE) phase. Whereas, when electron-donating methyl and

methoxy groups were served as terminal moieties, the mesophase of these LC materials do not show any SmE phase. Although the methoxy-substituted material (n-NPO-OMe) exhibits wider mesophasic temperature range than that of methyl-substituted materials (n-NPO-Me), choosing methoxy group as a terminal group of the mesogenic pendant in this research will encounter a synthetic problem by converting a methoxy group into a hydroxy group (synthetic step 5 of Scheme 1). Therefore, the methyl group becomes our best choice of the terminal group, besides 10-NPO-Me possess monotropic nematic and SmA phases along with the widest mesophasic temperature range (I 107 N 93 SmA 85 K) among these n-NPO-Me. Concluding the above-mentioned views, we can formulate the optimal structure (Na-OXD, 7b) that possesses decyloxy side-chain spacers and methyl terminal groups as electron-transporting mesogenic pendants, which are attached to the PF backbones. Comparatively, we also introduce non-mesogenic pendants (Be-OXD, 7a and carbazole, 7d) and mesogenic pendants (Bi-OXD, 7c, with wider mesophasic temperature range, i.e. K 134 SmA 187 N 195 I) to the PF backbones. In addition, polymers containing OXD pendants can provide large steric hindrance and reduce aggregation, which also have been reported.^{78, 99} To our best knowledge, the first series of PF copolymers containing PF backbones and electron-transporting mesogenic pendants are reported in this research.

Table 4.1 Molecular Weights and Thermal Properties of Polymers

Polymer	Yield (%)	M _n	M _w /M _n	T _d ^a (°)	T _g (°)	T _c (°) ^b
P1	53	10200	2.2	406	60	>300
P2	61	27000	2.1	414	80	>340
P3	79	55700	2.6	438	86	>340
P4	82	45600	1.8	438	83	>340

^a Temperature of 5 % weight loss measured by TGA in nitrogen.

^b Temperature measured by polarizing optical microscopy.

The average molecular weights of these PF copolymers obtained by GPC are given in Table 4.1. The number-average-molecular weights (M_n) of polymers are between 10200 and 55700 g/mol, and the polydispersity indexes (PDI) are between 1.8 and 2.6. The thermal stability of the polymers in nitrogen evaluated by thermogravimetric analysis (TGA) indicates that the degradation temperatures (T_d) of 5% weight loss in nitrogen are larger than 400 °C for all polymers (shown in Table 1). The mesomorphism characterized by polarizing optical microscopy (POM) and differential scanning calorimetry (DSC) thermograms are displayed in Figure 4.1. To avoid thermal decomposition, these polymers were heated to 280 °C then subsequently cooled to -40 °C at a heating and cooling rate of 10 °C/min, whereas their melting temperatures were not observed even up to 280 °C. The DSC results show the glass transition temperatures of these polymers are between 60 and 101 °C (demonstrated in Table 4.1). All these polymers are found to display the nematic and SmA phases, and reveal isotropization temperatures above 340 °C (except P1) where thermal decomposition occurred.

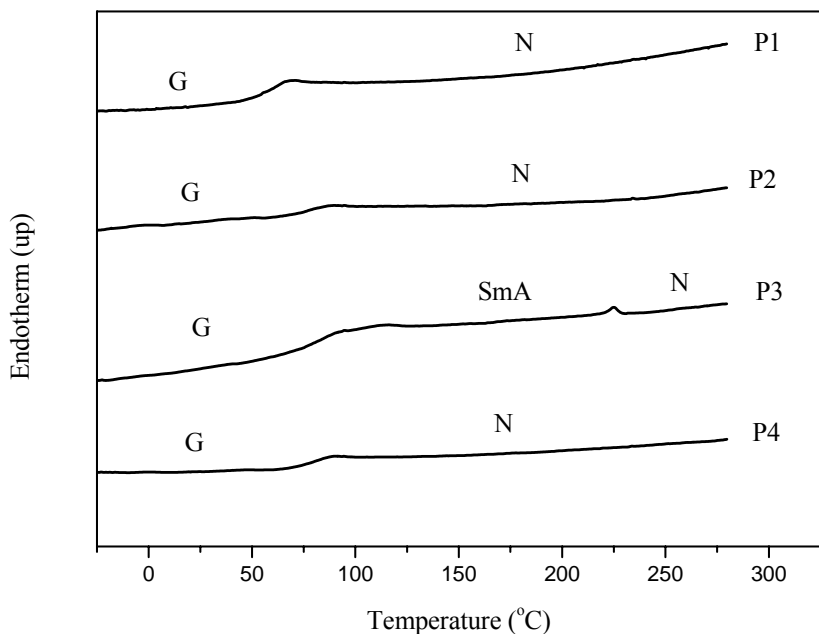
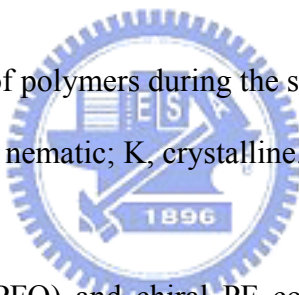


Figure 4.1 DSC thermograms of polymers during the second heating scan at 10 °C /min.

Symbols: G, glass; N, nematic; K, crystalline.



Poly(9,9-dioctylfluorene) (PFO) and chiral PF containing 2S-methylbutyl side groups have been reported to exhibit mesomorphism but with a strong tendency to crystallize on both heating and cooling processes.¹⁰⁰ Herein, we introduce electron-transporting Be-OXD (7a) groups, which do not exhibit mesogenic properties, to PF backbones to serve as pendants of the resulting polymer (P1). As revealed by DSC diagram (shown in Figure 4.1), P1 is an amorphous polymer with $T_g = 60$ °C and shows a stable glass-forming nematic phase corroborated by polarizing optical microscopy. P2 contains Na-OXD (7b) pendants, which is a monotropic mesogenic material with nematic and SmA phases, shows $T_g = 80$ °C and only exhibits a nematic phase without any SmA phase. On the other hand, P3 possesses Bi-OXD (7c) groups as pendants, Bi-OXD has wider mesophasic temperature range (K 134 SmA 187 N 195 I) than that of Na-OXD. The resulting polymer displays nematic and SmA

phases similar to their pendants with $T_g = 86$ °C. In comparison with P2, P3 shows two mesophases including the nematic and SmA phases. The divergence may result from the wide SmA temperature range (53 °C) of Bi-OXD pendants, which induces the resulting polymer to exhibit the SmA phase. In contrast to Bi-OXD, Na-OXD only has SmA temperature range of 8 °C and consequently can not effectively induce P2 to generate the SmA phase. Compare P1 and P2-P3, we can find that although Be-OXD (7a) do not exhibit mesogenic property, the large steric groups can still suppress the tendency of crystalline and enhance the mesophasic temperature range. On the hand, P4 (which is a random copolymer comprising carbazole and Be-OXD groups) is also an amorphous polymer with $T_g = 83$ °C, and exhibits a nematic phase without any propensity to crystallize on heating or cooling. From these results, we can draw two conclusions from these facts. First, the mesomorphism of these conjugated polymers are greatly affected by the nature of the pendants. Second, the mesophasic temperature range will be hugely promoted, comparing with the mesophasic temperature range of PFO (~100 °C), as well as the tendency of spontaneous crystallization of PF can be suppressed by the introduction of the OXD pendant groups.

Table 4.2 Absorption and PL Emission Spectral Data of Polymers in Chloroform Solutions and Thin Solid Films

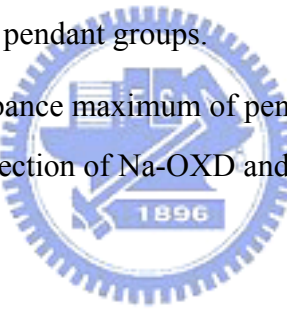
polymer	Optical						
	$\lambda_{\text{abs,sol}}$ (nm)	$\lambda_{\text{abs,silm}}$ (nm)	band gap	$\lambda_{\text{PL,sol}}$ (nm)	$\lambda_{\text{PL, film}}$ (nm)	$\Phi_{\text{PL}}^{\text{a}}$	$\Phi_{\text{PL}}^{\text{b}}$
	(eV)						
P1	300, 388	302, 389	2.95	417	427	1.06	0.80 ^c
P2	325, 389	334, 394	2.95	417	428	1.07	0.89 ^d
P3	320, 391	321, 395	2.95	417	428	1.09	0.95 ^d
P4	296, 392	299, 395	2.95	417	428	1.04	--

^a excited at 370 nm (the absorption region of polymer backbones).

^b excited at absorption region of pendant groups.

^c excited at the maximum absorbance maximum of pendant groups.

^d excited at the absorption intersection of Na-OXD and Bi-OXD pendant groups.



4.4.2 Optical Properties

The photophysical properties of the pendants (7a-7c) and polymers are summarized in Tables 4.2-4.3 and Figures 4.2-4.5 serially. It is noticed that all polymers exhibit two absorption bands (Figure 4.2). The shorter absorption range is originated from the absorption of the pendants, the longer wavelength peak in the region of 360-400 nm is attributed to the electron transition of the conjugated PF backbones. The optical band gaps of the polymers from the edge absorption of the polymer solutions are all equivalent (2.95 eV) regardless of various pendants, the value is exactly the same with the optical band gap of PFO reported by Janietz.¹⁰⁰ The identical band gaps illustrate that the different pendant groups do not appreciably change the excited state of the polymers, which implies similar distribution of effective conjugation lengths in the solution state of these polymers.

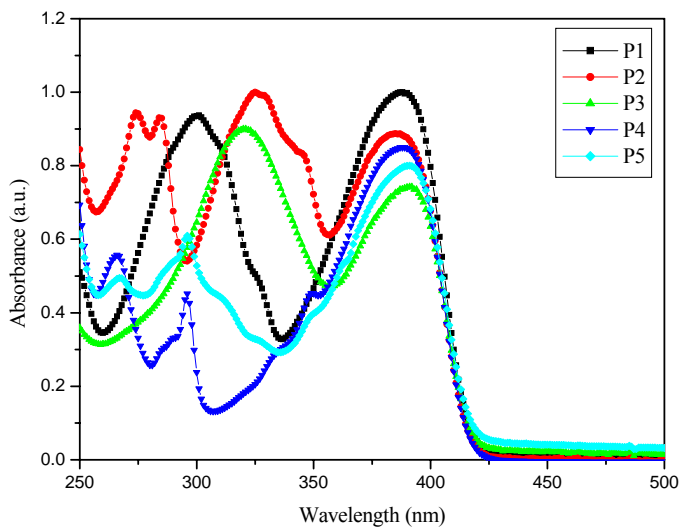


Figure 4.2 UV-visible spectra of polymer films.

The PL emission spectra in dilute solutions as well as in thin films are shown in Figure 4.3, where these polymers exhibit stable and strong purple-blue emissions from the PF backbones. Emissions from the OXD pendants are not observed, even when polymers are excited at the absorption peaks of the pendants. This indicates that the existence of efficient energy transfer from the pendants to the polymer backbones has occurred. Thin films and dilute solutions show nearly identical absorption values and shapes, indicating an absence of ground-state aggregation in the solid state. However, thin films show a red shift ca. 10 nm in PL peaks in contrast to dilute solutions, which suggests that light emission from a more planar structure has occurred in the solid state. The PL quantum yields are almost identical (Table 4.2) when these polymers are excited at the absorption region of the polymer backbone (370 nm). However, when these polymers are excited at the absorption region of pendants, the PL quantum yields (Table 4.2) will increase in the order of $P1 < P2 < P3$ according to the order of the quantum yield in each pendant (Table 4.3).

Table 4.3 Absorption and PL Emission Spectral Data of Pendants in Chloroform

Pendant group	$\lambda_{\text{abs}}^{\text{a}}$ (nm)	$\lambda_{\text{PL,sol}}^{\text{b}}$ (nm)	Rel. Φ_{PL}
Be-OXD (7a)	300	354	1 ^c
Na-OXD(7b)	323	374	1.59 ^d
Bi-OXD (7c)	319	386	1.75 ^d

^a Wavelength of the maximum absorbance.

^b Wavelength of the maximum emission.

^c excited at 300 nm and the PL quantum yield sets as 1.

^d excited at the absorption intersection of Na-OXD and Bi-OXD.



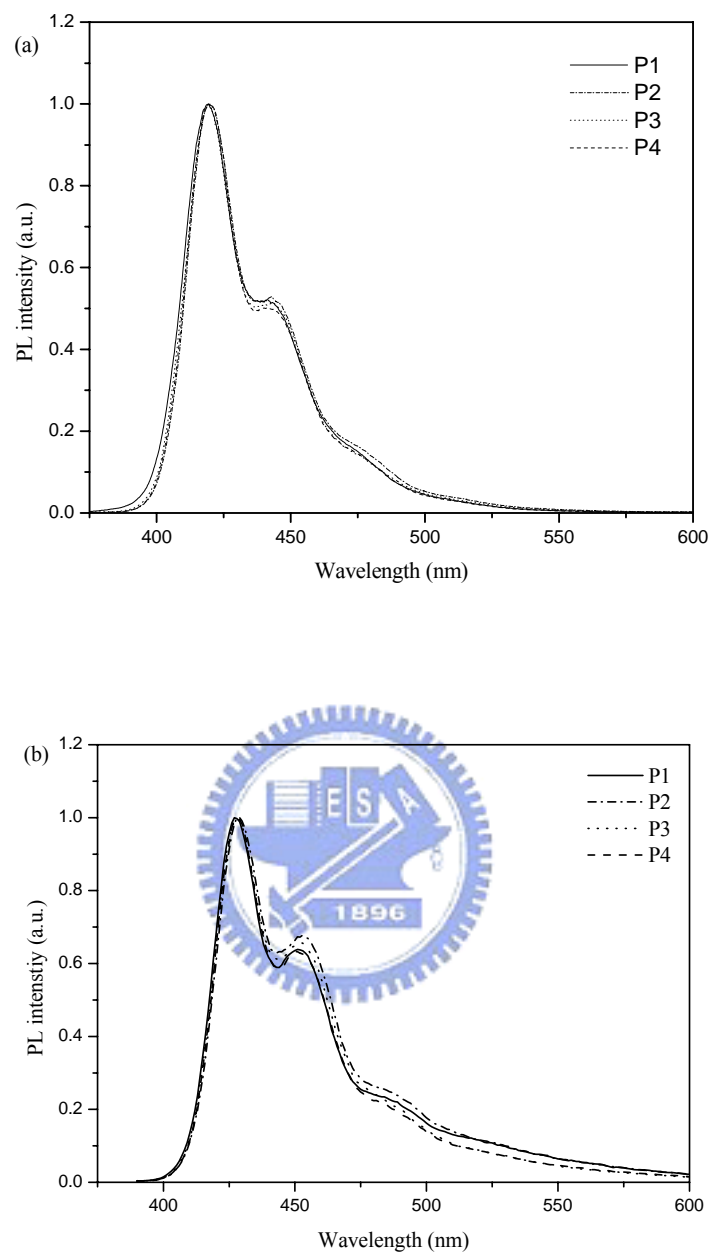


Figure 4.3 PL spectra of polymers (a) in dilute chloroform solutions. (b) in films.

Owing to the glass-forming LC property of these polymers, which make these polymers suitable to generate polarized emission. The anisotropic films are thermally annealed in the nematic temperature ranges on rubbing PI substrates for 30-60 min to align these polymers. As depicted in Figure 4-4, the shape of the annealed PL emissions is different from the thin film PL emissions, which indicates a more planar structure or aggregation formation in the annealed thin films. The PL dichroic ratios are 1.6~2.8 at 430 nm and 2.2~4.2 at 457 nm (Table 4.4), and these values are relatively lower than that of PFO. It is noted that thermally treated films in LC state show remarkable anisotropic properties under polarizing optical microscope (POM). Unfortunately, the annealed films result in a weakly anisotropic light while the aligned films are cold from LC states. This result of fast relaxation in alignment may be due to a complex alignment morphology originated from the competition of the polymer backbone and the pendants under thermal alignment. Conversely, while P3 is annealed in the temperature range of the SmA phase, the PL spectrum of annealed film shows a red-shifted emission peak at ca. 544 nm (Figure 4.5a). In order to identify the red-shifted emission peak which results from the aggregation (excimer formation) or the crystal packing (crystalline state) with different degrees of intermolecular interactions, P3 is sealed in an aligned LC cell with a thickness of 9 μm . The PL emission dichroic ratio is measured at 210 $^{\circ}\text{C}$ (which corresponds to the temperature range of the SmA phase) with different annealing time. As revealed in Figure 4.5b, the red-shifted peak becomes a dominated emission peak after 5 min thermal treatment and then becomes saturated after ca. 30 min treatment. From this result, we preferably assign the red-shifted emission band (ca. 544 nm) as an emission of the aggregation rather than the crystal packing. The dense packing of the smectic phase may be responsible for the formation of the aggregation. The data of PL dichroic ratios are summarized in Table 4.5, the emission dichroic ratios from polymer backbones and excimers are about 2.4 and 3.0, respectively, and these dichroic ratios are almost regardless of the annealing time.

Table 4.4 PL Emission Dichroic Ratios of Thermally Annealed Spin-Coated Films at Different Emission Peaks

Dichroic ratio	P1	P2	P3	P4	P5
R_{430}	2.7	1.6	2.8	1.6	1.9
R_{457}	3.8	2.4	4.2	2.2	2.9

^a PL emission dichroic ratio measured at emission peak of 430 nm.

^b PL emission dichroic ratio measured at emission peak of 457 nm.

Table 4.5 PL Emission Dichroic Ratios of P3 (at Different Emission Peaks) with Different Thermally Annealing Time at the Temperature Range of the SmA Phase

Dichroic ratio	1 min	5 min	10 min	30 min
R_{446}	2.2	2.6	2.4	2.3
R_{544}	3.0	2.9	2.9	3.0

^a PL emission dichroic ratio measured at emission peak of 446 nm.

^b PL emission dichroic ratio measured at emission peak of 544 nm.

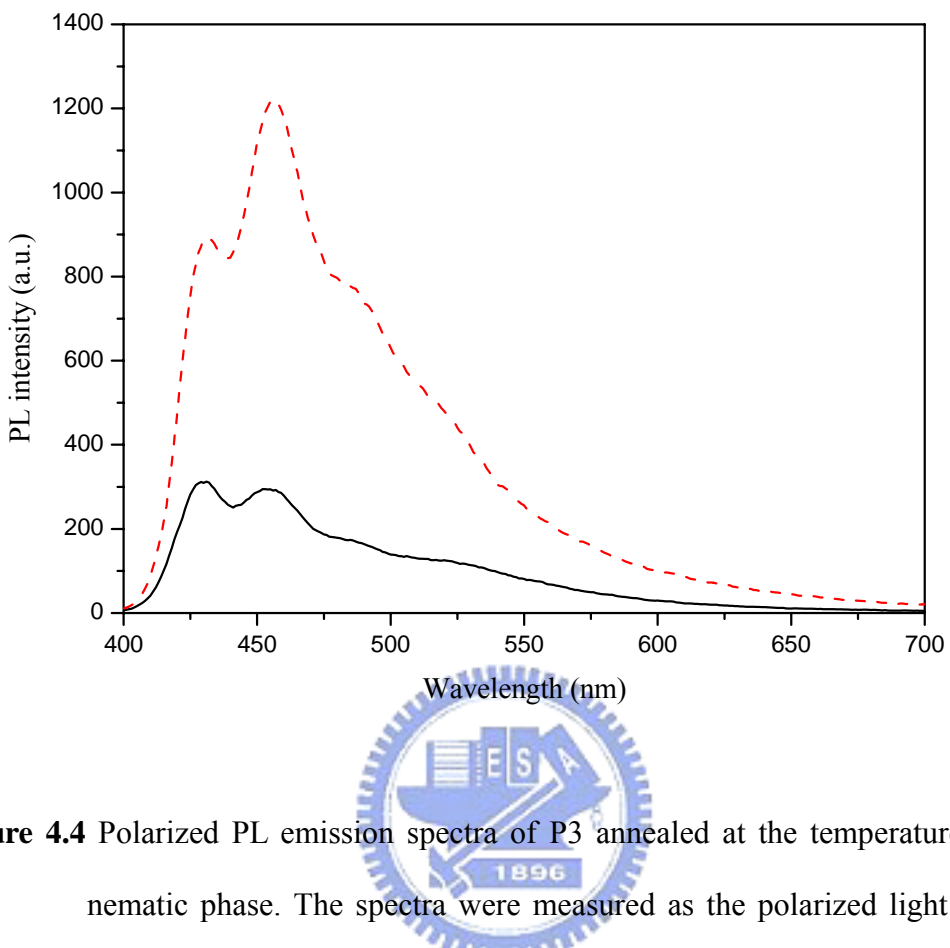


Figure 4.4 Polarized PL emission spectra of P3 annealed at the temperature range of the nematic phase. The spectra were measured as the polarized light parallel (dash line) and perpendicular (solid line) to the rubbing direction.

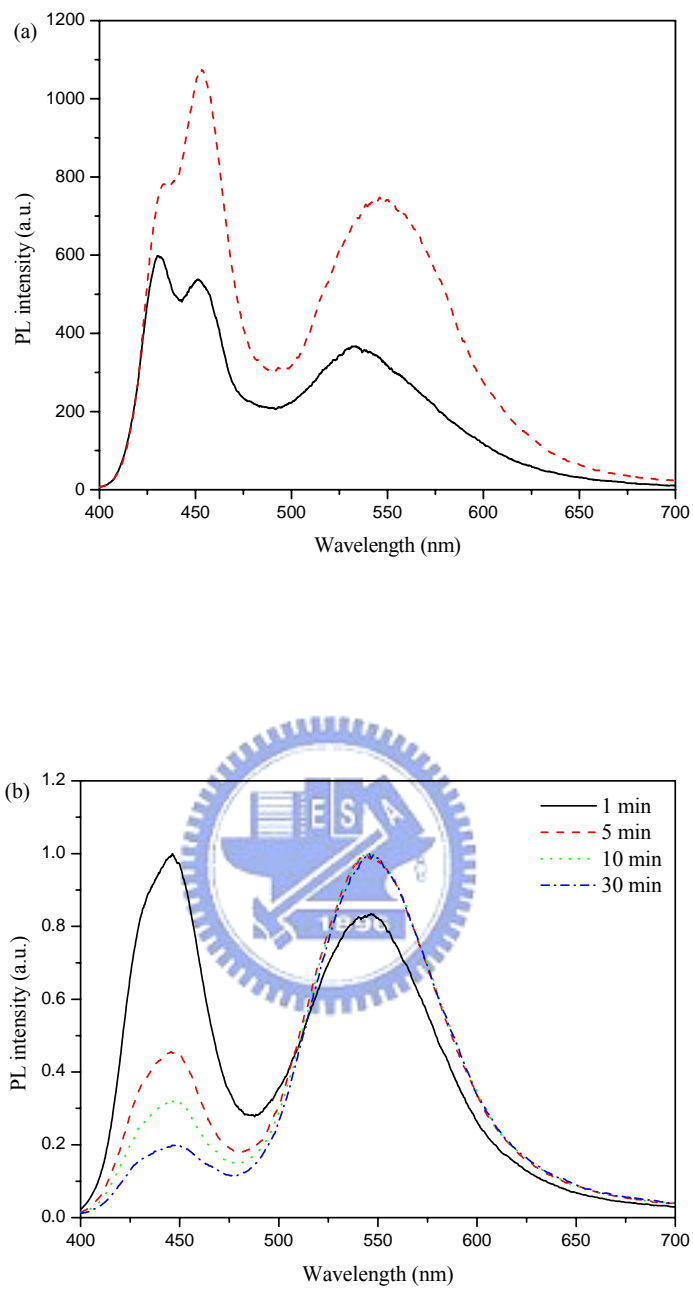


Figure 4.5 (a) Polarized PL emission spectra of P3 annealed at the temperature range of the SmA phase. The spectra were measured as the polarized light parallel (dash line) and perpendicular (solid line) to the rubbing direction. (b) Polarized PL emission spectra of P3 measured at 210 °C (the temperature range of the SmA phase) with different annealing time.

4.4.3 Electrochemical Properties

The redox behavior of polymer thin films were investigated by CV and the potentials were estimated by the reference energy level of ferrocene (4.8 eV below the vacuum level) according to the following equation:¹⁰¹ $E^{\text{HOMO}}/E^{\text{LUMO}} = [-(E^{\text{onset}} - 0.45) - 4.8] \text{ eV}$. The onset potentials were determined from the intersection of two tangents drawn at the rising and background currents of the CV measurements. As shown in Figure 6, these polymers possess two anodic peaks, which can be attributed to the oxidation of both pendants and polymer backbones. The OXD substituted polymers (P1-P3) show the onset potentials of oxidation between 1.46 and 1.52 V (Table 4.6) in the anodic scans. The onset potentials are similar to that reported value of PFO (1.4 V),¹⁰¹ and thus the onset potentials are due to the oxidation of the PF backbones. On the contrary, P4 has lower onset potentials of oxidation (ca. 1.31 V), and the lower value is attributed to the introduction of cabazole groups.¹⁰² In the cathodic scans, the onset potentials of reduction are remarkably promoted from -2.28 V of PFO to ca -1.9 V of these polymers by introducing OXD groups. The electrochemical results indicate that the incorporation of the OXD and cabazole groups into PF as pendants will efficiently reduce the LUMO energy levels and promote the HOMO energy levels, thus reduce the energy barrier of charge injection from electrodes to emitters.

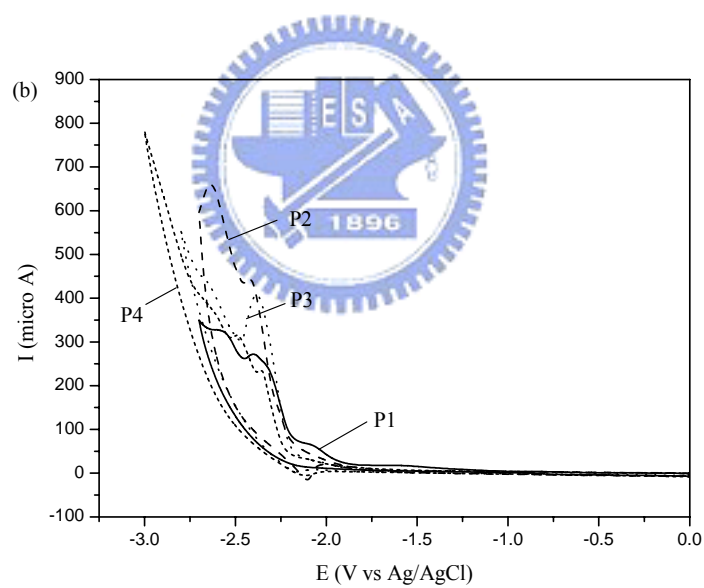
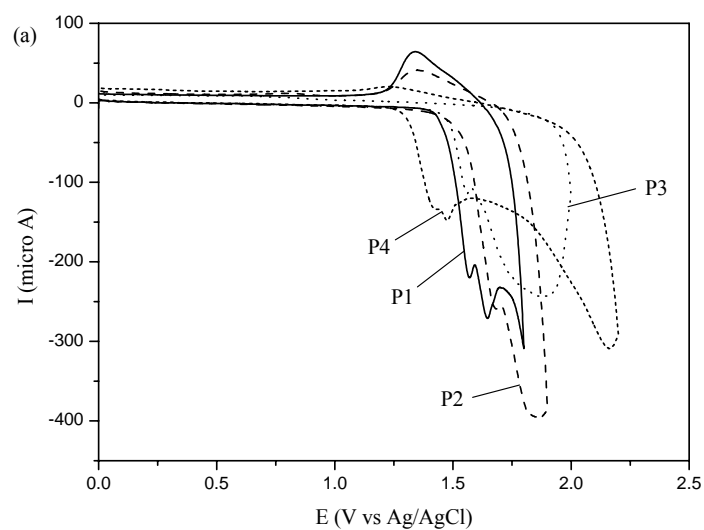


Figure 4.6 Cyclic voltammetry of polymers during (a) the oxidation process and (b) the reduction process.

Table 4.6 HOMO and LUMO Energies, and Electrochemical Properties of Polymers

Polymer	$E^{\text{red/onset}}$ (V)	$E^{\text{red/peak}}$ (V)	$E^{\text{ox/onset}}$ (V)	$E^{\text{ox/peak}}$ (V)	E^{HOMO} (eV)	E^{LUMO} (eV)	Band gap (eV)
P1	-1.91	-2.40,	1.46	1.57,	-5.81	-2.44	3.37
		-2.59		1.65			
P2	-1.94	-2.42,	1.52	1.69,	-5.87	-2.41	3.46
		-2.63		1.87			
P3	-1.86	-2.38,	1.47	1.56,	-5.82	-2.49	3.33
		-2.67		1.87			
P4	-1.90	-2.36,	1.31	1.47,	-5.66	-2.45	3.21
		-2.50		2.16			

4.4.4 Electroluminescent (EL) Properties of PLED Devices

The EL data are summarized in Table 4.7. The current-voltage and luminescence-voltage characteristics are displayed in Figure 4.7. All these devices show similar turn-on voltages for current and light at ca. 5 V. These similar turn-on voltages for current and light illustrate that a matched balance of injection and transportation in charges is achieved. The device with P1 as an emitter has the highest luminance of 2104 cd/m^2 at 10 V (with a power efficiency of 1.13 cd/A at 100 mA/cm^2) among these OXD substituted polymers (P1-P3). The devices based on these polymers (P1-P3) demonstrate a much higher brightness than the device made with poly(9,9-dihexylfluorene),¹⁰³ which had a maximum brightness 717 cd/m^2 . In addition these devices based on these polymers (P1-P3) also exhibit much better EL performance than the device made with poly[9,9-bis(2'-ethylhexyl)fluorene-2,7-diyl] (PBEHF)¹⁰⁴ and poly(9,9-dioctylfluorene) (POF).¹⁰⁵ From these results, we can conclude that the incorporation of electron-transporting moieties (OXD) into hole-transporting PF

backbones will improve the performance of the EL device. The device performance can be further improved by the incorporation of cabazole pendants into OXD-substituted PF (such as P4), a bright luminance of 2694 cd/m^2 at 11 V (with a power efficiency of 1.28 cd/A at 100 mA/cm^2) can be reached.

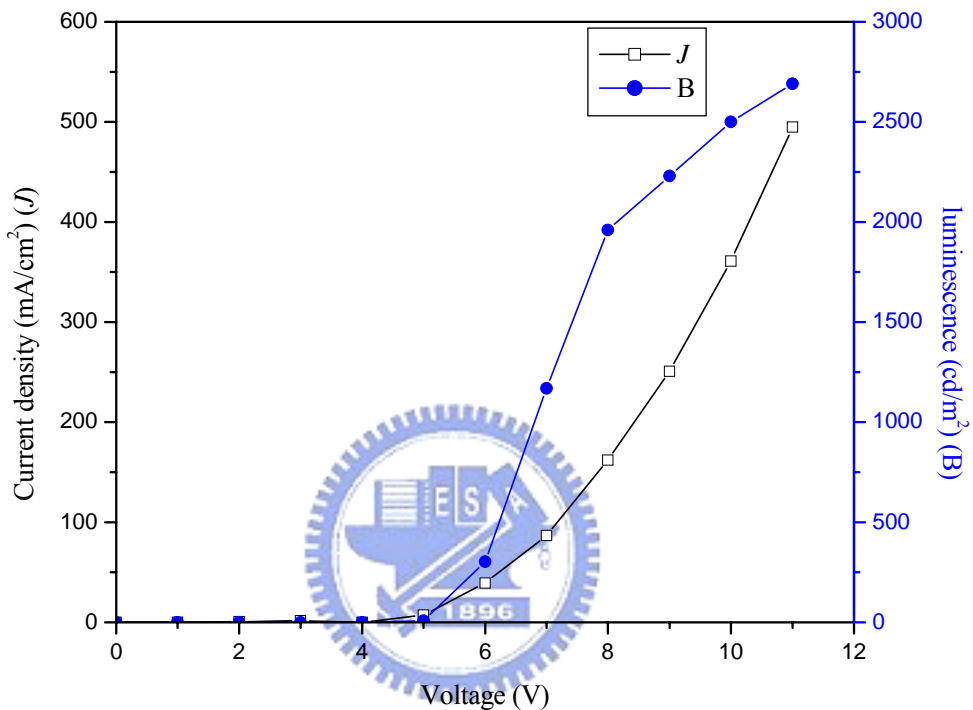


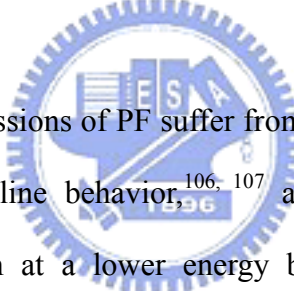
Figure 4.7 Current-voltage and luminescence-voltage characteristics of ITO/PEDOT:PSS/P4/Ca/Al device.

Table 4.7 PLED Devices^a Performance Data

Polymer	λ_{max} (nm)	Voltage ^b (V)	Brightness ^b (cd/m ²)	Power efficiency ^b (cd/A)	Luminance efficiency ^b (lm/W)	Max. brightness (cd/m ²) (V)
P1	424	7.8	1134	1.13	0.46	2104 (10)
P2	422	7.2	802	0.80	0.35	1672 (11)
P3	424	7.6	1070	1.07	0.44	2036 (11)
P4	422	7.1	1276	1.28	0.56	2694 (11)

^a Device structure: ITO/PEDOT:PSS/Polymer/Ca/Al.

^b Measured at 100 mA/cm².



It was reported that EL emissions of PF suffer from the excimer formation on the current flow due to its liquid crystalline behavior,^{106, 107} and results in an additional 100 nm bathochromic shifted emission at a lower energy band. As shown in Figure 4.8a, EL emission spectra of these polymers are almost the same at 8 V and exhibit stable EL emissions under forward biases. Figure 4.8b shows that the EL spectra of P3 are almost unchanged and without any low energy emission band as voltages increase from 6 V to 10 V. These EL spectra well matched with the corresponding PL emission spectra of thin films, which indicates that the similar radiatively excited states are involved in both EL and PL processes. Consequently, we can successfully suppress the excimer formation in the PF backbones by introducing OXD groups with long flexible side chains, even though these polymers possess unfavorable liquid crystalline behavior for PLEDs device.

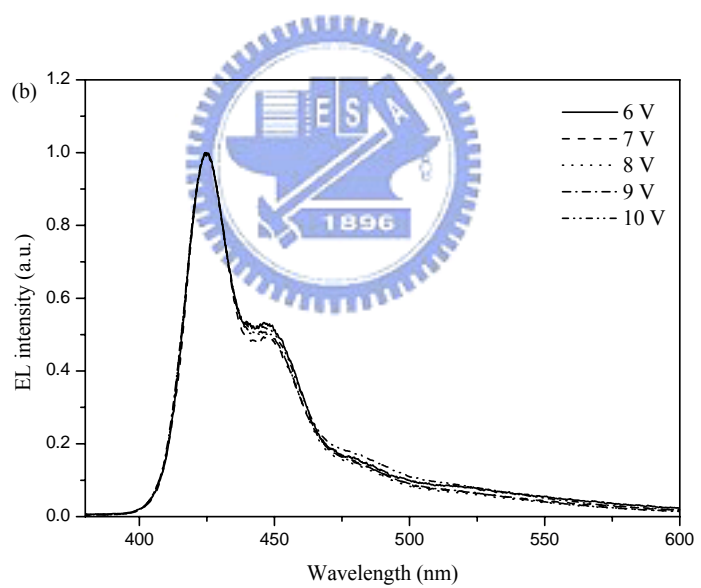
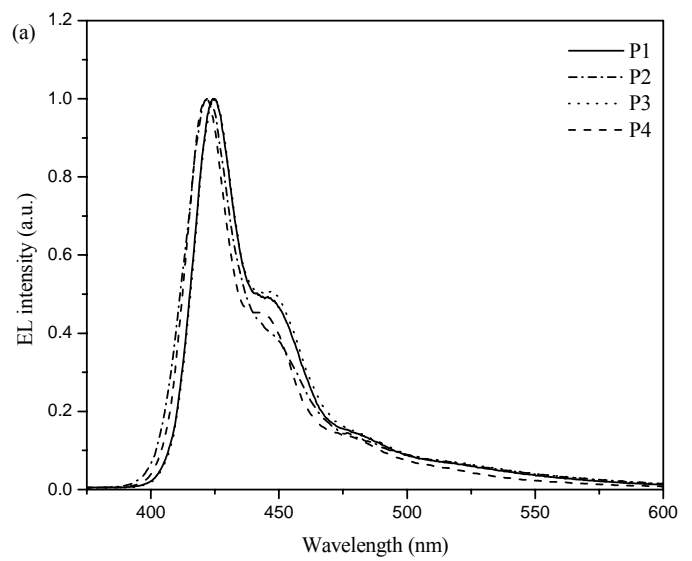


Figure 4.8 (a) Normalized EL spectra of ITO/PEDOT:PSS/Polymer/Ca/Al devices at 8 V.
 (b) Normalized EL spectra of ITO/PEDOT:PSS/P3/Ca/Al device at different voltages.

4.5 Conclusion

The thermal properties and mesomorphism of these glass-forming polymers are greatly affected by the nature of the pendants, these polymers exhibit stable mesogenic properties including the nematic and SmA phases. The incorporation of electron-transporting OXD pendants into PF backbones via long alkoxy spacers will effectively promote the mesophasic temperature range and depress the tendency of spontaneous crystallization of the PF backbones. For device performance, the introduction of charge-transporting pendants can not only tune the HOMO and LUMO energy levels but also suppress the formation of aggregation.

Acknowledgement. We thank the financial support from the National Science Council of Taiwan (ROC) through NSC 92-2113-M-009-016.



Chapter 5

Conclusion

A new class of mesomorphic molecules consisting of 1,3,4-oxadiazole-based mesogenic cores is prepared. These bent-shaped molecules exhibit the nematic and smectic A phases and exhibit a interesting schlieren texture consisting of only 2-brush disclinations and absence of 4-brush disclinations ($|s|=1$) in the nematic phase. In general, the mesogenic phases and optical properties of these oxadiazole-based LC materials have strong connections with their terminal functional groups. By increasing the terminal dipoles, the mesophase ranges are enhanced, and both of the absorption and photoluminescence spectra are shifted toward longer wavelengths.

A series of soluble alternating fluorene-based copolymers with OXD pendants were synthesized by palladium-catalyzed Suzuki coupling reaction. These polymers exhibit good thermal stability up to 400 °C and possess higher glass transition temperatures than that of the analogous dialkoxy-substituted polymer (PFPOC₆) consisting of the same backbone without OXD pendants. The photophysical and electrochemical properties of these polymers are not only affected by the OXD pendants, but also are affected by the polar effect (electron-withdrawing group, -CN, and electron-donating group, -R or -OR) and the size effect (the size of the grafted side chain) of the OXD pendants. Owing to the large steric hindrance of OXD pendants, the aggregation of these polymers in solid state is reduced, which results in almost identical PL emissions in both solution and solid states. The incorporation of OXD pendants into polymer backbone leads to mitigating the interchain interaction and improving the electron affinity and charge-injection properties effectively. Since only one emission peak is observed in both PL and EL spectra of these polymers, it is evidenced that effective energy transfer from the OXD pendants to the conjugated polymer

backbones has occurred and thus to eliminate the light emission from the OXD pendants. By comparing these polymers, we recognize that asymmetrical OXD substituted polymers possess better properties (higher quantum yield and lower aggregation in the solid state) than the symmetrical OXD substituted polymer. The symmetrical OXD substituted polymer has a longer PL emission wavelength than the asymmetrical OXD substituted polymers, which may be due to the improvement of the coplanarity between the polymer backbone and the symmetrical OXD pendants, and/or the introduction of two electron-withdrawing OXD pendants.

A series of soluble alternating poly(fluorene)-based copolymers containing electron-transporting 1,3,4-oxadiazole (OXD) and hole-transporting carbazole pendants attached to the C-9 position of fluorene units by long alkyl spacers were synthesized. All these polymers exhibit glass-forming liquid crystalline properties, including the nematic and smectic A (SmA) phases. The thermal properties and mesomorphism of these glass-forming polymers are greatly affected by the nature of the pendants. The incorporation of electron-transporting OXD pendants into PF backbones via long alkoxy spacers will effectively promote the mesophasic temperature range and depress the tendency of spontaneous crystallization of the PF backbones. For device performance, the introduction of charge-transporting pendants can not only tune the HOMO and LUMO energy levels but also suppress the formation of aggregation. A single layer device with P4 as an emitter shows a turn-on voltage of 5 V and a bright luminescence of 2694 cd/m^2 at 11 V with a power efficiency of 1.28 cd/A at 100 mA/cm^2 .

References

(1) Collings, P. J.; Hird, M.; "Introduction to liquid crystals" (Taylor & Francis).

(2) Burroughes, J. H.; Bradley, D. D.C.; Brown, A. R.; Marks, R. N.; Mackay, K.; Friend, R. H.; Burn, P. L.; Holmes, A. B. *Nature (London)* **1990**, *347*, 539.

(3) (a)Dai, L.; Winkler, B.; Dong, L.; Tong, L.; Mau, A. W. H. *Adv. Mater.* **2001**, *13*, 915. (b) Kraft, A.; Grimsdale, A. C.; Holmes, A. B. *Angew. Chem. Int. Ed.* **1998**, *37*, 402.

(4) (a) Kraft, A.; Grimsdale, A. C.; Holmes, A. B. *Angew. Chem., Int. Ed.* **1998**, *37*, 402. (b) Friend, R. H.; Gymer, R. W.; Holmes, A. B.; Burroughes, J. H.; Marks, R. N.; Taliani, C.; Bradley, D. D. C.; dos Santos, D. A.; Bredas, J. L.; Lögdlund, M.; Salaneck, W. R.; *Nature (London)* **1999**, *397*, 121.

(5) (a) Grell, M.; Bradley, D. D. C. *Adv. Mater.* **1999**, *11*, 895.

(6) (a) Friend, R. H.; Gymer, R. W.; Holmes, A. B.; Burroughes, J. H.; Marks, R. N.; Taliani, C.; Bradley, D. D. C.; dos Santos, D. A.; Bredas, J. L.; Lögdlund, M.; Salaneck, W. R.; *Nature (London)* **1999**, *397*, 121. (b) Johnson, M. J.; Sempel, A. *Inf. Disp.* **2000**, *2*, 12. (c) Dyreklev, P.; Berggren, M.; Inganäs, O.; Andersson, M. R.; Wennerstrom, O.; Hjertberg, T. *Adv. Mater.* **1995**, *7*, 43.

(7) (a) Wessling, R. A.; Zimmerman, R. G.; US-B 3401152, 1968 [*Chem. Abstr.* **1968**, *69*, 87735q]. (b) Wessling, R. A. *J. Polym. Sci. Polym. Symp.* **1985**, *72*, 55.

(8) (a) Lenz, R. W.; Han, C. C.; Stenger-Smith, J.; Karasz, F. E. *J. Polym. Sci. Polym. Chem.* **1988**, *26*, 3241. (b) Garay, R. O.; Baier, U.; Bubeck, C.; Mullen, K. *Adv. Mater.* **1993**, *5*, 561.

(9) (a) Bettenhausen, J.; Strohriegl, P. *Adv. Mater.* **1996**, *8*, 507. (b) Yeh, H. C.; Lee, R. H.; Chan, L. H.; Lin, T. Y. *Chem. Mater.* **2001**, *13*, 2788. (c) Salbeck, J.; Weissertel, F. *Macromol. Synth. Met.* **1997**, *91*, 209. (d) Wang, J. F.; Jabbour, G. E.; Mash, E. A.; Anderson, J. *Adv. Mater.* **1999**, *11*, 1266.

(10) (a)Liu, M. S.; Jiang, X.; Liu, S.; Herguth, P.; Jen, A. K. Y. *Macromolecules* **2002**, *35*,

3532. (b) Jenekhe, S. A.; Osaheni, J. A. *Science* **1994**, *265*, 765.

(11) Krebs, F. C.; Jorgensen, M. *Macromolecules* **2002**, *35*, 7200.

(12) Chen, Z. K.; Meng, H.; Lai, Y. H.; Huang, W. *Macromolecules* **1999**, *32*, 4351.

(13) Marsella, M. J.; Fu, D. K.; Swager, T. M. *Adv. Mater.* **1995**, *7*, 145.

(14) Gillissen, S.; Jonforsen, M.; Kesters, E.; Johansson, T.; Theander, M.; Andersson, M. R.; Inganas, O.; Lutsen, L.; Vanderzande, D. *Macromolecules* **2001**, *34*, 7294.

(15) (a) Wang, C.; Jung, G. Y.; Hua, Y.; Pearson, C.; Bryce, M. R.; Petty, M. C.; Batsanov, A. S.; Goeta, A. E.; Howard, J. A. K. *Chem. Mater.* **2001**, *13*, 1167. (b) Zhan, X.; Liu, Y.; Wu, X.; Wang, S.; Zhu, D. *Macromolecule* **2002**, *35*, 2529. (c) Lee, Y. Z.; Chen, X.; Chen, S. A.; Wei, P. K.; Fann, W. S. *J. Am. Chem. Soc.* **2001**, *123*, 2296. (c) Peng, Z.; Zhang, J. *Chem. Mater.* **1999**, *11*, 1138. (d) Chung, S. J.; Kwon, K. Y.; Lee, S. W.; Jin, J. L.; Lee, C. H.; Lee, C. E.; Park, Y. *Adv. Mater.* **1998**, *10*, 1112. (e) Kim, J. H.; Park, J. H.; Lee, H. *Chem. Mater.* **2003**, *15*, 3414.

(16) Adachi, C.; Tsutsui, T.; Saito, S. *Appl. Phys. Lett.* **1990**, *56*, 799.

(17) (a) Cui, Y.; Zhang, X.; Jenekhe, S. A. *Macromolecules* **1999**, *32*, 3824. (b) Jandke, M.; Strohriegl, P.; Berleb, S.; Werner, E.; Brutting, W. *Macromolecules* **1998**, *31*, 6434.

(18) (a) Jenekhe, S. A.; Zhang, X.; Chen, X. L.; Choong, V. E.; Gao, Y.; Hsieh, B. R. *Chem. Mater.* **1997**, *9*, 409. (b) Jen, A. K.; Wu, X. M.; Ma, H. *Chem. Mater.* **1998**, *10*, 3824.

(19) (a) Zhang, X.; Jenekhe, S. A. *Mater. Res. Soc. Symp. Proc.* **1998**, *488*, 539. (b) Wang, Y. Z.; Gebler, D. D.; Fu, D. K.; Swager, T. M.; MacDiarmid, A. G.; Epstein, A. J. *Synth. Met.* **1997**, *85*, 1179.

(20) (a) Ruiz, J. P.; Dharia, J. R.; Reynolds, J. R.; Buckley, L. J. *Macromolecules* **1992**, *25*, 849. (b) Chen, Z. K.; Meng, H.; Lai, Y. H.; Huang, W. *Macromolecules* **1999**, *32*, 4351. (c) Meng, H.; Yu, W. L.; Hunang, W. *Macromolecules* **1999**, *32*, 8841. (d) Pu, Y. J.; Soma, M.; Kido, J.; Nishide, H. *Chem. Mater.* **2001**, *13*, 3817. (e) Chen, Z. K.; Lee, N. H. S.; Huang, W.; Wu, Y. S.; Cao, Y. *Macromolecules* **2003**, *36*, 1009. (f) Wu, F. I.;

Reddy, S.; Shu, C. F.; Liu, M. S.; Jen, A. K. Y. *Chem. Mater.* **2003**, *15*, 269.

(21) Lam, J. W. Y.; Tang, B. Z. *J. Polym. Sci. Part A: Polym. Chem.* **2003**, *41*, 2607.

(22) Dyreklev, P.; Berggren, M.; Inganas, O.; Andersson, M. R.; Wennerstrom, O.; Hjertberg, T. *Adv. Mater.* **1995**, *7*, 43.

(23) Grell, M.; Bradley, D. D. C. *Adv. Mater.* **1999**, *11*, 895.

(24) Lin, H. C.; Lai, L. L.; Hsieh, W. P.; Huang, W. Y. *Liq. Cryst.* **1997**, *22*, 661.

(25) Semmler, K. J. K.; Dingemans, Samulski, E. T. *Liq. Cryst.* **1998**, *258*, 85.

(26) Tokuhisa, H.; Era, M.; Tsutsui, T. *Appl. Phys. Lett.* **1998**, *72*, 2639.

(27) Tokuhisa, H.; Era, M.; Tsutsui, T. *Adv. Mater.* **1998**, *10*, 404.

(28) Sato, M.; Ohta, R.; Handa, M.; Kasuga, K. *Liq. Cryst.* **2002**, *29*, 1441.

(29) Karamysheva, L. A.; Torgova, S. I.; Agafonova, I. F. *Liq. Cryst.* **2000**, *27*, 393.

(30) Cai, R.; Samulski, E. T. *Liq. Cryst.* **1991**, *9*, 617.

(31) Parra, M.; Alderete, J.; Zuniga, C.; Hidalgo, P.; Vergara, J.; Fuentes, G. *Liq. Cryst.* **2002**, *29*, 1375.

(32) Eichhorn, S. H.; Paraskos, A. J.; Kishikawa, E.; Swager, T. M. *J. Am. Chem. Soc.* **2002**, *124*, 12742.

(33) Dimitrowa, K.; Hauschild, J.; Zaschke, H.; Schubert, H. *J. Prakt. Chem.* **1980**, *331*, 631.

(34) Lai, C.; Ke, Y. C.; Su, J. C.; Shen, C.; Li, W. R. *Liq. Cryst.* **2002**, *29*, 915.

(35) Kim, B. G.; Kim, S.; Park, S. Y.; *Tetrahedron Lett.* **2001**, *42*, 2697.

(36) Haristoy, D.; TSIOURVAS, D. *Chem. Mater.* **2003**, *15*, 2079.

(37) Guller, R.; Binggeli, A.; Breu, V.; Bur, D.; Fischli, W.; Hirth, G.; Jenny, C.; Kansy, M.; Montavon, F.; Muller, M.; Oefner, C.; Stadler, H.; Vieira, E.; Wilhelm, M.; Wostl, W.; Matki, H. P. *Bioorg. Med. Chem. Lett.* **1999**, *9*, 1403.

(38) Debono, M.; Turner, W. W.; Lagrandeur, L.; Burkhardt, F. J.; Nissen, J. S.; Nichols, K. K.; Rodriguez, M. J.; Zweifel, M. J.; Zechner, D. J.; Gordee, R. S.; Tang, J.; Parr, T. R.

J. Med. Chem. **1995**, *38*, 3271.

(39) Dingemans, T. J.; Murthy, N. S.; Samulski, E. T. *J. Phys. Chem. B* **2001**, *105*, 8845.

(40) Fan, F. Y.; Culligan, S. W.; Mastrangelo, J. C.; Katsis, D.; Chen, S. H. *Chem. Mater.* **2001**, *13*, 4584.

(41) Collings, P. J.; Hird, M. "INTRODUCTION TO LIQUID CRYSTALS" (Taylor & Francis), pp.71.

(42) Chandrasekhar, S.; Nair, G. G.; Rao, D. S. S.; Prafeke, K.; Blunk, D. *Liq. Cryst.* **1998**, *24*, 67.

(43) Kishikawa, K.; Harris, M. C.; Swager, T. M. *Chem. Mater.* **1999**, *11*, 867.

(44) Dingemans, T. J.; Samulski, E. T. *Liq. Cryst.* **2000**, *27*, 131.

(45) Tao, Y. T.; Balasubramaniam, E.; Danel, A.; Jarosz, B.; Tomasik, P. *Chem. Mater.* **2001**, *13*, 1207.

(46) Wong, M. S.; Li, Z. H.; Tao, Y.; D'ioro, M. *Chem. Mater.* **2003**, *15*, 1198.

(47) Wawamoto, M.; Mochizuki, H.; Shishido, A.; Tsutsumi, O.; Ikeda, T.; Lee, B.; Shirota, Y. *J. Phys. Chem. B* **2003**, *21*, 4887.

(48) Burroughes, J. H.; Bradley, D. D.C.; Brown, A. R.; Marks, R. N.; Mackay, K.; Friend, R. H.; Burn, P. L.; Holmes, A. B. *Nature (London)* **1990**, *347*, 539.

(49) (a) Kraft, A.; Grimsdale, A. C.; Holmes, A. B. *Angew. Chem., Int. Ed.* **1998**, *37*, 402. (b) Friend, R. H.; Gymer, R. W.; Holmes, A. B.; Burroughes, J. H.; Marks, R. N.; Taliani, C.; Bradley, D. D. C.; dos Santos, D. A.; Bredas, J. L.; Lögdlund, M.; Salaneck, W. R.; *Nature (London)* **1999**, *397*, 121. (c) Johnson, M. J.; Sempel, A. *Inf. Disp.* **2000**, *2*, 12.

(50) (a) Gustafsson, G.; Cao, Y.; Treasy, G. M.; Klavetter, F.; Colaneri, N.; Heeger, A. J. *Nature* **1992**, *357*, 477. (b) Greenham, N. C.; Friend, R. H. *Solid State Phys.* **1995**, *49*, 1.

(51) (a) Liu, M. S.; Jiang, X.; Liu, S.; Herguth, P.; Jen, A. K. Y. *Macromolecules* **2002**, *35*, 3532. (b) Jenekhe, S. A.; Osaheni, J. A. *Science* **1994**, *265*, 765.

(52) Krebs, F. C.; Jorgensen, M. *Macromolecules* **2002**, *35*, 7200.

(53) Chen, Z. K.; Meng, H.; Lai, Y. H.; Huang, W. *Macromolecules* **1999**, *32*, 4351.

(54) Marsella, M. J.; Fu, D. K.; Swager, T. M. *Adv. Mater.* **1995**, *7*, 145.

(55) Gillissen, S.; Jonforsen, M.; Kesters, E.; Johansson, T.; Theander, M.; Andersson, M. R.; Inganäs, O.; Lutsen, L.; Vanderzande, D. *Macromolecules* **2001**, *34*, 7294.

(56) (a) Cui, Y.; Zhang, X.; Jenekhe, S. A. *Macromolecules* **1999**, *32*, 3824. (b) Jandke, M.; Strohriegl, P.; Berleb, S.; Werner, E.; Brutting, W. *Macromolecules* **1998**, *31*, 6434.

(57) (a) Jenekhe, S. A.; Zhang, X.; Chen, X. L.; Choong, V. E.; Gao, Y.; Hsieh, B. R. *Chem. Mater.* **1997**, *9*, 409. (b) Jen, A. K.; Wu, X. M.; Ma, H. *Chem. Mater.* **1998**, *10*, 3824.

(58) (a) Zhang, X.; Jenekhe, S. A. *Mater. Res. Soc. Symp. Proc.* **1998**, *488*, 539. (b) Wang, Y. Z.; Gebler, D. D.; Fu, D. K.; Swager, T. M.; MacDiarmid, A. G.; Epstein, A. J. *Synth. Met.* **1997**, *85*, 1179.

(59) (a) Wang, C.; Jung, G. Y.; Hua, Y.; Pearson, C.; Bryce, M. R.; Petty, M. C.; Batsanov, A. S.; Goeta, A. E.; Howard, J. A. K. *Chem. Mater.* **2001**, *13*, 1167. (b) Zhan, X.; Liu, Y.; Wu, X.; Wang, S.; Zhu, D. *Macromolecule* **2002**, *35*, 2529. (c) Lee, Y. Z.; Chen, X.; Chen, S. A.; Wei, P. K.; Fann, W. S. *J. Am. Chem. Soc.* **2001**, *123*, 2296. (c) Peng, Z.; Zhang, J. *Chem. Mater.* **1999**, *11*, 1138. (d) Chung, S. J.; Kwon, K. Y.; Lee, S. W.; Jin, J. L.; Lee, C. H.; Lee, C. E.; Park, Y. *Adv. Mater.* **1998**, *10*, 1112. (e) Kim, J. H.; Park, J. H.; Lee, H. *Chem. Mater.* **2003**, *15*, 3414.

(60) Adachi, C.; Tsutsui, T.; Saito, S. *Appl. Phys. Lett.* **1990**, *56*, 799.

(61) (a) Ruiz, J. P.; Dharia, J. R.; Reynolds, J. R.; Buckley, L. J. *Macromolecules* **1992**, *25*, 849. (b) Chen, Z. K.; Meng, H.; Lai, Y. H.; Huang, W. *Macromolecules* **1999**, *32*, 4351. (c) Meng, H.; Yu, W. L.; Hunang, W. *Macromolecules* **1999**, *32*, 8841. (d) Pu, Y. J.; Soma, M.; Kido, J.; Nishide, H. *Chem. Mater.* **2001**, *13*, 3817. (e) Chen, Z. K.; Lee, N. H. S.; Huang, W.; Wu, Y. S.; Cao, Y. *Macromolecules* **2003**, *36*, 1009. (f) Wu, F. I.; Reddy, S.; Shu, C. F.; Liu, M. S.; Jen, A. K. Y. *Chem. Mater.* **2003**, *15*, 269.

(62) (a) Moratti, S. C.; Cervimi, R.; Holmes, A. B.; baigent, D. R.; Friedn, R. H.; Greenham,

N. C.; Gruner, J.; Hamer, P. J. *Synth. Met.* **1995**, *71*, 2117. (b) Yang, J. S.; Swager, T. M. *J. Am. Chem. Soc.* **1998**, *120*, 5321.

(63) Bo, Z.; Zhang, C.; Severin, N.; Jurgen, P. R.; Schluter, A. D. *Macromolecules* **2000**, *33*, 2688.

(64) Liu, B.; Yu, W. L.; Lai, Y. H.; Huang, W. *Chem. Mater.* **2001**, *13*, 1984.

(65) Song, H. H.; Lin, H. C. *Liq. Cryst.* **2004**, in press.

(66) Xu, B.; Pan, Y.; Zhang, J.; Peng, Z. *Synth. Met.* **2000**, *114*, 337.

(67) Liu, M. S.; Jiang, X.; herguth, P.; Jen, A. K. Y. *Chem. Mater.* **2001**, *13*, 3820. (b) Wilson, J. N.; Windscheif, P. M.; Evans, U.; Myrick, M. L.; Bunz, U. H. F. *Macromolecules* **2002**, *35*, 8681.

(68) Egbe, D. A. M.; Cornelia, B.; Nowotny, J.; Gunther, W.; Klemm, E. *Macromolecules* **2003**, *36*, 5459.

(69) Redecker, M.; Bradley, D. D. C.; Inbasekaran, M.; Woo, E. P. *Appl. Phys. Lett.* **1998**, *73*, 1565.

(70) Grell, M.; Bradley, D. D. C.; Ungar, G.; Hill, J.; Whitehead, K. S. *Macromolecules* **1999**, *32*, 5810.

(71) Klaerner, G.; Miller, R. D. *Macromolecules* **1998**, *31*, 2007.

(72) Chen, X.; Liao, J. L.; Liang, Y.; Ahmed, M. O.; Tseng, H. E.; Chen, S. A. *J. Am. Chem. Soc.* **2003**, *125*, 636.

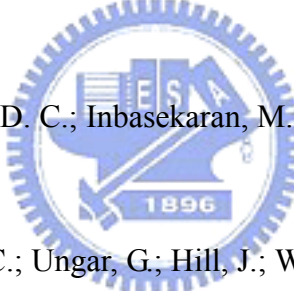
(73) Jenekhe, S. A.; Osaheni, J. A. *Science* **1994**, *265*, 765.

(74) Samuel, I. D. W.; Rumbles, G.; Collison, C. J. *Phys. Rev. B* **1995**, *52*, R11573.

(75) Ego, C.; Grimsdale, A. C.; Uckert, F.; Yu, G.; Srdanov, G.; Mullen, K. *Adv. Mater.* **2002**, *14*, 809.

(76) Stetayesh, S.; Grimsdale, A. C.; Weil, T.; Enkelmann, V.; Mullen, K.; Meghdadi, F.; List, E. j. w.; Leising, G. *J. Am. Chem. Soc.* **2001**, *123*, 946.

(77) Marsitzky, D.; Vestberg, R.; Blainey, P.; Tang, B. T.; Hawker, C. J.; Carter, K. R. *J. Am. Chem. Soc.* **1998**, *120*, 5321.



Chem. Soc. **2001**, *123*, 6965.

(78) Wu, F. I.; Reddy, S.; Shu, C. F.; Liu, M. S.; Jen, A. K. Y. *Chem. Mater.* **2003**, *15*, 269.

(79) Shu, C. F.; Dodda, R.; Wu, F. I.; Liu, M. S.; Jen, A. K. Y. *Macromolecules* **2003**, *36*, 6698.

(80) Scherf, U.; List, E. J. W. *Adv. Mater.* **2002**, *14*, 477.

(81) Grel, M.; Bradley, D. D. C.; Inbasekaran, M.; Woo, E. P. *Adv. Mater.* **1997**, *9*, 798.

(82) Hamaguchi, M.; Yoshino, K. *Appl. Phys. Lett.* **1995**, *67*, 3381.

(83) Geng, Y.; Chen, A. C. A.; Ou, J. J.; Chen, S. H. *Chem. Mater.* **2003**, *15*, 4352.

(84) Whitehead, K. S.; Grell, M.; Bradley, D. D. C.; Jandke, M.; Strohriegl, P. *Appl. Phys. Lett.* **2000**, *76*, 2946.

(85) Banach, M. J.; Friend, R. H.; Sirringhaus, H. *Macromolecules* **2003**, *36*, 2838.

(86) Grell, M.; Redecker, M.; Whitehead, K. S.; Bradley, D. D. C.; Inbasekaran, M.; Woo, E. P.; Wu, W. *Liq. Cryst.* **1999**, *26*, 1403.

(87) Miteva, T.; Meisel, A.; Knoll, W.; Nothofer, H. G.; Scherf, U.; Muller, D. C.; Meerholz, K.; Yasuda, A.; Neher, D. *Adv. Mater.* **2001**, *13*, 565.

(88) Schartel, B.; Wachtendorf, V.; Grell, M.; Bradley, D. D. C.; Hennecke, M. *Phys. Rev. B.* **1999**, *60*, 277.

(89) Sainova, D.; Zen, A.; Nothofer, H. G.; Asawapirom, U.; Scherf, U.; Hagen, R.; Bieringer, T.; Kostromine, S.; Neher, D. *Adv. Funct. Mater.* **2002**, *12*, 49.

(90) Culligan, S. W.; Geng, Y.; Chen, S. H.; Klubek, K.; Vaeth, K. M.; Tang, C. W. *Adv. Mater.* **2003**, *15*, 1176.

(91) Geng, Y.; Trajkovska, A.; Katsis, D.; Ou, J. J.; Culligan, S. W.; Chen, S. H. *J. Am. Chem. Soc.* **2002**, *124*, 8337.

(92) Geng, Y.; Culligan, S. W.; Trajkovska, A.; Wallace, J. U.; Chen, S. H. *Chem. Mater.* **2003**, *15*, 542.

(93) Song, H. H.; Lin, H. C. *Liq. Cryst.* **2004**, *31*, 831.

(94) Peng, Z.; Bao, Z.; Galvin, M. E. *Chem. Mater.* **1998**, *10*, 2086.

(95) Ranger, M.; Rondeau, D.; Leclerc, M. *Macromolecules* **1997**, *30*, 7686.

(96) Contoret, A. E. A.; Farrar, S. R.; O'Neill, M.; Nicholls, J. E.; Richards, G. J.; Kelly, S. M.; Hall, A. W. *Chem. Mater.* **2002**, *14*, 1477.

(97) Barry, J.; Bram, G.; Decodts, G.; Louupy, A.; Orange, C. *Synthesis* **1985**, *1*, 40.

(98) Liu, S. P.; Chan, H. S. O.; Ng, S. C. *J Polym Sci Part A: Polym Chem* **2004**, *42*, 4792.

(99) Sung, H. H.; Lin, H. C. *Macromolecules* **2004**, *37*, 7945.

(100) Geng, Y.; Trajkovska, A.; Katsis, D.; Ou, J. J.; Culligan, S. W.; Chen, S. H. *J. Am. Chem. Soc.* **2002**, *124*, 8337.

(101) Janietz, S.; Bradley, D. D. C.; Grell, M.; Giebel, C.; Inbasekaran, M.; Woo, E. P. *Appl. Phys. Lett.* **1998**, *73*, 2453.

(102) Xia, C.; Advincula, R. C. *Chem. Mater.* **2001**, *13*, 1682.

(103) Liu, M. S.; Jiang, X.; Herguth, P.; Jen, A. K. Y. *Chem. Mater.* **2001**, *13*, 3820.

(104) Hwang, D. H.; Kim, S. K.; Park, M. J.; Lee, J. H.; Koo, B. W.; Kang, I. N.; Kim, S. H.; Zyung, T. *Chem. Mater.* **2004**, *16*, 1298.

(105) Gong, X.; Iyer, P. K.; Moses, D.; Bazan, G. C.; Heeger, A. J. *Adv. Funct. Mater.* **2003**, *13*, 325.

(106) Weinfurtner, K. H.; Fujikawa, H.; Tokito, S.; Taga, Y. *Appl. Phys. Lett.* **2000**, *76*, 2502.

(107) Bradley, D. D. C.; Grell, M.; Long, X.; Mellor, H.; Grice, A. *Proc. SPIE* **1998**, *3145*, 254.